Aalto University
School of Engineering

Rizwan Ullah

Guidelines for Dimensional Accuracy and Machining Allowances of 3D Printed Metal Parts

Master's thesis submitted for examination of the degree in Master of Science (Technology)

Espoo 04.02.2019

Supervisor: Professor Esko Niemi

Advisor: Professor Esko Niemi

Aalto University
School of Engineering

Aalto University, P.O. BOX 11000, 00076
AALTO
www.aalto.fi

Abstract of master's thesis

Author Rizwan Ullah		
Title of thesis Guidelines for dimensional accuracy and machining allowances of 3D printed metal parts		
Master programme Mechanical Engineering		**Code** ENG25
Thesis supervisor Professor Esko Niemi		
Thesis advisor(s) Professor Esko Niemi		
Dated 04.02.2019	**Number of pages** 69+33	**Language** English

Abstract

In this research, characteristics of 3D printed metal parts are investigated. Main objectives are to find dimensional accuracy and define machining allowances for 3D printed metal parts. To achieve this goal internal threads were manufactured, and their quality was examined.

Method of this study was to examine quality of M5 and M8, internal threads. For this purpose, pre-holes were printed in flat plates in 5 different printing inclinations to build plate. Aluminium and maraging steels were main materials used in this research. Printing-machine's recoater angle was varied to observe its effect in determining part's dimensional accuracy. Printed parts were examined in as-built condition and after heat treatment. Physical properties measured during experimentation were surface roughness, flatness, hardness, porosity near surface, hole size and drilling forces. Thread strength was measured using thread stripping forces and thread profile was analyzed with optical microscope.

In results, effect of printing inclination on material properties was investigated. Comparison of different recoater angles and heat treatments were done separately. Results revealed that printing inclination and recoater angle do not affect material properties significantly and that threads are equally strong in all directions. Machining allowances, due to material surface defects, are recommended to be 0.2 mm for aluminium and 0.1 mm for maraging steel components. Making a pre-hole during printing reduces drilling forces up to 80%. To avoid off-centering effects during drilling, pre-hole size is recommended to be 1 mm smaller than nominal diameter.

Funding for this project was provided by Aalto University, Department of Mechanical Engineering, "FIN3D" research project. Equipment from laboratories of Production Engineering and Material Science of Mechanical Engineering, Aalto University, were utilized in the research. EOS Finland provided metal printed parts and valuable information.

Keywords: Additive manufacturing, Metal printing, Machining allowances, Geometric tolerances, Drilling, Tapping, Internal threads.

Acknowledgement

Above all, I am grateful to Almighty God for His blessings.

This thesis was part of Aalto University, Mechanical Engineering department, research project, "FIN3D". EOS Finland, based in Turku, supported this research by providing all printing materials and technical information.

First and foremost, I would like to thank my supervisor and advisor, Professor Esko Niemi for trusting in my abilities and providing this unique opportunity. He was always available for guidance and took keen interest throughout this research. I extend my acknowledgement to Dr. Sampsa Laakso who provided constructive feedback and practical information about experimentation techniques. Roy Björkstrand was key personnel from our group, for holding meetings with EOS Finland and managing thesis progress overall. I extend my deepest regard to him. In addition, I am grateful to EOS Finland for providing printing materials and feedback during meetings. Without their help, thesis would not have been possible.

Janne and Seppo, I am grateful for your support. Your professionalism has inspired me. In addition, materials science group personnel, Kim Widell and Laura Tiainen have helped me a lot in performing experiments, so special thanks to them.

As I am about to complete my master's degree in mechanical engineering, I would like to thank Aalto University for selecting me in first place and providing me best platform for learning and contributing to knowledge.

Espoo, 25.01.2019

Rizwan Ullah

Table of Contents

Abbreviations

AB-35	As-built, build plate temperature 35 ºC (cold processed)
AB-200	As-built, build plate temperature 200 ºC (hot processed)
ABS	Acrylonitrile Butadiene Styrene
AM	Additive Manufacturing
ASTM	American Society of Testing and Materials
CAD	Computer Aided Design
CNC	Computer Numerical Control
DMLS	Direct Metal Laser Sintering
EDM	Electron Discahrge Machining
FDM	Fused Deposition Modeling
ISO	The International Organization for Standardization
LED	Linear Energy Density
PBF	Powder Bed Fusion
PC	Polycarbonate
PLA	Polylactic Acid
SLM	Selective Laser Melting
SLS	Selective Laser Sintering
SM	Subtractive Manufacturing
ST	Solution Treatment
Stl	Stereolithography

1 Introduction

A growing interest in manufacturing is additive manufacturing (AM). In this manufacturing process, material is deposited point by point and layer by layer, thus no material is lost as with the conventional methods. Manufacturing has never been as flexible as with AM, which enables complex geometries like molds and valves to be created near net shape. Application areas comprise a wide range of industries such as medical, tooling, aerospace and automotive.

Although it is promoted as a free-form process in which any shape can be manufactured, there are certain limitations; notably:

- Not all engineering materials can be used
- Post-processing is required to achieve better surface finish and to remove surface defects
- The size of printed products is limited by printer dimensions.

According to ISO/ASTM 52900:2015 (en) standard, seven approved techniques are adopted, and the field is rapidly expanding. For production of metal parts, powder bed fusion, binder jetting and directed energy deposition are frequently employed [1]. PBF (powder bed fusion), which is powder technology wherein micro-sized metal particles are fused together with laser.

With the advent of AM, some unresolved issues have also surfaced. A plausible question in first stages of development of AM, is about dimensional accuracy and printing quality which will be examined in this research.

This study investigates holes printed in various inclinations in aluminium and maraging steel manufactured by EOS's 3D printing machine, M290. DMLS (Direct metal laser sintering), which is a PBF method, is a registered trade mark of EOS [24] where LASER sintering is used for metal deposition. Drilling and tapping then followed and resulted in internal threads. Surface porosity, axial drilling forces, hardness, roughness, flatness, hole diameter, thread stripping force and thread profile are examined. The analysis also explores isotropy of printed material in as-built condition and after heat treatment. Machining issues linked to tool wear are briefly reported. Machining allowances will be outlined. Finally, some guidelines are recommended to acquire accurate holes and threads in metal printed parts.

1.1 Background Problem

Defects most common to PBF methods in AM are dross, warping, shrinkages, porosity, poor surface roughness in downskin surfaces, support rupturing and color changes [25, Appendix E. Page 1-3]. As material is built vertically upward, some material properties, e.g. percentage elongation become weak in one direction compared to other ones [9, page 252]. ST is done mostly to relieve thermal stresses and to acquire uniform properties of material [24]. To what extent this anisotropy exists in materials produced by PBF, must be investigated.

In addition to manufacturing defects, geometrical variation occurs in PBF methods. Geometrical tolerances are not yet defined for AM processes. As material is built up in 3 dimensions, i.e. horizontal XY plane and vertical Z axis, material properties can vary depending on direction of build. Dross, i.e. partially melted particles attached to downskin surfaces, and surface finish depends on printing inclination. A comparison of as-built and heat treatment can also give more insight to material properties.

1.2 Research Questions

In view of above problems, following specific questions are raised for DMLS process.

1. Do different materials behave differently and if there is any anisotropy present in AM prints?
2. How strong are the threads made in AM prints in different inclinations?
3. How much porosity is there in AM metal prints? How is it distributed? What is the biggest pore present? Is it crucial for surface properties?
4. How is dross deposited in holes or with how good an accuracy of a hole of particular size can be built up?
5. What is the pre-hole diameter that should be printed for machining a certain hole size?
6. How much machining allowance should be added to AM prints in design phase?
7. How big cutting forces take place during machining? Do these forces vary in different printing inclinations?
8. How flat surfaces can be built and how does it vary at different printing inclinations?
9. What is the surface finish of DMLS parts at various inclinations?

1.3 Objective

In this study, core idea is to define geometrical accuracy and machining allowances of additive manufactured parts made by DMLS method. For this purpose, a round hole, very basic shape, is used. These holes are made in a rectangular bar, printed in various inclinations. Pre-hole sizes are investigated to acquire strong internal threads.

1.4 Scope

Powder bed fusion method, DMLS, is employed for metal printing. Different pre-hole diameters, representing various machining allowances, are printed in 5 printing inclinations i.e. 0º, 30º, 45º, 60º and 90º using aluminium and maraging steel. Two internal threads M5 and M8 are made to these pre-holes using drilling and tapping. Quality of threads is determined using thread stripping test and via optical microscopy. Some physical properties including flatness, surface roughness, hardness, porosity near surface and drilling forces are determined in printed material.

2 Additive Manufacturing

In AM, almost no material is lost during production. Previously it was employed mostly for rapid prototyping, but these days it is increasingly a production process [9, page 109,200]. Compared to conventional manufacturing processes, it does not require any special tooling and arrangements like fixturing. AM technology has made possible making of complex shapes in few steps, but the downside is, it is time consuming process.

In all AM processes, part is sliced in extremely small sized layers, usually 5-100 μm thick [9, page 47], using some commercial software like Ultimaker Cura. Required part features are converted from CAD (Computer Aided Design) file into a set of G and M codes. These are mostly machine instructions, where material needs to be deposited. As most of time, material is built layer by layer, some effect of isotropy remains in components although it can be minimised, in certain technologies.

2.1 ASTM approved AM technologies

AM technology is swiftly developing, and new methods are commercialized. ASTM (American Society of Testing and Materials) has advertised the list of following 7 approved technologies. This will help in understanding principles of AM manufacturing.

Vat photopolymerization

First AM process developed, was stereolithography, also known as vat photopolymerization. This technique makes use of photocurable polymers in a vat where laser beam cures material along directed paths defined by scanning mirrors. Part moves down, and sweeper/spreader traverses horizontally so that no defects remain in newly formed layer. Final part accuracy is good and relatively bigger size components can be made. Down sides are limited materials that can be processed and removal of resins and supports. Figure 1 shows schematic of vat photopolymerization.

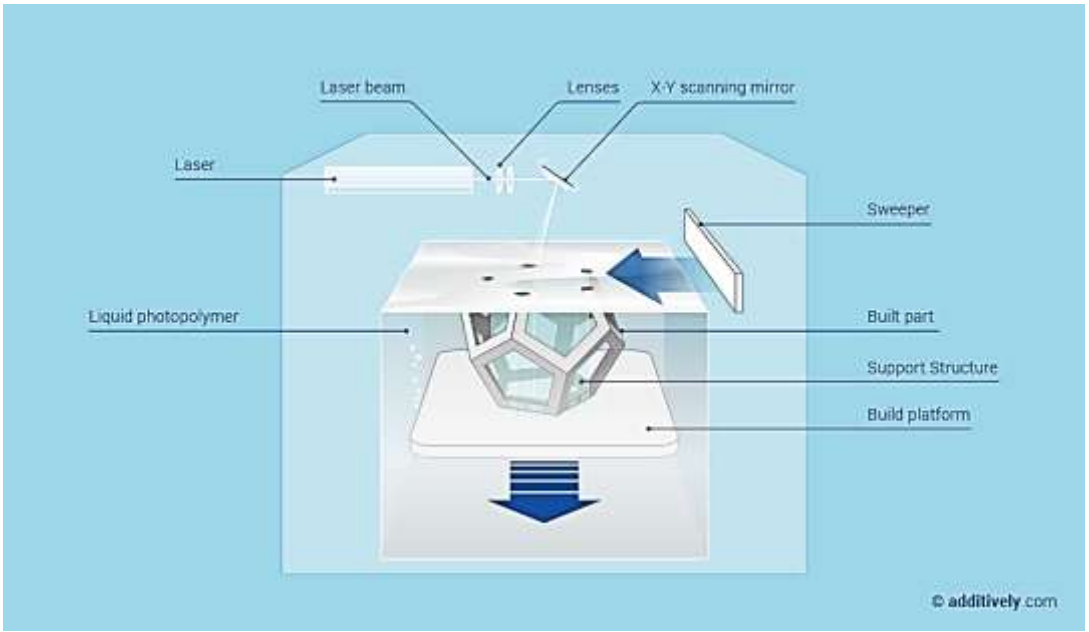

Figure 1: Schematic of vat photopolymerization [1]

Powder bed fusion

In PBF, high power laser melts the powder and part is built layer by layer. It is mostly used for metals production and is less common for plastics. SLS and SLM are terms often used for the same technology where laser melts and sinters the powder. DMLS is registered trademark of EOS which prints parts by SLS process. Powder can be used as support, but it is relatively poor conductor of heat. Supports are

mostly built of the same powder and since these do not have functional requirement in part, so must be removed afterward. Lattice structures are preferred in designing supports. Isotropic effect can be reduced by heat treatment process. Surface of R_a 4-10 microns and 99.9% [1] dense material can be achieved which makes it superior for metal production.

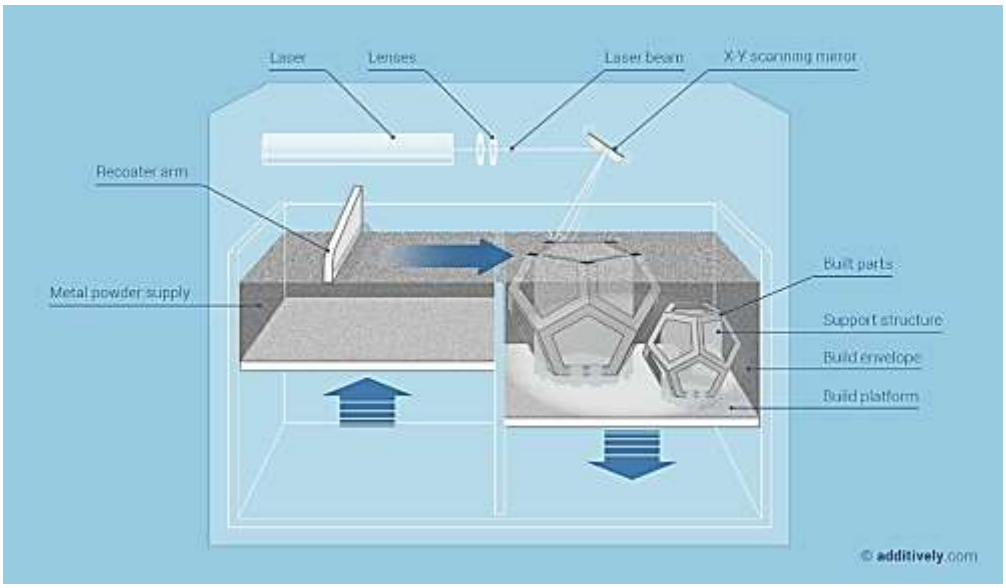

Figure 2: Schematic of Powder bed fusion, [1]

Material extrusion

In FDM (Fused Deposition Modeling) or Material extrusion two different materials, i.e. build material and support material, are used. Two nozzles, used separately, extrude these materials. After building the required part, supports are removed, mostly by heating. Build materials typically used are ABS, polyamide, polycarbonate, polyethylene, polypropylene, and waxes.

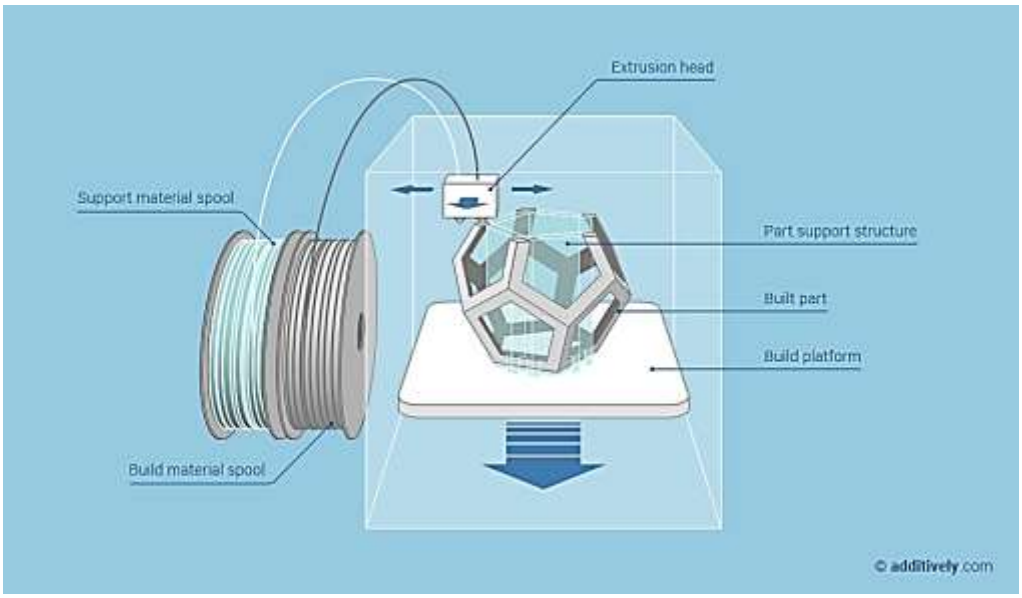

Figure 3: Schematic of Fused Deposition Modeling, [1]

Material jetting

In this technique inkjet printer head transfers wax droplets as build material, on certain areas according to the demand, which is defined by CAD model of component. Support material is separately used for creating support structures which will be later removed. No recoater is used and material fall by action of gravity. Making wax patterns, is main application area that are used for making jewellery and investment casting. Some application areas are also in medical and dentistry.

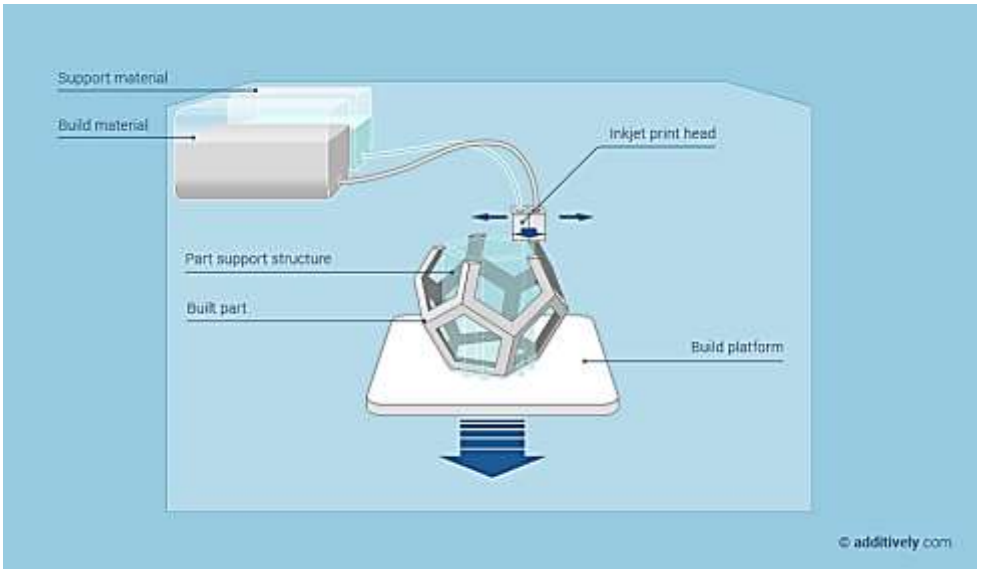

Figure 4: Sschematic of Material jetting [1]

Binder jetting

In this technique, adhesive bonding liquid is used to cement powder raw material, spread by roller. Parts produced are delicate and have lower strength unless they are sintered. Supports are not needed, and many parts can be nested in same build space. This technique also makes possible of colours in printing process. Overall this is a rapid and inexpensive process of making prototypes. Sand moulds made by this technique can produce high quality castings.

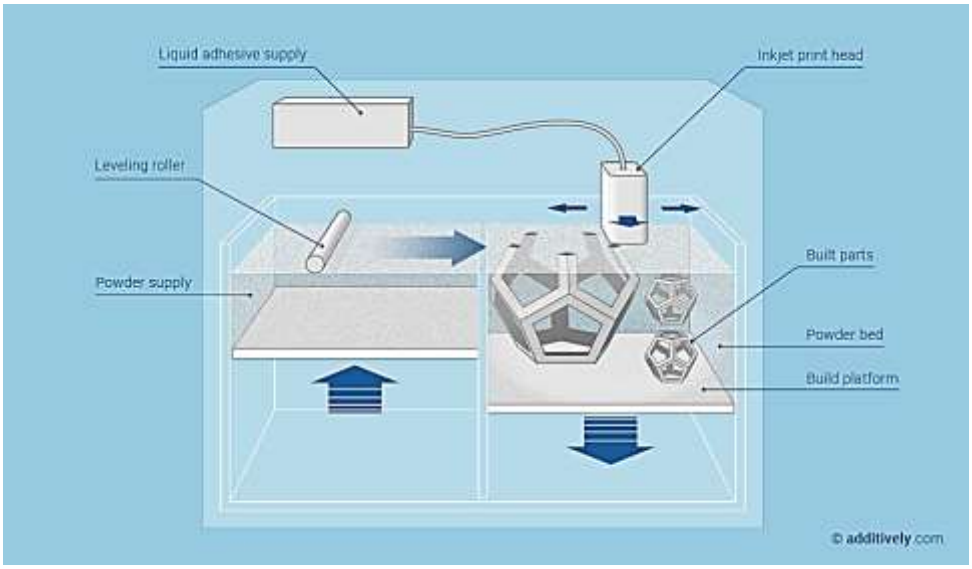

Figure 5: Sschematic of Binder jetting [1]

Sheet lamination

In this technique, material in form of sheet is cut with a laser or knife and stacked on top of one another. Newly formed layers are pressed by heated roller or can be glued together. Materials processed can be paper or plastic sheets. Process itself is rapid and low-cost. An adequate amount of material is lost in the form of cut rolls that can be recycled but needs additional processing. Application areas are model makings, prototypes and topography maps.

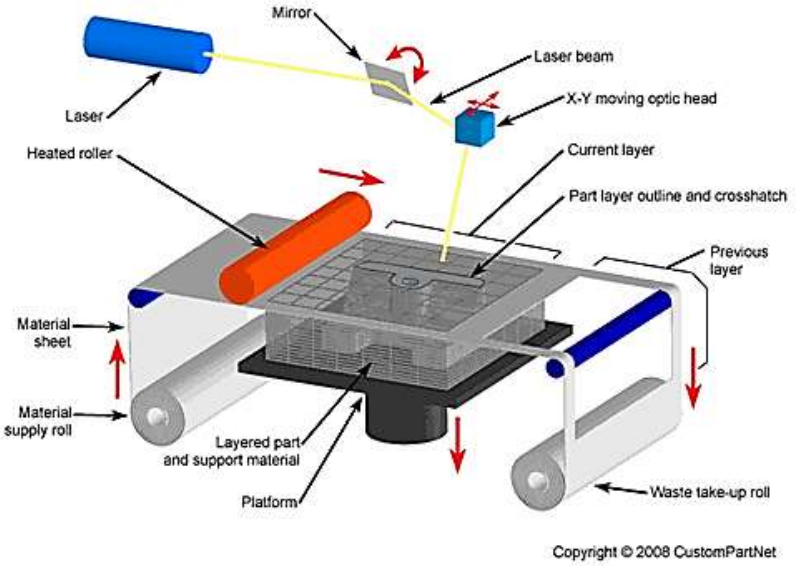

Figure 6: schematic of sheet lamination [2]

Directed energy deposition

Also known as electron beam melting in which high energy beam of electrons melts powder material directly. Supports are needed for improved heat transfer. Compared to selective laser melting processes, electron beam melting produced less thermal affects. Very compact (higher than 99%) [1] components are formed by this technique. Surface produced by this technique is rough compared to SLM process.

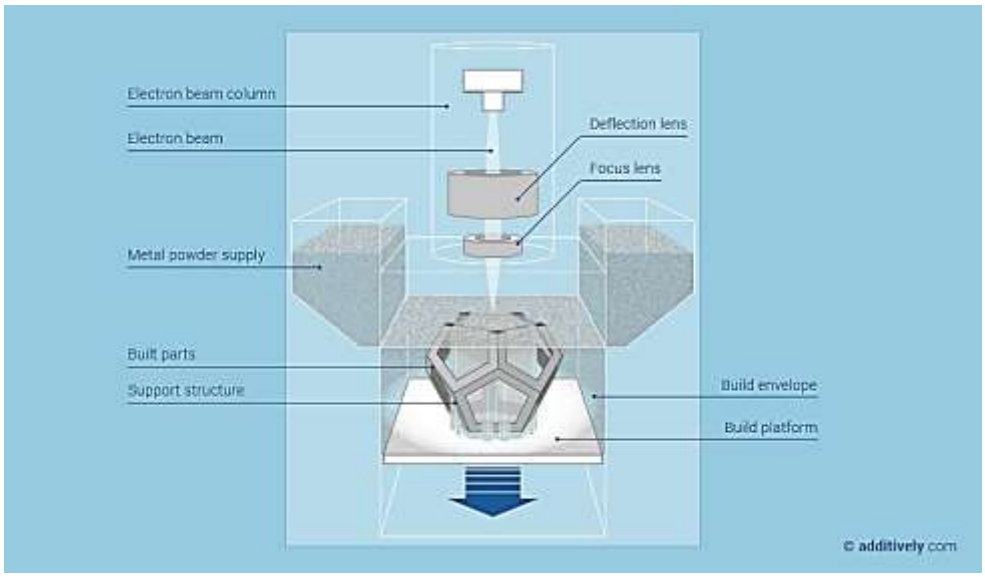

Figure 7: schematic of electron beam melting [1]

2.2 AM processed materials

Among metals, most commonly used materials include aluminium, cobalt chrome alloy, nickel, titanium alloys, maraging steel and stainless steel. Plastic materials available are, but not limited to, ABS, nylon, PLA and PC. Ceramics and sand can also be processed.

2.2.1 Aluminium and alloys

Aluminium and its alloys have significant applications in aerospace and automotive industry. Though silicon is inclusion in Aluminium alloys, yet it is beneficial for improving fluidity and castability [20, page 759]. Figure 8 shows formation of binary phase alloy in Al-Si alloys. Eutectic point exists at about 11.7% of Si, where all liquid changes to solid at a sharp temperature. So, this amount of silicon is preferable for high silicon aluminium alloys to avoid intermetallic compounds [29, page 35-50]. This kind of transformation results in more homogenous material which contain alpha aluminium and silicon.

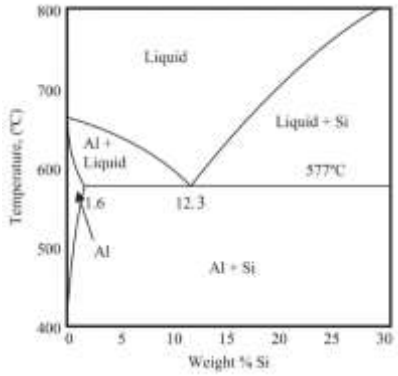

Figure 8: AL-Si phase diagram [3, page 2]

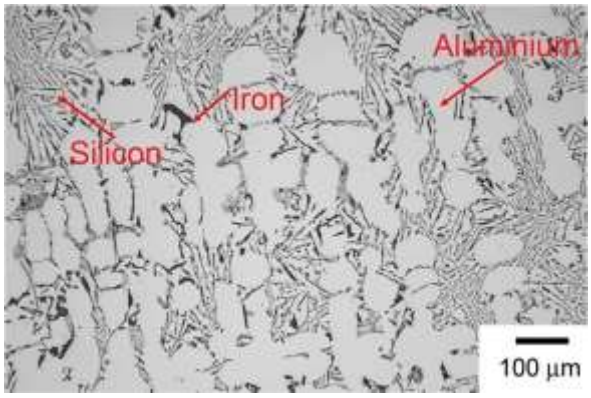

Figure 9: Optical micrograph of as-built AlSi10Mg [4]

Figure 9 shows microstructure of as-built AlSi10Mg where large columnar alpha grains (white) and silicon in fine needle like structure is noticeable.

Takata et. all [4] observed columnar α-Al grains and fine silicon particles, dispersed in microstructure of AlSi10Mg. According to their findings, annealing at higher temperature was found to be beneficial as it resulted in coarsening of Si particles which maintain characteristic microstructure and result in stable intermetallic forms.

2.2.2 Maraging steel

In maraging steel, carbon content is kept very low to avoid formation of TiC, which increases brittleness. For maraging steel austinitezation temperature is 850 C°. Slow cooling results in formation of martensite which is relatively soft compared to quenched martensite, owing to presence of nickel in it. Ni_3Mo, Ni_3Ti, Ni_3Al and Fe_2Mo precipitates are formed in martensitic matrix. Cobalt helps in homogenous dispersion of these precipitates. Aging process increases hardness and strength of maraging steel can rise to 2000 MPa [5].

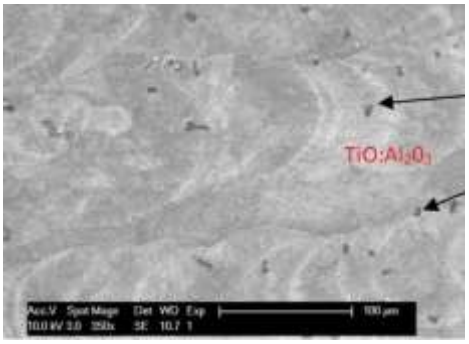

Figure 10: SEM result of maraging steel 300 [6]

Du et al., [7] measured grain size of wrought components higher than SLM components which validated the fact that SLM components have higher hardness. They determined microstructure of wrought samples to be isotropic and SLM components to be anisotropic.

2.3 Anisotropy

Wrought samples usually have more homogenous properties than SLM components. For same square cross-sectional shape of long rectangular bars, ultimate tensile strength and yield strength are higher in XY plane, compared to Z orientated samples [8].

Nakata et al., [4] study also revealed that as-built AlSi10Mg strength that does not depend upon shape of component. However, ductility was found to be dependent on build orientation and fractures occur along melt boundaries. For solution treated samples, ductility was not observed to be dependent on direction.

2.4 Characteristics of Metal laser sintering

2.4.1 Process parameters

Process parameters for PBF process are classified in 4 groups [9].

I. Based on laser characteristics

These include adjusting laser power, spot size, pulse duration and pulse frequency. Most of these parameters have direct influence on energy delivered to melt pool. For materials possessing higher melting point, high power laser is mandatory.

Though no proper definition of high-power laser exists about laser material processing, it usually ranges from few hundred watts to kilo watts of power [10]. Among high power commercially available lasers, including CO_2 laser, fiber laser and neodymium-doped yttrium aluminium garnet (Nd: YAG) laser. Neodymium can be replaced with ytterbium, erbium, thallium or holmium doping [11]. Fiber laser also use some rare earth elements as doping. Being very compact, this laser type is widely employed in material processing applications. Its wavelength is about 0.5 to 2 µm. CO_2 is molecular gas-based laser having wavelength of 10.6 µm and power ranges from tens of watts to kilowatts. Application areas are laser material processing including cutting, marking and welding of aluminium and steel [12].

II. Scanning

Scanning refers to laser traversing backward and forward for melting powder. Scanning speed, scan spacing, and scan pattern are critical parameters controlling energy input and melt pool properties.

Scanning strategies are often revealed when SLM process is outlined. For better fusion of laser scanning tracks, scanning strategies are employed. With single laser head, continuous tracks

build material by traversing linearly scanning in XY plane. Often layers are rotated 67° every time, with addition of each layer. One such example is 'island' scanning strategy. It is also intended to reduce residual stresses and distortions in component [7].

Laser scanning forms melt pools which overlap and thus a dense material is formed. This melt pool appears to be in semi cylindrical shape. Melt pool height as measured by Rosenthal [13], was 150 µm and width as 300 µm, at hatch spacing of about 200 µm, which produced a 33% overlap among adjacent traces and layers.

Figure 11: Melt pool formed in AlSi10Mg [13]

According to Xubin Su and Yongqiang Yang [14], as overlapping of solidified layers increases in adjacent position, fabrication defects affect surface quality. They suggested interlayer stagger scanning strategy using path manipulation for staggering of tracks to some distance. Track space should be such that powder in blank spaces is melted completely and dense solid is formed. Too much scan space will result in tracks that barely overlap. Selection of laser power, scanning speed and track space must be checked to get high density.

According to Guo et al., [15], higher LED i.e. ratio of laser power and scanning speed, increases melt pool width and depth. Higher laser power gives continuous tracks even at different scanning speeds. Lowering scanning speed also reduces balling phenomenon. They suggested that hatch distance (scan space) should always be shorter than width of track.

III. Depending on powder attributes
Powder size and distribution substantially matters in printing process. Fine powder produces better surface finish of finished part and as they offer more surface area, absorbs energy efficiently. Powder bed thickness is carefully selected based on particle size. Commonly used particle size varies from 20 to 75 µm.

IV. Temperature related
In PBF method, parts are built on a build-plate, which is kept at some specific temperature based on material being processed. This can also be adjusted to make cooling rate faster or slower and will affect printing process to great extent as heat generated by rapid melting and solidification must be dissipated.

2.4.2 Build orientation

In case of non-symmetrical part design, AM produces somewhat different mechanical properties in different printing inclinations. Fortunato et al., [16] researched effect of build orientation on hardness, surface roughness and cutting forces. It was found out that hardness of AM parts is not altered in two build orientations i.e. 0° and 90°. Surface roughness of as built AM part at built at 0° is better as compared to 90°. They also found out that cutting forces are increased in AM parts built at 90° build orientation.

2.4.3 Recoater direction

During DLMS process, it is usual practice to place parts at inclined angle relative to recoater for avoiding recoater damage, however doing so limits maximum printing dimensions available on build plate. Kranz et al., [17] found out that for angle of build varying between 45°- 90° and recoater angle of 0°-180°, maximum deviation in part accuracy is of 0.1 mm for any combination. Wall thickness of 0.4 mm is successful at any build orientation and recoater angle. A schematic of recoater angle is presented in Figure 12.

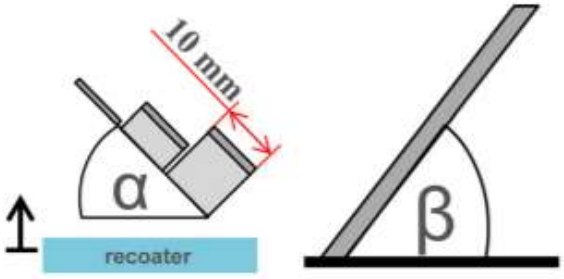

Figure 12: α: angle between recoater device and components; β: printing inclination to the building platform [17]

2.4.4 Supports

For simple and bulky geometric features, it is preferred to build the part directly on build plate. Supports often become inevitable for longer protruded sections and weak structures. Prime purpose is to provide stiffness and better heat conduction. Combination of lattice support and solid or pin support results in getting benefits of both support structures. Lattice supports reduce printing material and time while solid supports provide better stiffness and heat conductivity. Parts usually undergoes stress relieving before removal from build plate. At 45° printing inclination, supports are not required [25, page 131]. Therefor printing at angle higher than 45°, can be used for creating lattice structures, which are self-supporting.

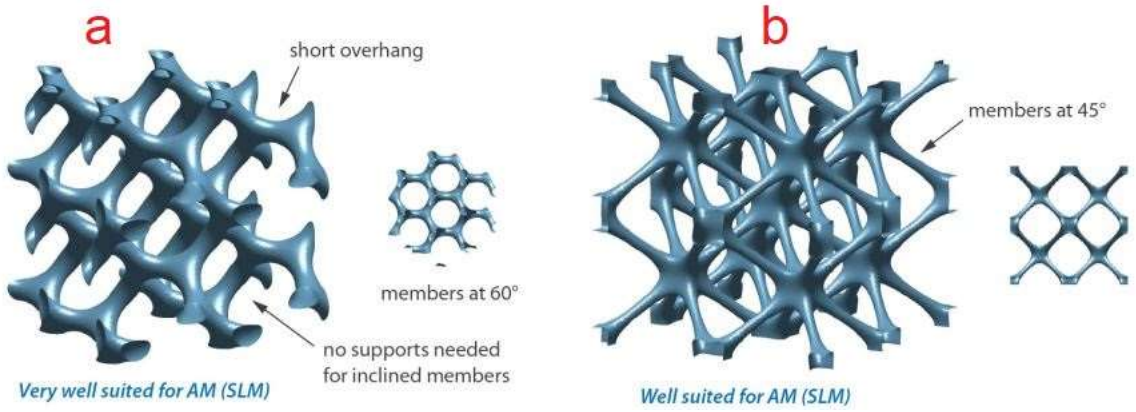

Figure 13: lattice structure well-chosen for SLM process (a) at 60° (b) at 45° [25]

2.4.5 Loading stl file in machine setup

Any CAD modelling software can be used to make 3D part model which is then saved in '.stl' (stereolithography) file format. A third-party software is used to process '. stl' file wherein orientation is done in 3D space and supports are generated. Slicing converts this part in number of layers that can be processed later by SLM machine.

2.4.6 Inert gas

A specific inert gas is used for some powder materials, e.g. nitrogen gas is used for making parts of stainless steel, cobalt-chrome alloys and nickel alloys, while argon is used for aluminium or titanium alloys [18].

2.4.7 Safety factors

Metal powder, high power laser and filter system used, are some factors involved in SLM process that can affect users in adverse way. As laser is contained in build chamber only, a lot of its harmful effects are mitigated. Risk of inhaling metal powder could be adverse, so respirators are used by operators to feed powder inside machine. Some metal powders become explosives when these encounters enough oxygen content in air or in presence of moisture. So proper safety protocols are followed [18].

2.5 Heat treatment of aluminium and maraging steel

Aluminium

As-built components are referred to as those printed components that are produced directly from printer, without any heat treatment. Solution treatment (ST), i.e. normal stress relieving cycle can be used as heat treatment process for aluminium. Li et. al [19] demonstrated that as-built components have highest tensile and yield strength whereas solution-treated components have resulted in lower values. As solution-treatment temperature is increased from 450°C to 550°C, these mechanical properties reach their lowest level. Ductility on other end is improved in ST samples. Artificial aging and solution treatment decrease solubility of Si atoms which in turn reduced brittleness and improve ductility. [4]

Maraging steel

Fortunato et al., [16] researched the effect of heat treatment of maraging steel on hardness, surface roughness and cutting forces. Samples were categorized as non-heat-treated (NT), partially heat-treated PT (solution annealed) and TT totally heat-treated (aged). Hardness of PT samples is lowest among all whereas NT samples are somewhat harder and TT samples showed most hardness. Cutting forces in TT samples are highest while in PT sample these are lowest and in NT samples are moderate. At lower cutting speed all samples PT, NT and TT showed same surface roughness after milling.

2.6 Surface roughness achieved for SLM components

Surface roughness can vary due to difference in powder adhesion or variation in powder gain size. In SLM, material is built up by overlapping of adjacent melted powder layers so whenever a slanted or protruded edge is required, these layers add up to get the required shape. In doing so surface quality gets affected. This effect is more prominent on downskin surface, i.e. surface facing in downward direction.

Surface roughness depends on printing inclination and layer thickness [25, Appendix E, page 2]. Surface roughness (Ra) is smaller (8-10 μm) at higher angles (≥ 50°) of inclination with build plate and higher (18-30 μm) at angle (≤ 40°) of inclination with build plate. Surface roughness of up-facing surfaces is better than down-facing surfaces [17].

2.7 Size limitation of hole size

In practice, holes are not printed but only inverse space from material is left out during printing and so holes are formed. For simplicity this will be referred as ‘hole printing’ in this research report. Holes of diameter ≤ 2 mm, failed in printing process, due to lack of powder adhering to surface. Vertical holes, i.e. hole axis perpendicular to build plate, showed better quality than parallel holes, i.e. hole axis is parallel to build plate. Vertical holes have no restraint on printable hole size. For perpendicular holes,

accuracy is dependent on hole size. For bigger diameter (≥ 12 mm), vertical or inclined holes require support structure. So, printable hole size depends mostly on printing inclination. [17].

2.8 AM part defects

Due to rapid solidification and melting of powder large number of defects can form in SLM components. Some of these exist because of selection of inappropriate manufacturing parameters like laser power, scanning speed, hatch distance and nature of supports. Some common defects found in metal components built by SLM are outlined here.

2.8.1 Support rupturing

Since powder is troublesome for providing support because of its low stiffness [25, appendix C, page 3], other supports are usually required for overhanging features in components. Lattice supports, and solid supports are two broad categories. Primary requirement of support is to provide higher conduction rate and stiffness to bear load of protruded components [25, appendix C, page 3]. In lattice supports, a thin solid frame of material is developed. By doing so, they reduce material used in making of supports compared to solid supports. Solid supports will consume more material and time in its construction, but on other end yield more accuracy in printing process.

These supports are optimized for certain materials and printing parameters are optimized so that no defects appear due to supports. Different design and manufacturing parameters can determine such supports. In case of higher thermal stresses, supports will split and affect parts accuracy.

2.8.2 Porosity

Porosity can be very common in SLM components notably near the surface and therefore must be removed. During printing process, melted layers are fused together to form solid material and to avoid any gaps. Some porosity however exists in components after printing process that could be due to humidity in powder or extreme laser power. Uniformly dispersed pores may not be able to effect on part integrity. Surface porosity observed in SLM components in shown in Figure 14 as an example. Such pores can be avoided by carefully optimizing printing parameters.

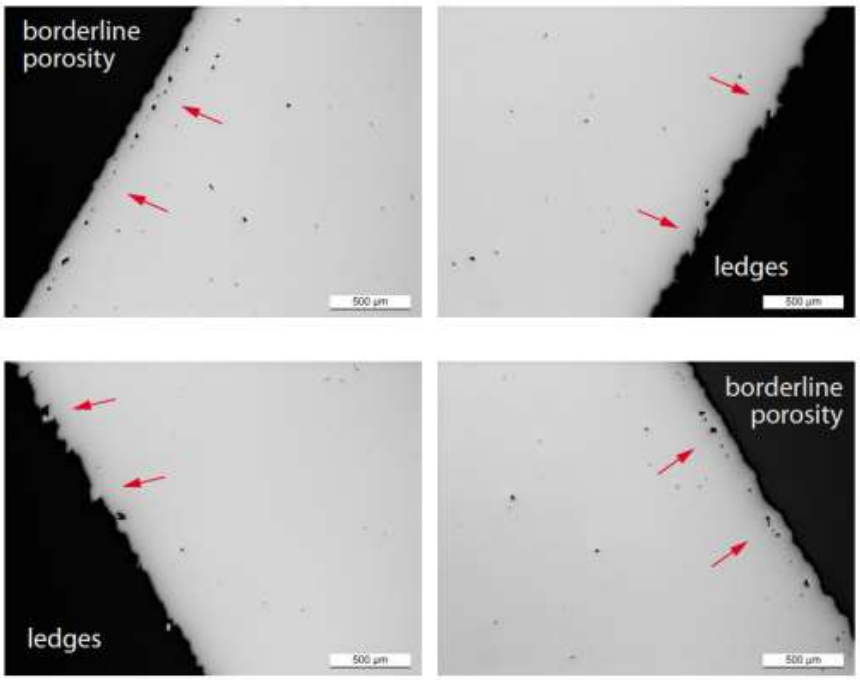

Figure 14: Borderline porosity in SLM component, at 5X magnification [25]

2.8.3 Dross formation

Term ‘dross’ is used for partially melted powder particles attached to solid material during SLM process. Primarily dross exists on underskin surfaces i.e. facing downward to printing direction. Dross formation affects surface quality and needs machining process for its removal. Holes printed at inclination angle less than 45° contain dross.

Figure 15: Dross formed in downskin surface of SLM component [25]

2.8.4 Balling phenomenon

Balling phenomenon is mainly attributed due to low energy transferred to melt pool. Low laser power or fast scanning speed result in balling phenomenon which is melt splashing [21]. Due to this splashing unmelted powder particles exist in melt and affect material uniformity. Pore formation in SLM is also attributed to balling phenomenon [22].

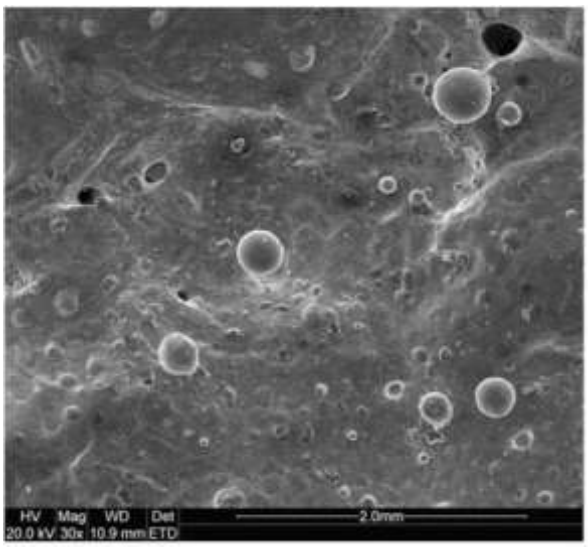

Figure 16: SEM image of balling in 316L Stainless steel, SLM component [21]

2.8.5 Warping

Sometimes, due to thermal stresses built up during printing process, warping occurs, and flat faces show curved profile. This kind of effects appear when components are not stress relieved. One such example is displayed in Figure 17.

Figure 17: warping in Inconel, VTT [25]

2.8.6 Burs

Burs can exist on very sharp corners. These can be avoided by creating fillets [25].

2.8.7 Colour changes

Distorted colors appear due to high thermal activity during printing process in presence of oxygen. Burn marks can form due to high laser power.

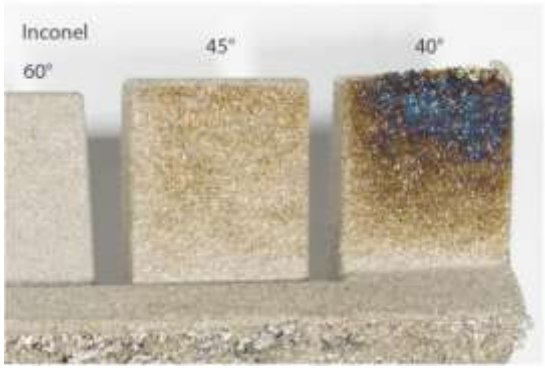

Figure 18: Colour distortion in SLM components [25]

2.9 Machining of AM components

SM (Subtractive manufacturing) often becomes inevitable owing to insufficient accuracy, surface roughness and defects prone to AM, e.g. porosity and requirement for removal of support structure. In some cases, subtractive machining is integrated with AM process to get finished product in single step [7]. This trend is becoming more popular as it unites benefits of both subtractive and additive manufacturing. Parts are designed in such a way that their subsequent machining operations can be performed with the least human assistance.

Wire EDM is sometimes employed, at earlier stages of post-processing of AM, to remove components from build plate. Supports are either sawn away or broken manually. This is rapid way of getting rid of support structures. Fine powder particles sticking to support structures often causes difficulty in milling, as it reduced friction between tool and workpiece.

It is observed that cutting forces are higher for SLM samples than for wrought components of maraging steel. This difference expands with higher feed rates. [7] [28]

3D CAD model is decomposed to multifaceted triangles using slicing software used in AM. These triangular faces are then printed by SLM process into required component shape. So, machining strategy must be adopted to produce better surface finish. Gibson et al., [9] suggested that selection of adaptive stepover distances would give better surface roughness after machining of AM components. They also proposed finding sharp edges in stl file and defining tool paths accordingly [9]. However, in practice, during machining of AM parts, these detailed modifications are not needed and can be neglected.

Chips formation

M. shunmugavel et al. [32] observed that as-built and heat-treated components have no substantial effect on chips formed during machining of Ti–6Al–4V. Gael Le Coz et al. [33] confirmed that chips morphology is similar during micro cutting for SLM produced and hot rolled titanium allow.

2.9.1 Cutting forces

Fortunato et al. [16] observed that higher cutting speeds and forces are not reduced due to thermal stresses for maraging steel produced by SLM process, contrary to general trend experienced in machining of most metals. More tool wear causes higher cutting forces during machining. They also observed that 90° printing inclination has higher cutting forces than 0° printing inclination; inferring to anisotropy in material.

Gael Le Coz et al. also observed higher cutting forces in SLM produced Ti-6Al-4V alloy compared to same hot rolled and annealed sample [33].

2.10 Limitation of AM processes

In addition to its emerging benefits, AM has some process restrictions. Supports are required for printing process and needs to be removed manually afterwards. Limited commercial engineering materials, restricted printer size and thermally induced defects are AM's present day's shortcomings. Geometrical tolerances resulting from AM process are not properly outlined and authentic knowledge is needed to determine machining allowances.

2.11 Summary

Discussion based on previous knowledge can be summarized in form of the following fish bone diagram with section numbers, referring to chapter 2 headings. It represents various factors that affect part accuracy and must be carefully selected. Manufacturing parameters listed in Figure 19 are the most commonly relevant ones. Machining processes typically used for hole and thread making are drilling, reaming and taping. VTT has proposed machining allowances for some components as mentioned here [25, page 131]. This research will investigate defects occurring in printed metal parts and recommend machining allowances accordingly.

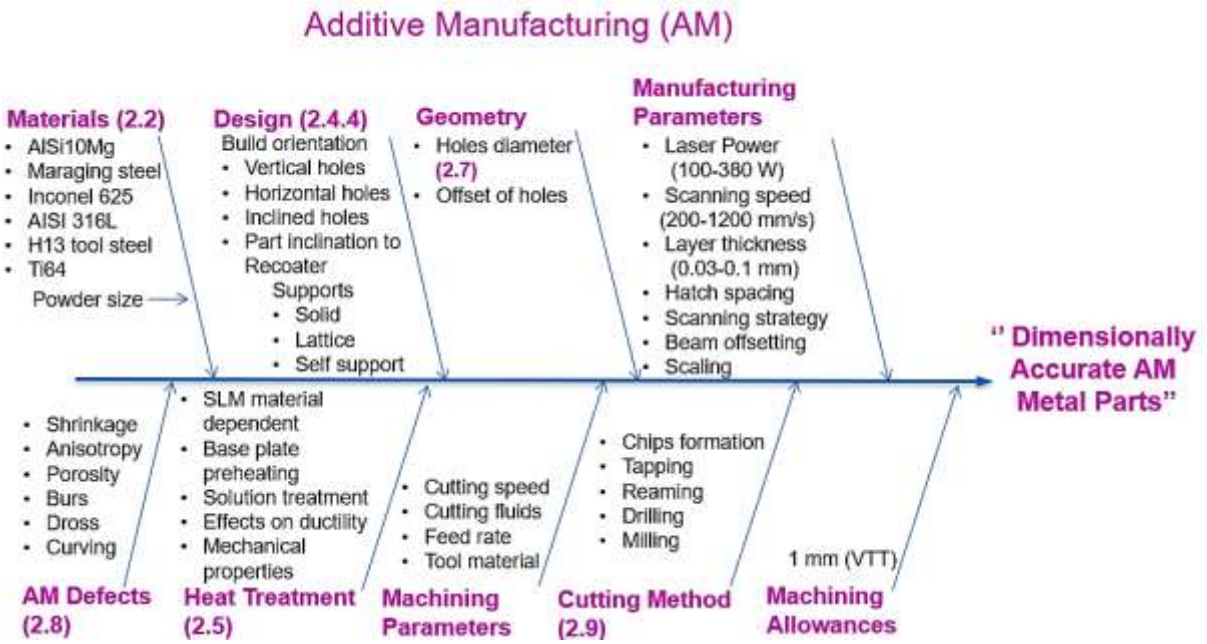

Figure 19: Summary of SLM process parameters for accurate part features

3 Methodology

In this study, machining processes are performed on AM metal parts. Objective of this study is to define guidelines for geometrically accurate features and machining allowances that should be added in part design. For this purpose, two materials i.e. aluminium and maraging steel are provided by EOS Finland [24]. Flat plates are built in 5 printing inclinations shown in Figures 20 and 21 and in two orientations to recoater Figure 22, for spreading powder on the bed for SLM process. It must be noted that in Figure 22, each recoater angle is used to print one set of plates/components. So, there will be 10 plates for one material i.e. 5 printing inclinations and 2 recoater orientations. In Figure 21, supports are added to print test part at various inclinations. Later, these supports will be milled away, resulting in flat plates. Recoater travels linearly and spreads powder before laser melting.

Figure 20: Flat plates printed in 5 orientations

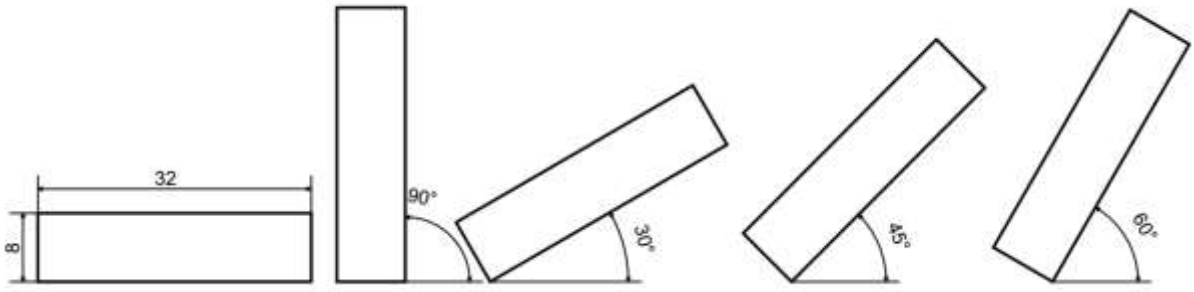

Figure 21: Schematic of flat plates

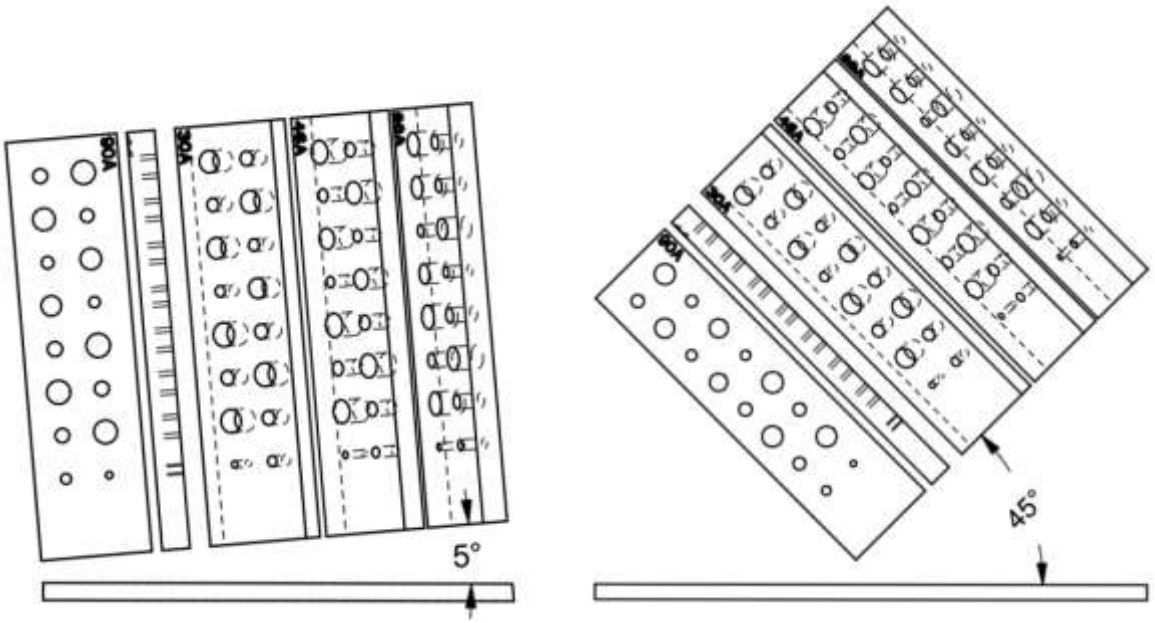

Figure 22: Recoater orientation to work pieces

3.1 Test part geometry

Test part is an additive manufactured flat plate, having printed pre-holes of various diameters. As literature suggests that marginal porosity exits near surfaces [25], some increment in diameter is given as machining allowance in test part. Figures 23 and 24 show drawings of pre-hole diameters and their positions on flat plate. Drilling and tapping (thread making) are machining processes performed on test part.

For making M5 thread, 4.2 mm drill diameter is required. So, to get 4.2 mm hole from AM process, pre-holes of various pre-hole diameters are printed. These pre-holes include 4.3 mm, 4.2 mm and 4.1mm, having increment of 0.1mm from nominal diameter and 3.8 mm, 3.5 mm, 3.2 mm having increment of 0.4 mm, 0.8 mm and 1 mm from nominal diameter respectively. An additional pre-hole of 2 mm, that is far less than required drill diameter is printed as well. These increments in pre-hole diameter are the allowances added in test part design to get accurate and stronger threads. Some space is left intentionally next to smallest pre-hole, in plates for directly drilling and tapping in solid material. This will provide more accurate results for drilling force measurement, as there will not be any off-centering possible due to drill wandering.

Similarly, for producing M8 thread, different pre-hole diameters are printed in the same test part. Nominal diameter required for M8 thread is 6.8 mm. Pre-hole sizes are as following: 6.9 mm, 6.8 mm, 6.7 mm (with 0.1 mm increment) and 6.4 mm, 6.1 mm and 5.8 mm with increment of 0.4mm, 0.8 mm and 1 mm, respectively, from nominal pre-hole required for tapping. Again, a 3 mm pre-hole is printed in same test part to make a comparison with drilling and tapping in zero-pre-hole case. For drilling a hole in solid material, some space is allocated for direct drilling and tapping of M8.

Summing it up, based on machining allowances already known from VTT report on ‘’Design guide for additive manufacturing of metal components by SLM process’’ [25] and during discussion with EOS Finland personnel, different machining allowances are incorporated in test part design to determine which pre-hole diameter gives sufficiently strong and accurate thread.

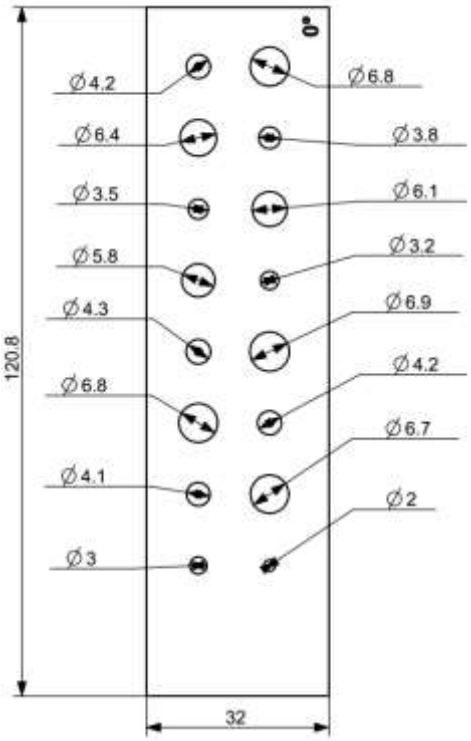

Figure 23: Test part Hole Diameters

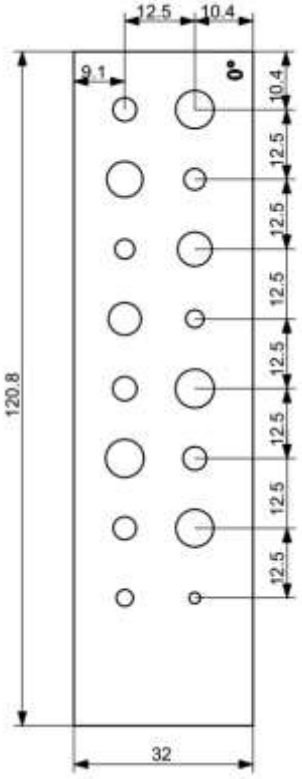

Figure 24: Inter-hole distances

3.2 Test Parameters

Among many geometric features only hole and thread making will be in focus in this experimental plan. This study will check the following parameters:

1. Two-hole size diameters required for making M5, M8 threads
2. Machining allowances varied with incremental values for these two-hole sizes
3. Work pieces printed at five printing orientations i.e. 0°, 30°,45°, 60° and 90° to horizontal plane
4. Recoater angle to work pieces i.e. 5° and 45°
5. Two engineering materials, AlSi10Mg and Maraging steel
6. Heat treatment: as-printed, solution treated (ST)

Since there was no restriction on printing all these work pieces, all possible combinations (1-5) are tested in this study.

Heat treatment plan: As-built AM parts are carrying thermal stresses and therefore require annealing to release these stresses. The annealed components are machined, and comparison is made.

Characteristics of AM components are determined by calculating:

1. Surface roughness of flat surfaces
2. Flatness of printed surfaces
3. Macro hardness of material
4. Porosity analysis via image analysis technique
5. Cutting forces i.e. axial forces during drilling
6. Hole size calculation
7. Mechanical strength of internal threads using ISO-892-2 test [26]

3.3 Heat treatment of aluminium and maraging steel

Aluminium test parts are used in two as-built conditions, i.e. no heat treatment process is utilized. First one is as-built 35 °C, where build plate temperature is maintained at 35 °C and this is referred to as cold-processed. In this state recoater angle to parts is 5°. Other one is as-built 200 °C, where recoater angle used are 5° and 45°. Build plate temperate is 200 °C and this one is referred to as hot-processed.

For maraging steel, as-built parts are used; printed at 5° to recoater. Solution treatment is done for parts printed at 5° and 45° to recoater.

3.4 Machine tool

Matsura MX-520 five-axis vertical machining center (Figure 25) is used for drilling and tapping process. It has a highly accurate spindle and can serve as a reliable resource for this research. GibbsCAM software prepares executable file for MX-520, including coordinates and machining parameters for drilling and tapping.

Figure 25: Matsura, 5-axis Vertical machining center

3-axis vertical milling shown in Figure 26 was used for side and end milling for removing supports from AM flat work piece.

Figure 26: Milling machine

Figure 27: Centering microscope

3.5 Centering microscope

Since AM parts can have variations during printing process affecting geometric features so drilling and tapping requires determination of center point of pre-holes. For this purpose, a centering microscope, Figure 27 is employed. These coordinates are then used as center points for drilling and tapping in Matsura.

3.6 Cutting tools

Walter TITEX [27] drills and taps are used for drilling holes and thread tapping. Since this is not a machining parameter study, manufacture's recommended values for feed and cutting speeds, as listed in Tables 1 and 2 are used for drilling and tapping.

Table 1: Drill and machining parameters

Material to be drilled	Drill Product code	Drill diameter	feed (mm/rev)	Cutting speed (m/min)	Point Angle	Number of flutes
Maraging steel	A3293TTP-4.2	4.2	0.078	60	140	2
	A3293TTP-6.8	6.8	0.11	60	140	2
AlSi10Mg	A3299XPL-4.2	4.2	0.11	200	140	2
	A7191TFT-6.8	6.8	0.08	60	140	2

4.2 mm and 6.8 mm drills used for drilling operation, are shown in Figures 28 and 29.

Figure 28: A3293TTP-4.2 & 6.8 mm, 2 flutes, Solid carbide drills with coolant-through [27]

Figure 29: A3299XPL-4.2 & 6.8 mm, 2 flutes, Solid carbide drills with coolant-through [27]

Table 2: Tapping tool and machining parameters

Material to be tapped	Tap Product code	Tapp material	Tapp coating	Pitch	Cutting speed (m/min)
AlSi10Mg	E2031466-M5	HSS	TiN	0.8	(20-27)
	E2031466-M8	HSS	TiN	1.25	(20-27)
Maraging steel MS1	S2021305-M5	HSS	TiN	0.8	(10-15)
	S2021305-M8	HSS	TiN	1.25	(10-15)

M5 and M8 taps used for tapping operation, are shown in Figures 30 and 31.

Figure 30: E2031466-M5 & M8, 4 flutes, High speed steel tap [27]

Figure 31: S2021305-M5 and M8, 3 flutes, High speed steel tap [27]

3.7 Cutting force calculations

During drilling process, axial thrust force and torque are applied, remove the material for making hole. In this study, axial thrust force and torque for drilling process will be determined.

To calculate axial force and torque, various power law models applicable for specific materials have been defined. Equations (1-4) are outlined by Sandvik Coromant [23], to evaluate drilling force, power consumption and torque during drilling for selected materials.

Power consumed during drilling is given as:

$$P_c = \frac{(f_n * V_c * DC * k_c)}{240} \qquad \text{Eq.1}$$

$$k_c = k_{c1} * (f_z * sin\ KAPR)^{-mc} * (1 - \frac{\lambda_o}{100}) \qquad \text{Eq. 2}$$

Torque due to drilling action:

$$M_c = \frac{P_c * 30 * 10^3}{\pi * n} \qquad \text{Eq. 3}$$

Feed force is approximated as:

$$F_f \approx 0.5 * k_C * \frac{DC}{2} * f_n * sin\ KAPR \qquad \text{Eq. 4}$$

Where

$f_n =$ $feed\ (mm/rev)$

$f_z =$ $feed\ per\ edge\ (mm)$

$V_c = cutting\ speed\ (m/min)$

$DC =$ $drill\ diameter\ (mm)$

$k_c =$ $specific\ cutting\ force\ (N/mm\text{^}2)$

mc=material constant

$\lambda_o = entering\ angle$

$n =$ spindle speed (rpm)

$KAPR = {}^{point\ angle}/_{2}$

Walter TITEX's cutting speed and feed, as mentioned in Tables 1 and 2 are used to calculate axial drilling force and torque for drilling. Approximate values of *mc and* k_c (specific cutting force) are used [24]. This is done for comparison purpose.

Table 3: Theoretical calculation of Force and Torque for drilling

Workpiece material	Drill	Dc (mm)	Feed, Fn (mm/rev)	Fz (mm/edges .rev)	Vc (m/min)	Point angle	N, rpm	mc	kc, N/mm^2	Feed Force Ff, (N)	Torque Mc (Nm)	Power Pc (W)
Maraging steel	A3293TTP-4.2	4.2	0.078	0.039	60	140	4550	0.25	4800	369	0.83	393
	A3293TTP-6.8	6.8	0.11	0.055	60	140	2810	0.25	4404	774	2.80	824
AlSi10Mg	A3299XPL-4.2	4.2	0.11	0.055	200	140	15165	0.25	1028	112	0.25	396
	A7191TFT-6.8	6.8	0.08	0.040	60	140	2810	0.25	1113	142	0.51	151
Al 6082	A3299XPL-4.2	4.2	0.11	0.055	200	140	15165	0.25	661	72	0.16	254
Al 6082	A7191TFT-6.8	6.8	0.08	0.040	60	140	2810	0.25	725	93	0.34	99

Drilling and tapping was done for Al 6082 (a cold rolled aluminium), to compare results with SLM parts. Exact values of mc and kc are not known for SLM processed parts, so it is expected that these drilling force values might not represent true drilling forces and torques.

3.8 Cutting force measurement

Kistler 9271 A sensor (Figure 32), is used to measure axial thrust force during drilling. This sensor can measure 0-20,000 N force and 100 Nm torque with a sensitivity of 2.01 pC/N and 1.56 pC/Ncm respectively. Operating range for this sensor is 0-70° C.

Piezoelectric sensor is used in Kistler 9271A, which converts mechanical load to proportional voltage. A charge amplifier then amplifies this voltage and a data acquisition device is used to convert amplified voltage to a digital signal. DaqView software is used to record this numerical data into ASCII file. Schematic of force measurement equipment is shown in Figure 34.

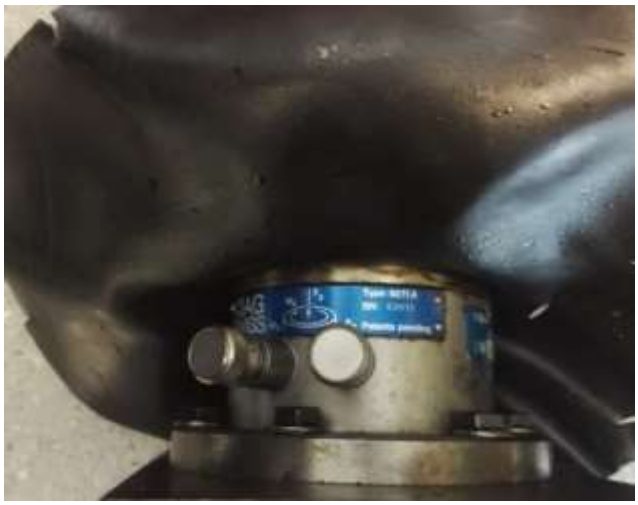

Figure 32, Kistler sensor

Figure 33, Vice mounted on top of Kistler sensor

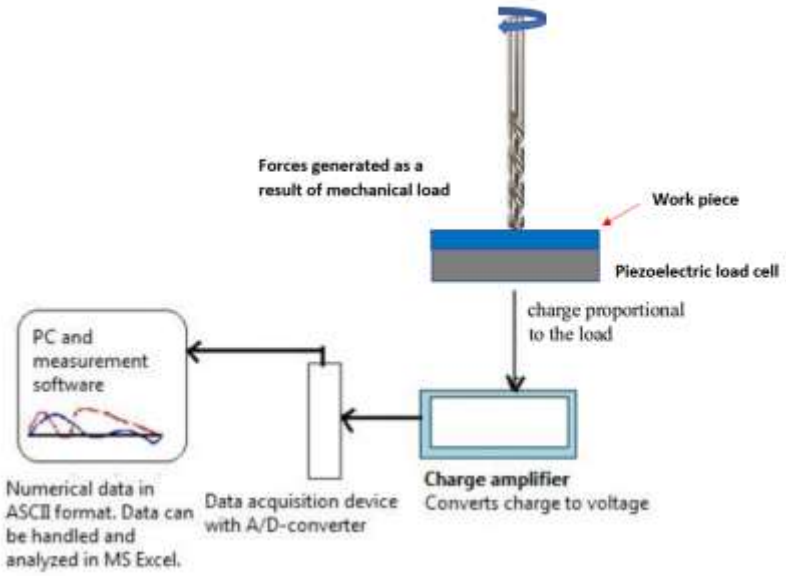

Figure 34: Schematic of data acquisition in Cutting force measurement

Calibration

Calibrating sensor is vital in force and torque measurement. In calibration process, dependence of known input variables i.e. weight and moment on measured output (voltage) is determined. Assuming linearity between input and output, a calibration line is defined. During actual force and moment measurement, voltage values are obtained from sensor, which are converted to real force and moment values using these calibration line. During calibration, scaling factor can be changed if forces and torques are exceeding the limit set by previous scaling factor so that output voltage remains in ±10 V range.

Two loads (5kg*9.8 ms^{-2}) 49N and (10 kg*9.8 ms^{-2}) 98N are applied on the sensor in vertically down direction and voltages for axial force are recorded. Similarly, for calibrating torque, two torques of (5 kg*9.8 ms^{-2}*0.5 m) 24.5 Nm and (10 kg*9.8 ms^{-2}*0.5 m) 49 Nm are applied using a spring scale and 0.5 m long lever.

Resulting calibration curves along with calibration lines are shown in Figure 35.

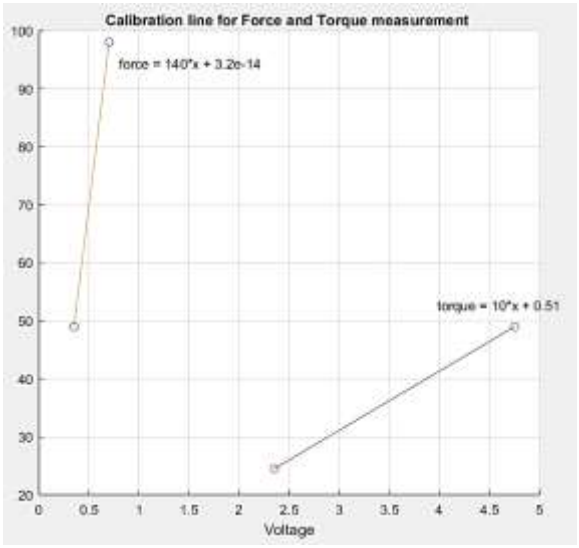

Figure 35: Calibration lines for force measurement

3.9 Cutting forces in AL6082

Before measuring drilling forces for DLMS parts, drilling and tapping forces were measured in Al 6082 grade, for comparison purpose. Resulting M5 and M8 threads are shown in Figure 36.

Figure 36: Reference M5 and M8 made in Al 6082

Results of axials drilling force and torque are displayed in Figure 37. Drilling forces, for M5 and M8 were measured as 275 N and 375 N respectively whereas torque was found out to be 0.5 Nm and 1 Nm respectively. Torque values obtained, are so small in magnitude compared to axial forces, that these are not included in this research study because during experimentation, noise and vibrations can influence the voltage signal easily.

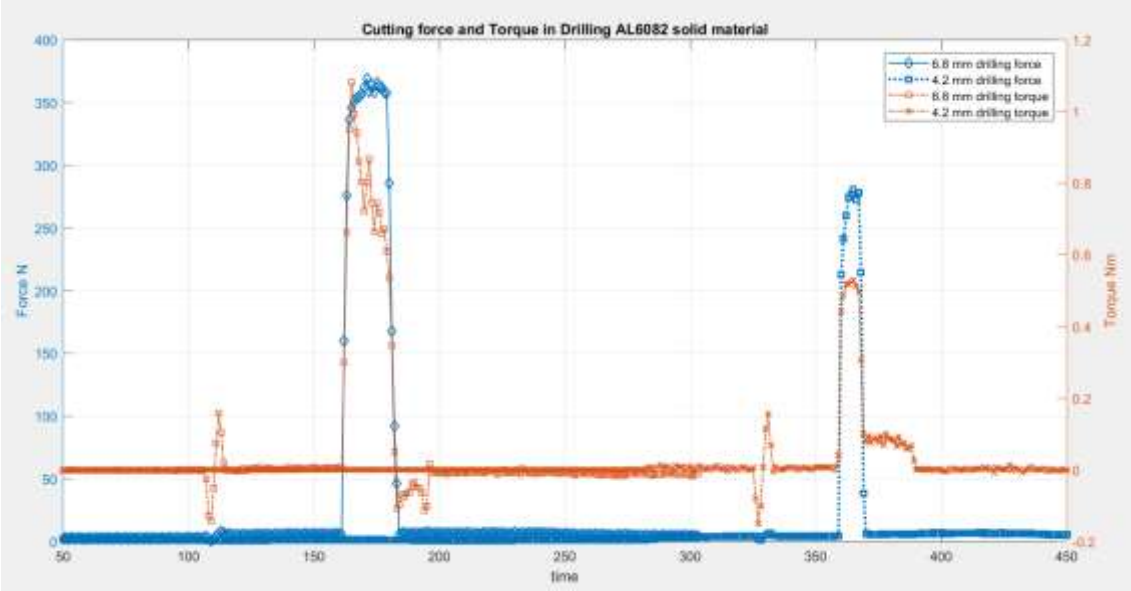

Figure 37: Drilling force and torque in Aluminium 6082 for two drills

Experimental drilling force values (Figure 37) are approximately 4 times higher for Al 6082 compared to numerically determined values shown in Table 3. So, there is discrepancy in determining drilling forces by numerical method. Since a calibration system was used for determining of experimental drilling force values, these (Figure 37) are more reliable compared to numerically determined values.

3.10 Macrographs preparation

AlSi10Mg

As discussed in literature, some surface porosity exists in DLMS process [25, page 131]. A section of AlSi10Mg (shown in Figure 50), was cut from printed parts and examined under optical microscope. Keller's reagent was used to observe general surface of material and to look for any surface porosity. Composition of this reagent is given in Table 4.

Table 4: Etchant (Keller's Reagent) composition used for AlSi0Mg

H_20	HCl	HF	HNO_3
95 ml	1.5 ml	1 ml	2.5 ml

Although there was an effort made to measure porosity quantitatively, it was still hard to describe it explicitly by a numerical number. So then only qualitative approach was used to visualise printed surface.

Maraging steel

Picric acid works better for maraging steel for etching [31, page 212], but most of laboratories are discouraged to use picric acid due to its explosive nature. So, an alternative option was employed for selection of etchant. Chemical composition of this etchant used for viewing macrostructure of maraging steel is shown in Table 5. Etching time used was 2 minutes.

Table 5: Etchant used for maraging steel

water	ethyl alcohol	methyl alcohol	HCl	CuCl2	FeCl3	HNO3
50 ml	50 ml	50 ml	50 ml	1 g	2.5 g	2.5 ml

4 Results and Discussion

4.1 Aluminium AlSi10Mg

Among additive manufacturing of metals, aluminium is the difficult one. High thermal conductivity, light weight and reflective nature are probable causes in casting and sintering process. Aluminium products, owing to their light weight are commonly used in automotive and aerospace industries. In this study AlSi10Mg test parts printed by EOS M290 were used. Material composition as given by manufacturer EOS is tabulated in Table 6.

Table 6: AlSi10Mg material composition [24]

Element	Al	Si	Fe	Cu	Mn	Mg	Ni	Zn	Pb	Sn	Ti
Weight	balance	9-11	≤ .55	≤ .05	≤ .45	.2-0.45	.05	≤ .1	≤ .05	≤ .05	≤ .15

Figure 38 shows as-built AlSi10Mg material printed using printing parameters termed as 'Surface 1.0', i.e. built for higher surface properties. Due to inappropriate supports and build plate temperature, rupturing occurred at the interface of flat plate and supports. These printed components, termed as 'as-built' in subsequent study, are not annealed and therefore carrying thermal stresses built up during laser sintering process.

During 3D printing, build-plate was at 35 °C, and parts are printed at 5° to recoater and will be referred as AB-35 in next discussion.

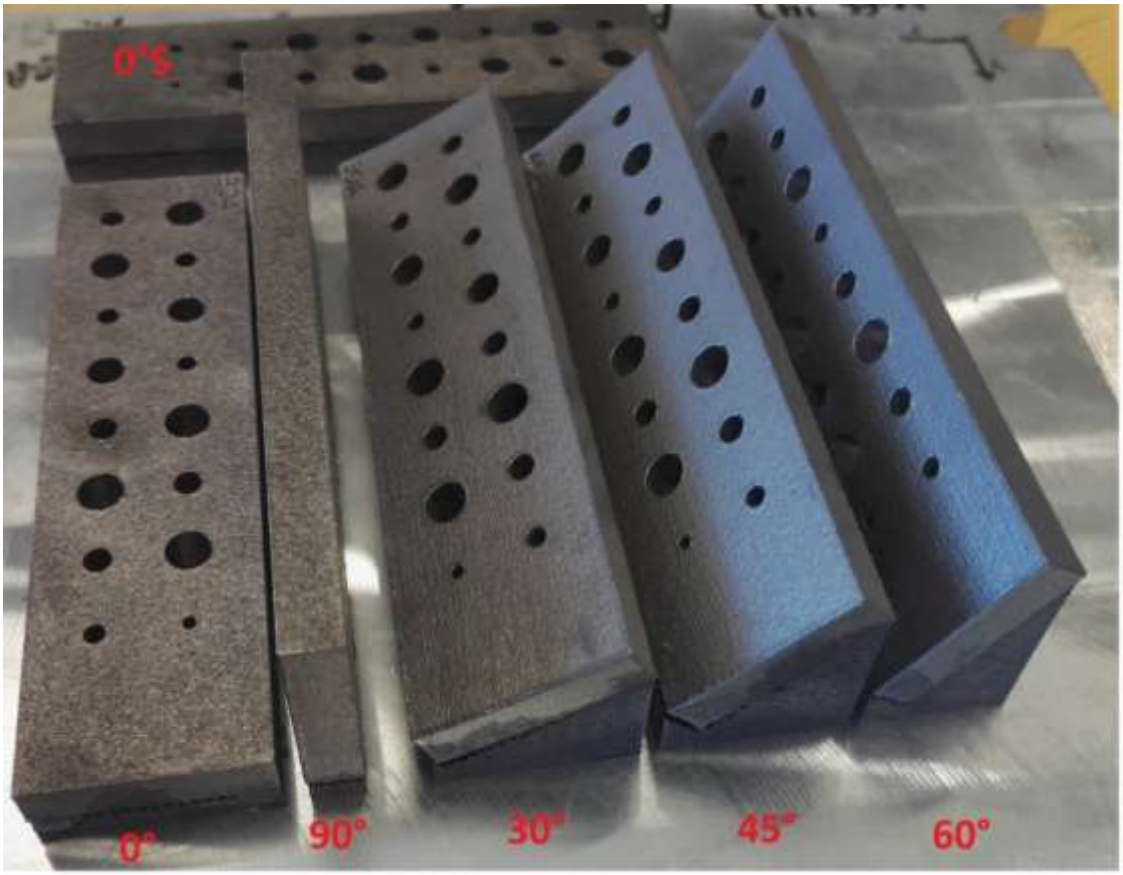

Figure 38: AlSi10Mg, As-built-35, 5° recoater angle, in various printing inclinations

Here inclination angle means angle between the main flat surface of part and horizontal plane.

AlSi10Mg (As-built) was printed in two different orientations relative to recoater, i.e. 5° and 45° with build plate at 200 °C, shown in Figures 39 & 40 respectively. These will be termed as AB-200 in further discussion.

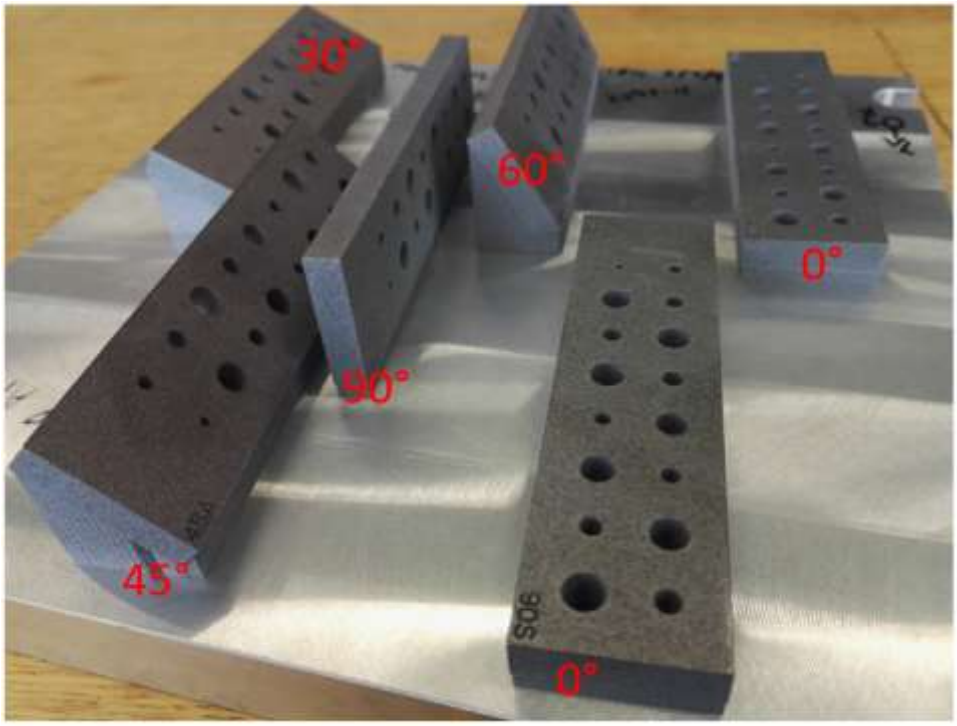

Figure 39: AlSi10Mg, AB-200, 5° recoater angle

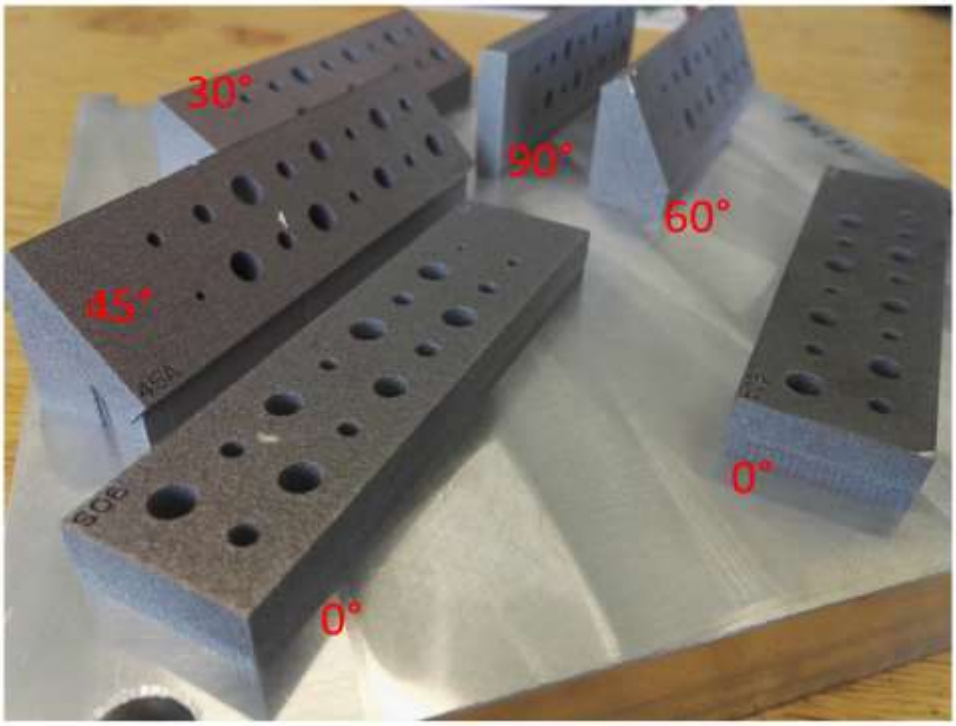

Figure 40: AlSi10Mg, AB-200, 45° recoater angle

Heat treatment
Typically, T6 solution treatment is used for heat treatment of cast aluminium alloys. For DMLS, when there is fast melting and solidification, T6 cycle is not used, instead components are placed in a stress relieving cycle with 2 hours at 300° C. Doing so will releases most thermally induced stresses and reduce anisotropy [24].

Aluminum components used in this research are as-built, i.e. no solution treatment was performed.

4.1.1 Flatness measurement

Three different measurement methods were employed to gauge flatness of printed parts.

Coordinate measuring machine (CMM)
Using CMM, flatness of top surface of each work-piece is measured. Accuracy of CMM used is around 20 µm. Figure 41 shows flatness measured in micro meter before and after base plate was removed from printed parts with wire EDM process. During these measurements, 60 points were selected randomly, and each surface was measured three times to get reliable data.

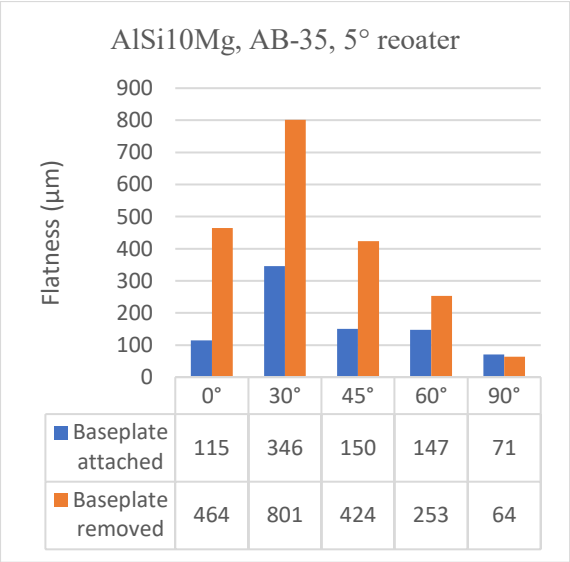

	0°	30°	45°	60°	90°
Baseplate attached	115	346	150	147	71
Baseplate removed	464	801	424	253	64

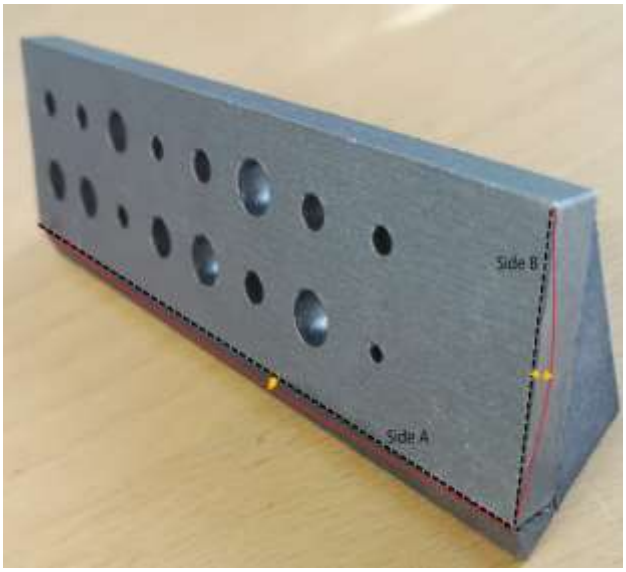

Figure 41: Flatness measurement with CMM

Figure 42: schematic of flatness measured using feeler gauges

Discussion

Higher flatness implies more uneven surface. As expected, test parts are more warped after being removed from build plate. Accuracy of flatness measured values are also verified by manual measurement using feeler gauges, as shown in Table 7 and by using gom-Atos optical scanning, shown in Figures 43 and 44.

Feeler gauges
Table 7 shows result of maximum distance measured by feeler gauges, between flat surface and curve formed along sides A and B. A schematic is shown in Figure 42. This data cannot be more accurate as top edges were having raised edges due to contour printing along corners in test parts and because flatness could vary from place to place.

Table 7: Flatness measured with feeler gauges. **educated guess* *--values missing*

Printing Inclination	Before support removal (µm)		After support removal (µm)	
	side B	side A	side B	side A
0°	40	--	<40*	400
30°	470	60	510	310
45	330	90	370	320
60°	125	50	140	100
90°	20	--	<40*	30

Discussion

One can see that, for build plate not removed, flatness of side B was higher than side A. After parts removal, side B did not show significant change, but side A has warped significantly. So, curving has occurred along both faces.

3D Metrology

gom Atos scanner was used to observe variations in printed parts compared to CAD geometry as shown in Figure 44. Scanner has an accuracy of 80 µm. Retrospective points were used during scanning process. Although data cloud collected was not enough, but still it provided some idea of where exactly variation have occurred.

Figure 43: Data points obtained from GOM Atos scanner

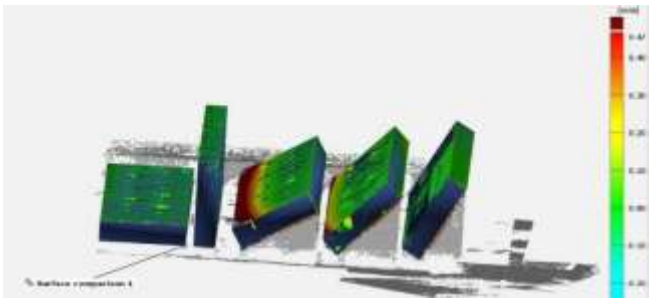

Figure 44: comparison of scanned data and CAD geometry

Discussion

Data obtained from this scanning process has proved the fact that the same method can be employed for scanning of curved surfaces or distorted printed parts. Result obtained in Figure 44, clearly shows that variation is higher than 0.47 mm which is in accordance with results of CMM and feeler gauges.

Flatness comparison of Solution treated AlSi10Mg

As the accuracy of CMM was validated by comparing its results with manual and optical method, it was used to measure and compare flatness of printed parts at 5° and 45° to recoater for AB-200 prints, shown in Figures 45.

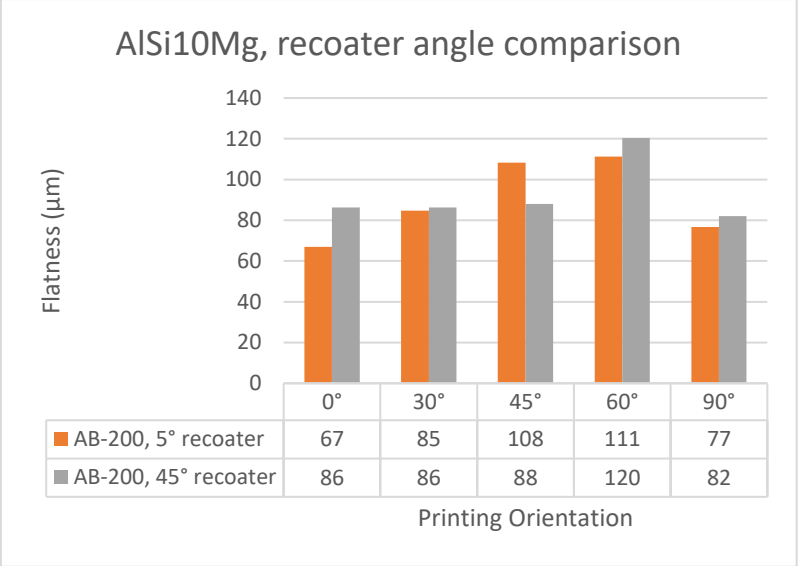

Figure 45: Flatness achieved with different value of recoater angle and printing orientation

Discussion

It was observed from that flatness varied between 67µm to 120 µm; which is not that significant. Differences in flatness value of ST components printed at 5° and 45° is minute. So, it can be inferred that having parts placed differently on build plate i.e. different recoater angle, flatness will not change.

4.1.2 Surface roughness

For AB-35 parts, surface 1.0 parameters were used [24] for producing better surface properties. For AB-200 parts, speed 1.0 parameters were employed; which can be printed faster. Top and bottom surface of AM prints are shown in Figure 48. Laser scan lines can be seen at upper side and holes do not have sharp edges at lower side compared to top surface.

Surface roughness is measured with Taylor-Hobson equipment Figure 49, according to EN ISO 4288 standard. Surface roughness, Ra, of flat faces, measured for various printing inclinations are presented in Figure 46.

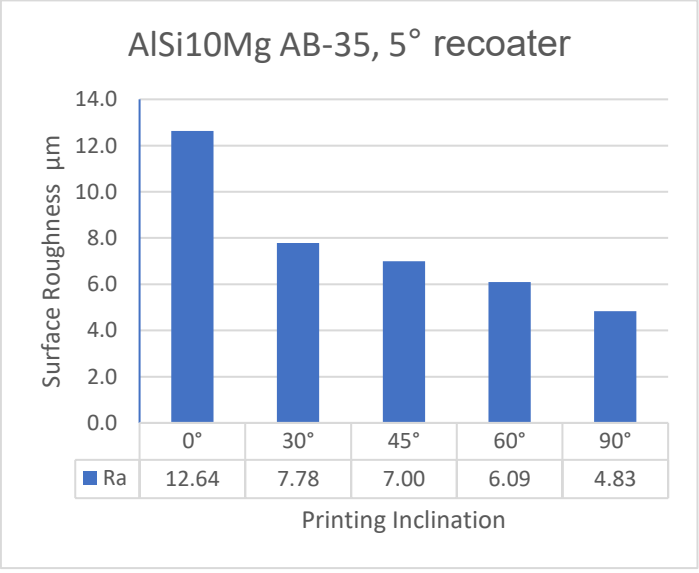

Figure 46: Surface roughness of ALSi10Mg, AB-35

Discussion

Horizontal component (0°) is rougher compared to the component built at 90°. Surface properties are improved when inclination angle is increased from 30° to 60° as can be seen from Figure 46.

This is due to stair case effect produced between adjacent layers.

Roughness comparison of AB-200 for different recoater angles

For AB-200 parts, printed at 5° and 45° to recoater, surface roughness values are presented for different printing inclinations in Figure 47

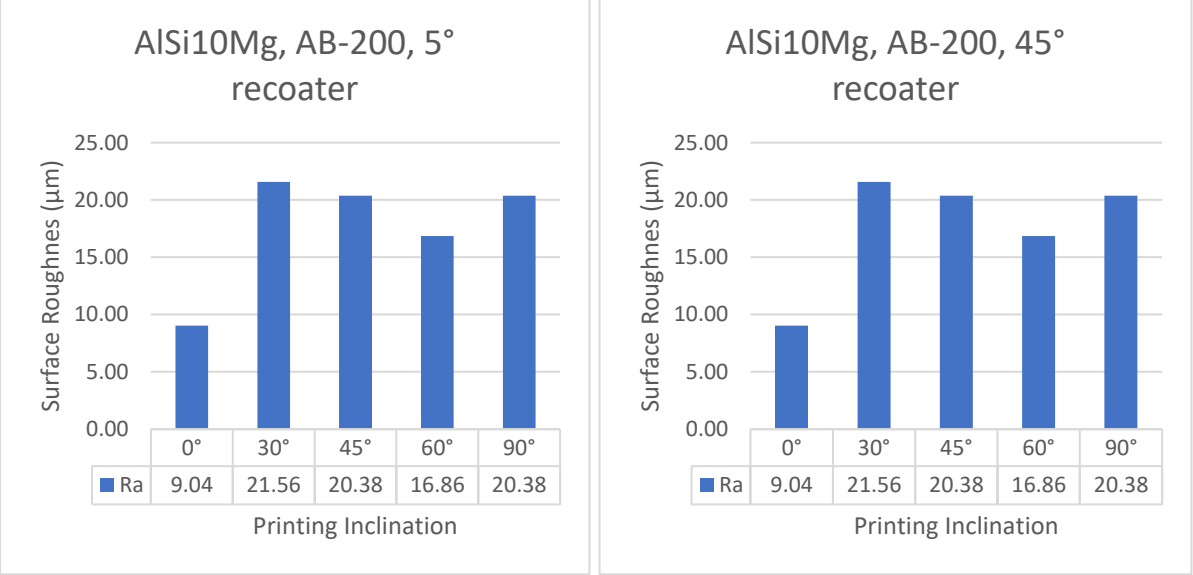

Figure 47: Surface roughness comparison of AlSi10Mg, AB-200, 5° recoater angle (left), 45° recoater angle (right), speed 1.0

Discussion

For both 5° and 45° components, similar kind of trend is observed. At 0° printing inclination, surface roughness is least; which is good. For other printing inclinations, flatness has increased 2 times or more. Surface roughness is increased significantly for AB-200 parts compared to AB-35 because of different printing parameters employed by manufacturer.

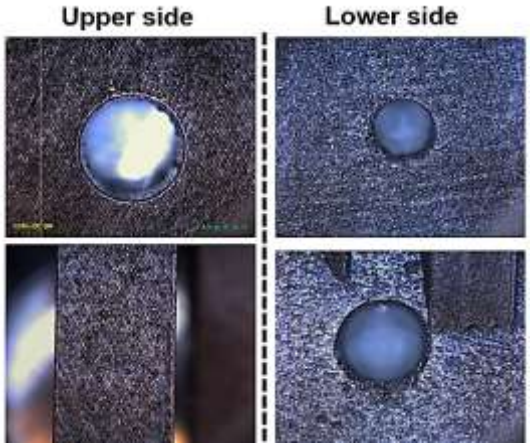

Figure 48: as built surface

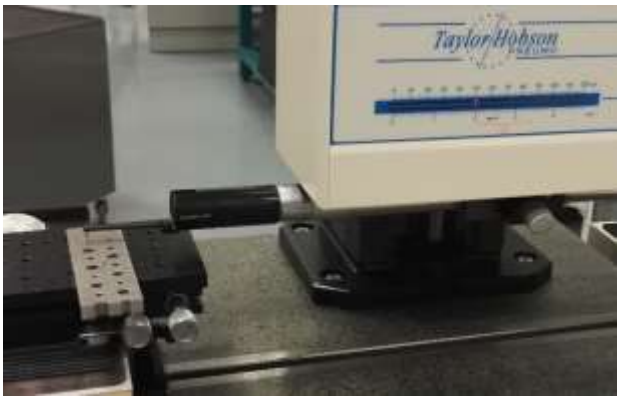

Figure 49: Surface measurement Taylor Hobson equipment

4.1.3 Hardness

Hardness of AB-35 parts is checked by Vickers hardness method, using V10 scale. A section of printed plate is cut with wire EDM and hardness is measured along face A as shown in Figure 50.

Figure 50: section cut from printed part

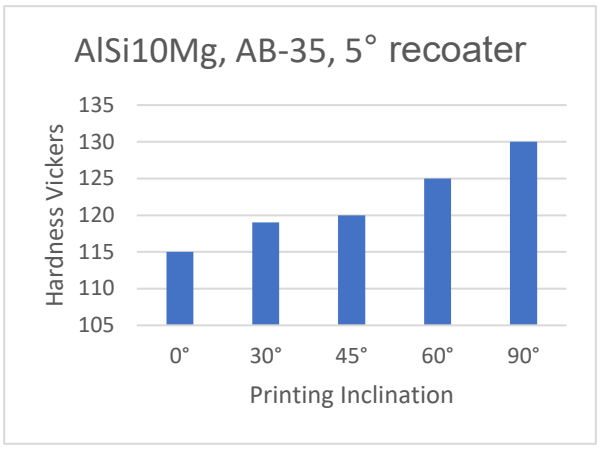

Figure 51: Vickers 10 scale Hardness, AlSi10Mg, AB-35, 5° recoater angle

Discussion

From Figure 51, it is evident that hardness is increasing with increase in printing inclination. Results pointed out that vertically (90°) printed part is harder than horizontally printed one, i.e. (0°). This could be due to high surface contact of horizontal components with base plate as compared to vertically printed, which has least contact with baseplate. Second factor is height of components from build plate and since horizontal plate has least height and more direct surface contact, so it can have higher cooling rates and be softer. On the other hand, with increased height and less direct surface contact; as it was in case of 90° component, harder will be the material. This refers to anisotropy of material i.e. hardness is varying depending upon direction of printing.

Hardness comparison of AB-200 Parts

Similarly, hardness of AB-200 components, printed at 5° and 45° to recoater, was measured and results are presented in Figure 52.

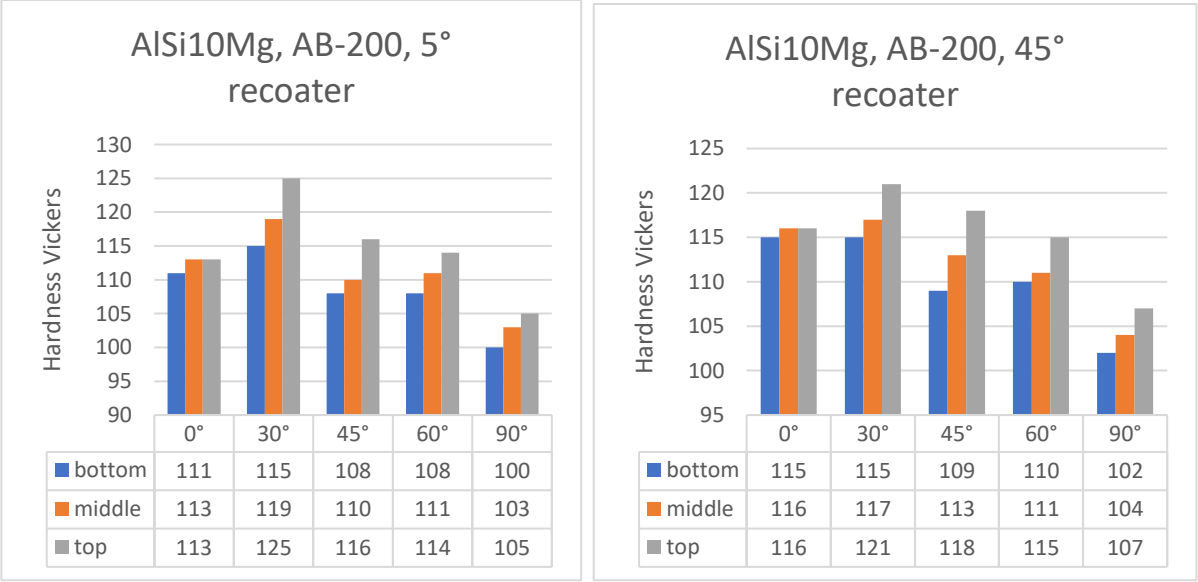

Figure 52: Hardness (Vickers) comparison of AlSi10Mg, AB-200, 5° recoater angle (left), 45° recoater angle (right)

Discussion

For AB-200 parts, range of hardness remained same for both 5° and 45° oriented components, compared to hardness of AB-35 components. Hardness was measured at three different locations i.e. bottom, middle and top of printed plates, along face A. From Figure 52, it appears that height affects hardness of printed material in all inclinations. Material at top, is harder than at the bottom. Harness is not varying for material printed at 0°; which confirms the hypothesis that height has some influence on hardness of printed parts.

Trend of hardness observed for AB-200 parts is opposite to AB-35 components. As contact area of supports is decreasing along printing inclinations (from 0° to 90°), hardness is also declining. This was different in case of AB-35 parts. So, it can be concluded that though height might have small effect on hardness, parts contact area is main factor defining hardness of material.

Lower areas of part are overaged and resulted in lower hardness while at top areas, peak aging has occurred which showed higher hardness. AB-200 have resulted in better buildability (stress relieving and part accuracy) but this aging/over aging variation has resulted in variance in material properties, e.g. hardness.

4.1.4 Hole diameter

Printing pre-holes is logical for making holes and internal threads. It will reduce material consumption and printing time. Downside is that there will be shrinkages resulting in undersized holes. Dross will also exist on downskin surfaces in pre-holes; that must be removed. Once pre-holes are printed, measuring new coordinates is a laborious task and off-centering effect may result in drill-wandering that will form bad shape of hole.

Figure 53 visualizes schematically nominal diameter, difference of nominal diameter to printed diameter and dross (difference of d_2 and d_1). Printed holes size, d_1 is termed as major diameter and d_2 as minor diameter. Due to dross (unmelted particles attached to downskin surfaces) d_1 , and d_2 are not equal.

Diameter of holes printed in various inclination are measured with small hole gauge and micro meter and results are attached in appendix A. Based on these results, Figures 54-56 enlist dross formed in these pre-holes and difference to printed pre-holes to nominal diameter i.e. 4.2 mm and 6.8 mm.

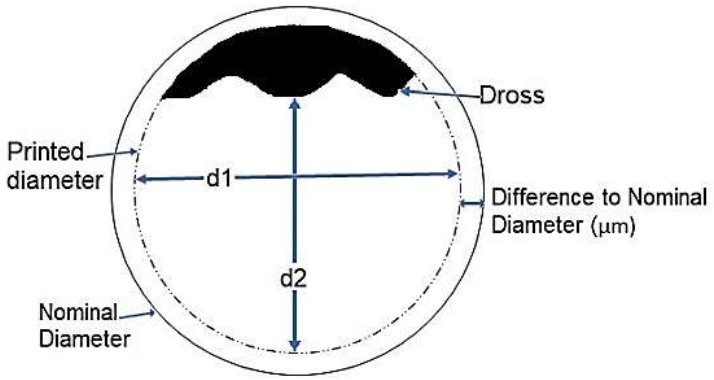

Figure 53: A schematic of diameter measurement

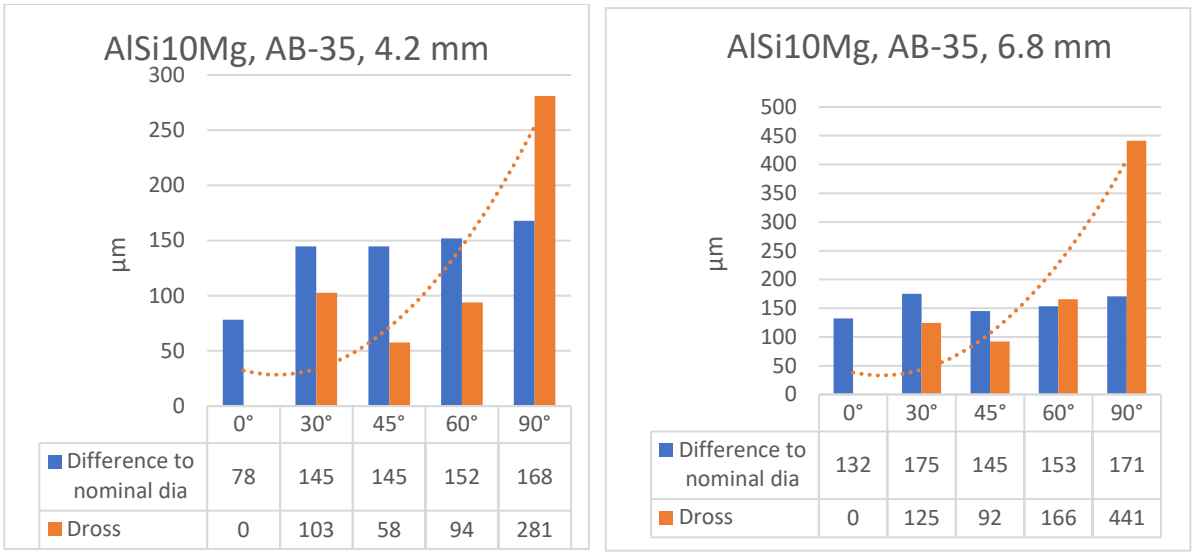

Figure 54: Hole size variation in AB-35, 5° recoater angle, 4.2 mm left, 6.8 mm right

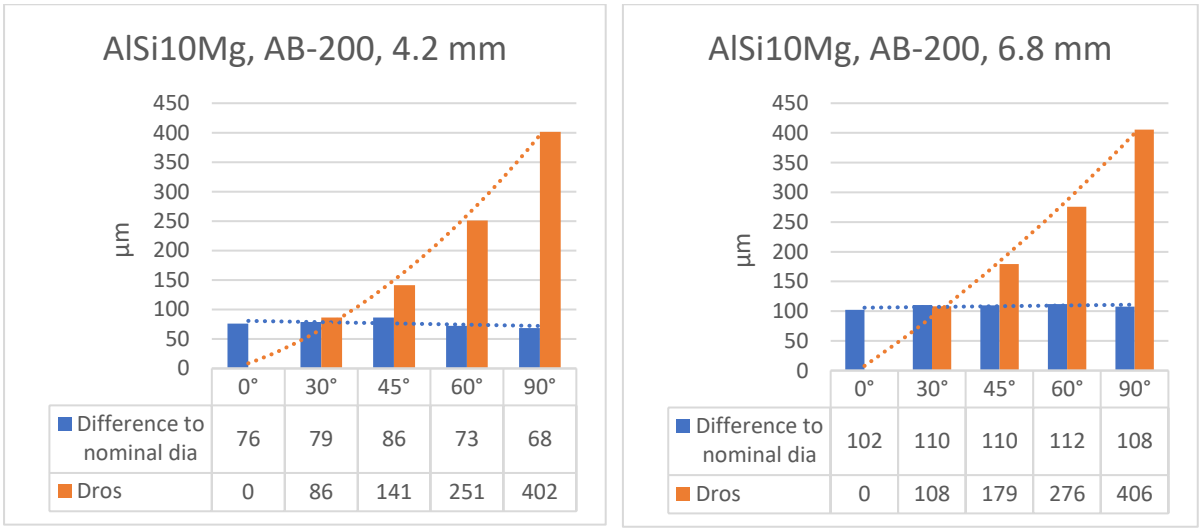

Figure 55: Hole size variation in AlSi10Mg, AB-200, 5° recoater angle, 4.2 mm left, 6.8 mm right

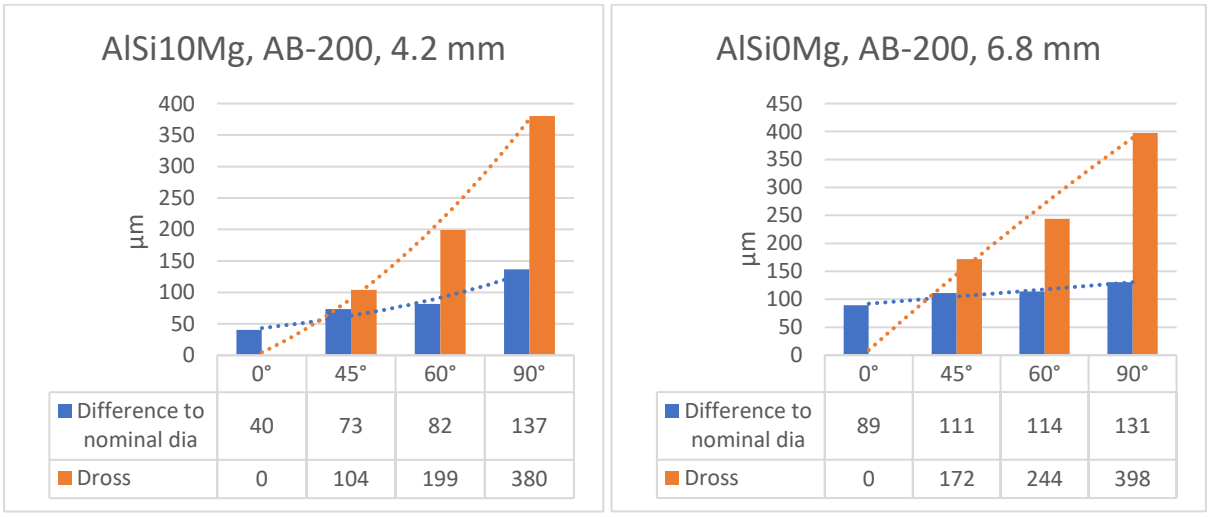

Figure 56: Hole size variation in AlSi10Mg, AB-200, 45° recoater angle, 4.2 mm left, 6.8 mm right

Discussion

Diameter measurement showed that printed pre-holes are undersized compared to nominal dimensions. There could be effect of scaling down that might reduce dimensions on all sides. It is also possible that shrinkage has occurred during cooling process. As there might be number of factors affecting shrinkages, it is challenging to control it.

These graphs shown in Figures 54-56, point out that difference of printed diameter to nominal diameter, represented by blue bars, is somewhat constant but dross increases with increase in printing inclination. It seems logical that dross is maximum for 90° inclination (horizontal holes).

No dross will form for vertical holes i.e. in 0° printing inclination, so printing pre-holes will result in better quality holes. Only issue would then be that printed hole diameter would not be the same as was required. Since these pre-holes will be undersized, so either their nominal diameter must be increased approx. by 0.15 mm or by removing 0.15 mm material after printing. Removing material via drilling is not always easy. To drill these holes, center coordinates must be measured using accurate devices such as CMM. For smaller holes even that becomes problematic, as measuring probes are limited in sizes and might not fit in smaller pre-holes, e.g. diameter < 3 mm.

In practice, when d_1 is drilled to nominal diameter, all dross will be removed.

With right measuring probe in CMM, program must be designed such that both diameter and center are measured from up-skin surfaces so that dross cannot affect measurement process. Direct drilling has advantage of avoiding off-setting during drilling process and needs lesser arrangement for drilling.

4.1.5 Cutting forces

During drilling pre-holes in printed AlSi10Mg, cutting forces are measured using Kistler sensor Figure 32 and principles shown in Figure 34. Main purpose was to observe any effect of anisotropy along different printing inclinations in both as-built and solution treated condition. Machining parameters selected for drilling and tapping of aluminium are listed in Tables 1 and 2. It is already well-established fact that with increase in pre-hole diameter, axial drilling forces are reduced [30, page 220]. For printed material, this will be checked for various pre-hole diameters. Different colors are used to indicate the trend in cutting forces among different pre-holes and printing inclination shown in Tables 8-10.

AlSi10Mg, AB-35, 5° to recoater

Axial drilling forces measured for AlSi10Mg, AB-35, printed at 5° to recoater direction are given in Table 8. Zero pre-hole means that hole is drilled in solid material. This will result in accurate and reliable result for drilling forces. For other pre-holes, off centering can have effect on drilling forces. Values presented in Table 8-10 are extracted from cutting forces measured individually for each pre-hole and annexed in appendix B.

Table 8: Axial drilling forces (N) for 4.2 mm and 6.8 mm drill

Printing Inclination	0°	30°	45°	60°	90°		
Pre-hole diameter (mm)	Force (N) for drilling 4,2 mm hole					Mean Force (N)	Range (N)
0	247	247	251	262	237	249	26
2	62	66	64	61	60	63	6
3,2	27	39	30	26	28	30	13
3,5	22	31	20	22	20	23	11
3,8	16	16	9	8	17	13	9
Mean Force (N)	75	80	75	76	72		

Printing Inclination	0°	30°	45°	60°	90°		
Pre-hole diameter (mm)	Force (N) for drilling 6,8 mm hole					Mean Force	Range (N)
0	366	382	396	399	375	384	34
3	130	127	129	130	126	128	5
5,8	36	35	34	35	33	35	3
6,1	26	34	28	25	29	28	9
6,4	18	19	18	20	19	19	2
Mean Force (N)	115	120	121	122	117		

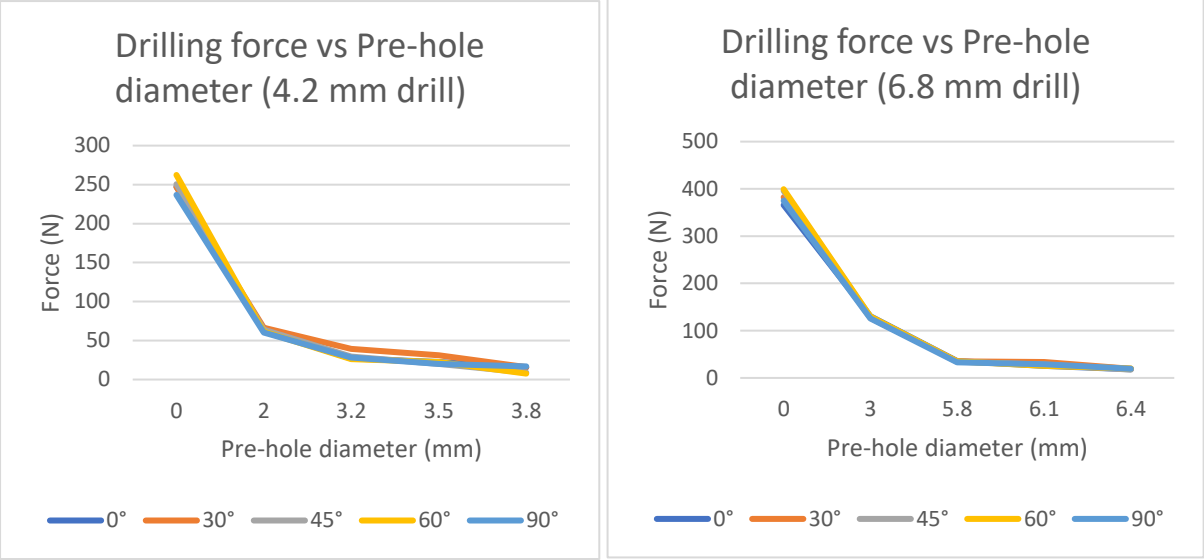

Figure 57: Axial drilling force variation with pre-hole sizes in AlSi10Mg, AB-35, 5° recoater angle

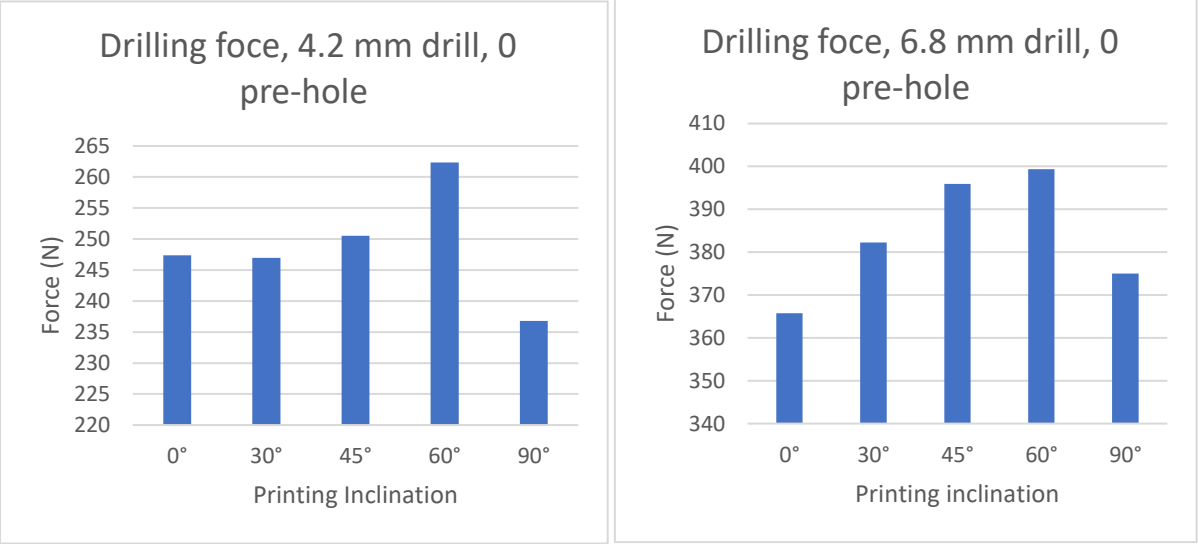

Figure 58: Drilling force variation with printing inclination in AlSi10Mg, AB-35, 5° recoater angle

Discussion

Figure 57 clearly indicates the fact that with increase in pre-hole size, axial drilling forces are reduced. With a pre-hole of 2 mm for 4.2 mm drill, axial force is reduced 75% approx. compared to drilling force for 0 pre-hole. Decrease in force is also significant for a pre-hole of 3 mm for 6.8 mm drill. This proves the point that having a pre-hole is beneficial in AM part design compared to direct drilling in solid material. Especially for structural component, it will be beneficial to make pre-holes and therefore reduce axial drilling thrust.

Table 8 presents axial drilling forces for various pre-holes and respective printing inclinations in newton (N). Variation of force is higher in case of drilling in solid material, i.e. 0 pre-hole for both 4.2 mm and 6.8 mm drill. Axial force is increasing until 60° for both drills and then decreases (Figure 58). Hardness value increases from 0° to 90° as shown in Figure 51 and so does cutting forces, except for 90° inclination. Only thing common in 0° to 60° printing inclination is that plates have more contact area with build plate compared to 90° inclination (Figure 38).

As expected, for bigger diameter drill, drilling forces are higher. Figure 58 presents drilling forces in solid material to avoid any chances of off-centering. Since a reasonable difference exist in drilling force values so it can be said that material behaves in an anisotropic way in AB-35 condition.

AlSi10Mg, AB-200, 5° to recoater

In Table 9, drilling forces for AlSi10Mg, AB-200 components with 5° recoater angle are presented.

Table 9: Axial drilling forces (N) for 4.2 mm and 6.8 mm drill

printing inclination	0°	30°	45°	60°	90°		
pre-hole diameter (mm)	Force (N) for drilling 4.2 mm hole					Mean Force (N)	Range (N)
0	310	299	299	300	298	301	12
2	54	59	58	57	64	59	10
3.2	23	25	24	24	24	24	2
3.5	20	21	20	18	21	20	3
3.8	10	11	15	12	15	12	5
Mean Force (N)	83	83	83	82	84		

printing inclination	0°	30°	45°	60°	90°		
pre-hole diameter (mm)	Force (N) for drilling 6.8 mm hole					Mean Force (N)	Range (N)
0	422	420	422	425	430	424	10
2	135	141	140	145	145	141	10
5.8	35	34	35	36	35	35	1
6.1	24	23	24	22	23	23	2
6.4	18	14	15	14	18	16	5
Mean Force (N)	127	127	127	128	130		

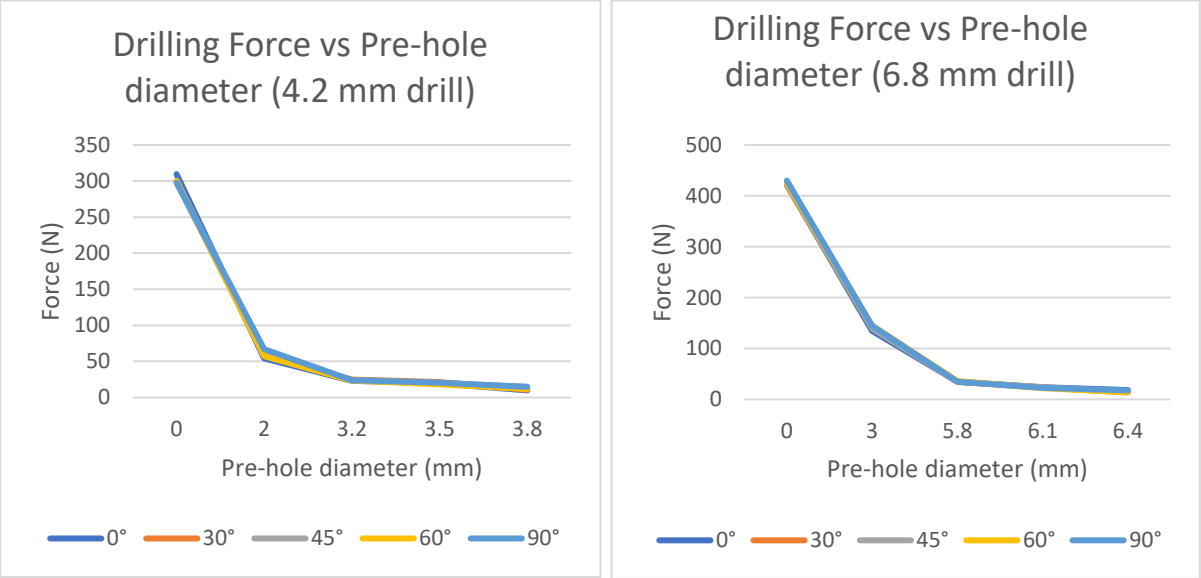

Figure 59: Axial drilling force variation with pre-hole sizes in AlSi10Mg, AB-200, 5° recoater angle

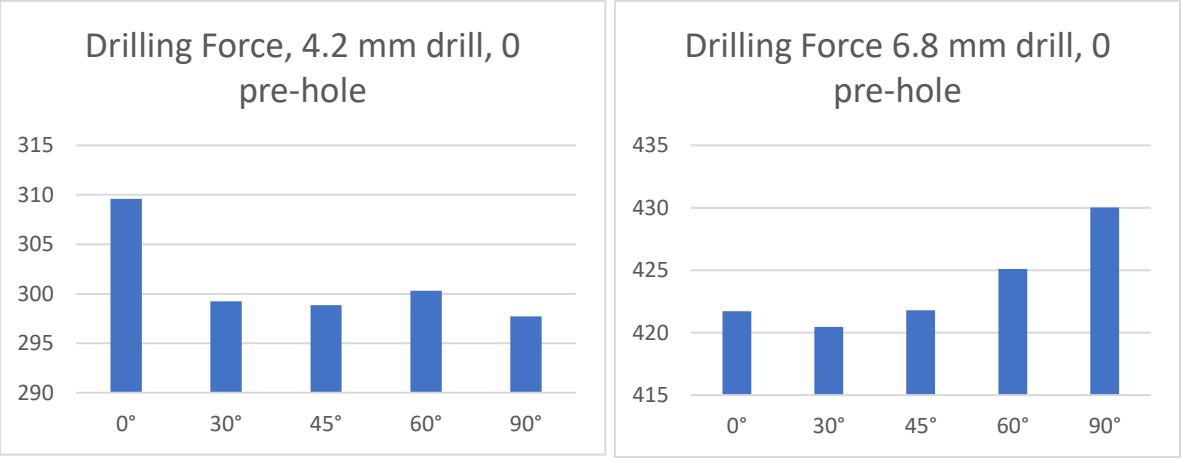

Figure 60: Drilling force variation with printing inclination in AlSi10Mg, AB-200, 5° recoater angle for 0 pre-hole

Discussion

Drilling forces are higher in AB-200 parts than AB-35 parts. For AB-200 parts, drilling force variation among different printing inclinations, for 0 pre-hole is less than that observed for AB-35. Since differences among forces are smaller along different printing inclinations and trend is different for 4.2 mm drill and 6.8 mm drill depicted in Figure 60, it cannot be asserted for sure that drilling forces will be higher for which printing inclination. It can conclude that material behaves isotopically in AB-200 condition based on fact that range of forces is smaller among printing inclinations.

AlSi10Mg, AB-200, 45° to recoater

For parts placed differently to recoater direction, i.e. 45°, drilling forces are calculated and tabulated in Table 10.

Table 10: Axial drilling forces (N) for 4.2 mm and 6.8 mm drill '--' values missing

Printing inclination	0°	30°	45°	60°	90°		
pre-hole diameter (mm)	Force for drilling 4.2 mm hole					Mean Force (N)	Range (N)
0	--	271	291	288	296	287	25
2	--	59	56	57	63	59	7
3.2	--	24	27	24	27	26	3
3.5	--	--	20	21	22	21	2
3.8	--	--	--	12	12	12	0
Mean Force (N)				80	84		

Printing inclination	0°	30°	45°	60°	90°		
pre-hole diameter (mm)	Force for drilling 6.8 mm hole					Mean Force (N)	Range (N)
0	431	434	429	425	429	429	9
3	145	145	145	147	145	145	2
5.8	36	36	35	36	36	36	1
6.1	24	23	24	24	25	24	2
6.4	15	17	16	21	18	17	6
Mean Force (N)	130	131	130	130	131		

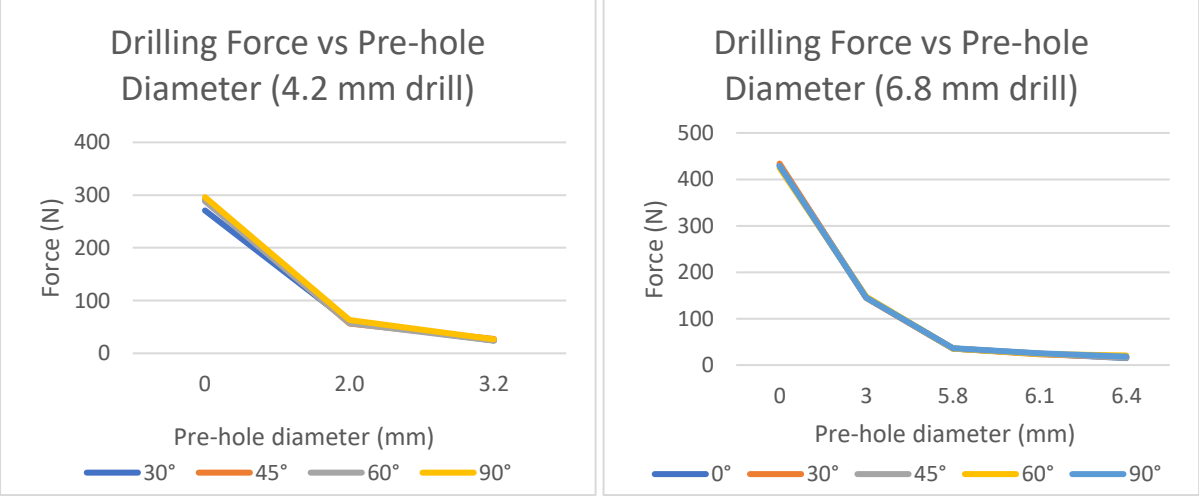

Figure 61: Axial drilling force variation with pre-hole sizes in AlSi10Mg, AB-200, 45° recoater angle

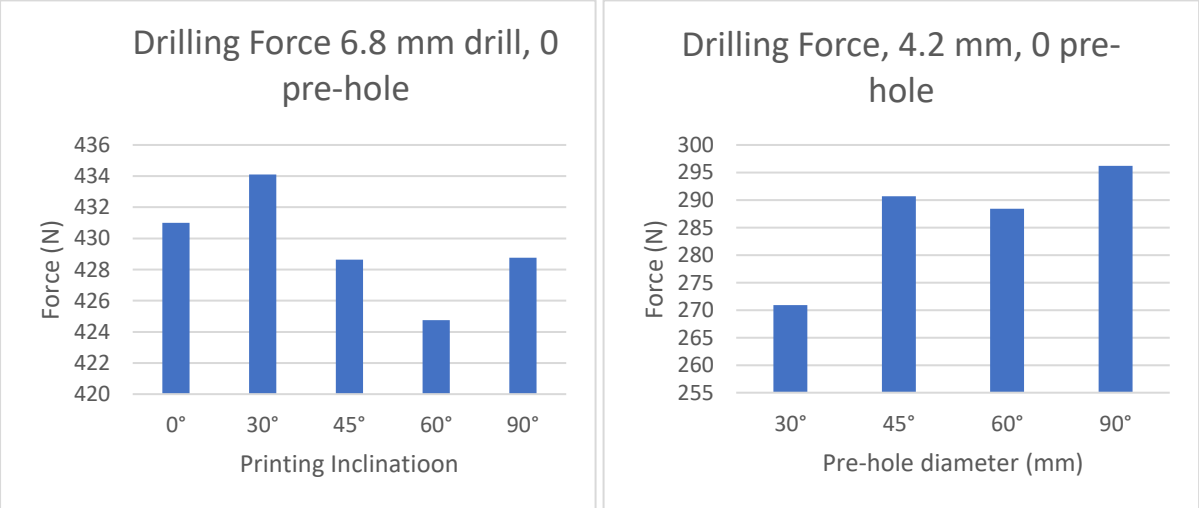

Figure 62: Drilling force variation with printing inclination in AlSi10Mg, AB-200, 45° recoater angle

Discussion

Variation of force between different printing inclinations is higher for 4.2 mm drill but smaller for 6.8 mm drill. Still average force values are close to previous forces for 5° to recoater. So, it can be said that part placement to recoater does not affect nature of material.

Conclusion

Summing it up, it can be stated that average drilling forces are almost same in wrought aluminium 6082 (displayed in Figure 37) and those observed for AB-35 parts. Drilling forces are higher for AB-200 parts compared to AB-35 components indicating the fact the build plate temperature has some effect on material properties. Material is anisotropic for AB-200 parts, i.e. printing inclination has no significant influence on cutting forces and parts placement to recoater do not affect cutting forces. For weak structural components it is better to select pre-hole to reduce axial drilling force. Any pre-hole size that is close to nominal diameter will reduce drilling forces by 75-80%.

4.1.6 Macrographs

Results shown in Figures 63-77 are macrographs that are captured using optical microscope and magnified 2.5X. These macrographs are taken for 6.8 mm semi-circle. Before observing in microscope, these samples were ground with SiC paper of grit size 800, 1200 and 2000 successively. By doing so, peak to peak value reduced to 15 µm. Mechanical polishing then followed with diamond paste of size 3 µm and 1 µm successively.

Samples were then etched for 25-30 seconds in Keller's reagent. Washing and drying with methanol was final step before observing in microscope.

AlSi10Mg, AB-35, 5° recoater angle

Figures 63-67 represent macrographs of AlSi10Mg, AB-35 printed in different inclinations indicated by red arrow.

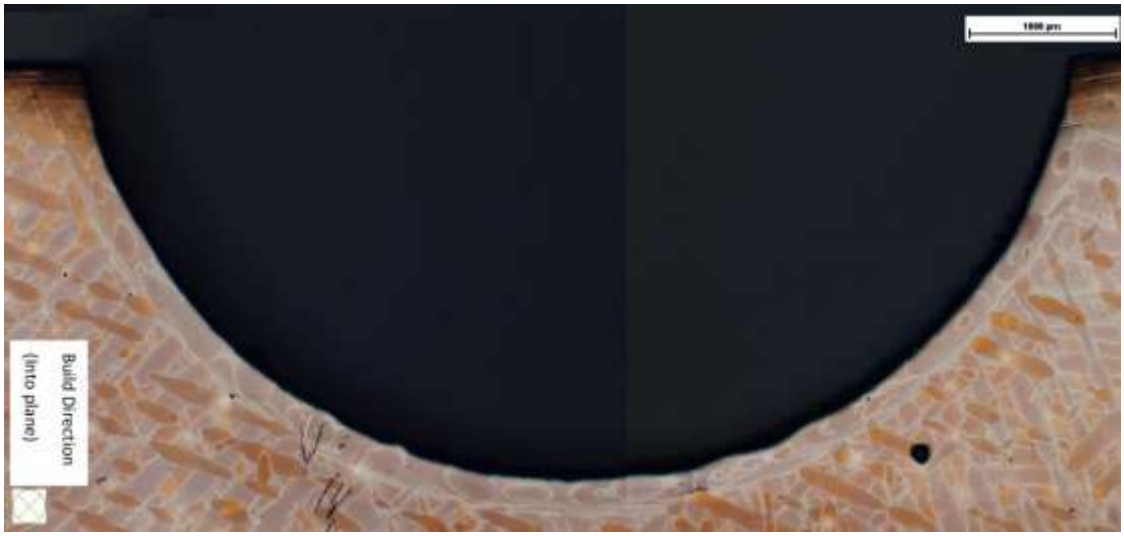

Figure 63: Porosity observed in AlSi10Mg, AB-35, 6.8 mm semi-circle, Printing Inclination 0°, Objective 2.5 X

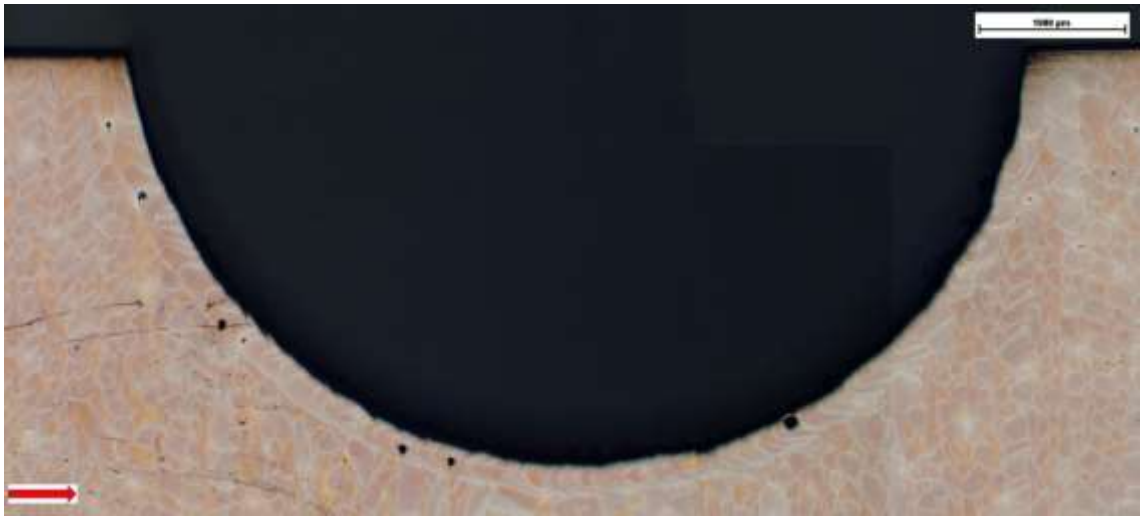

Figure 64: Porosity observed in AlSi10Mg, AB-35, 6.8 mm semi-circle, Printing Inclination 30°, Objective 2.5 X

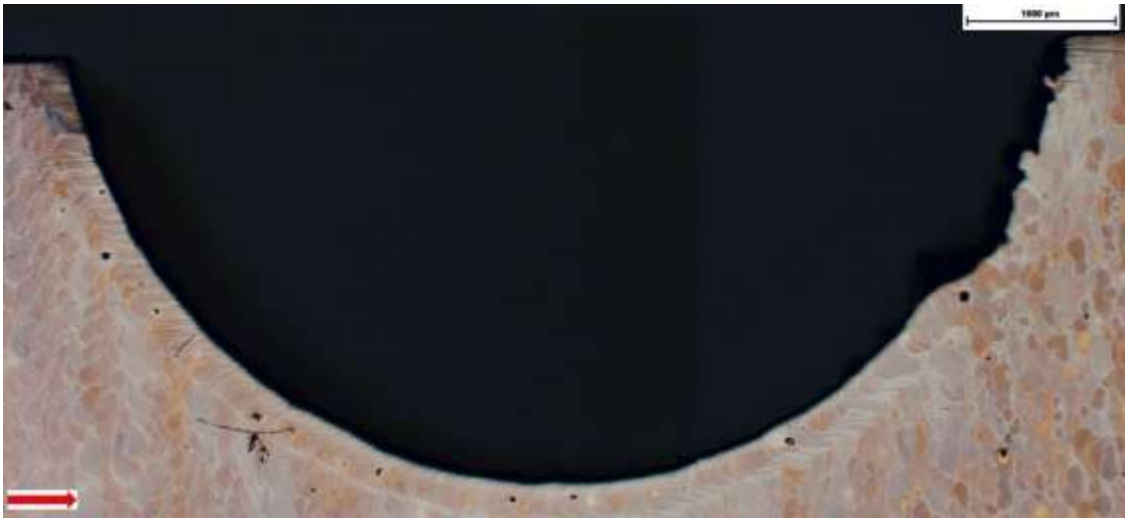

Figure 65: Porosity observed in AlSi10Mg, AB-35, 6.8 mm semi-circle, Printing Inclination 45°, Objective 2.5 X

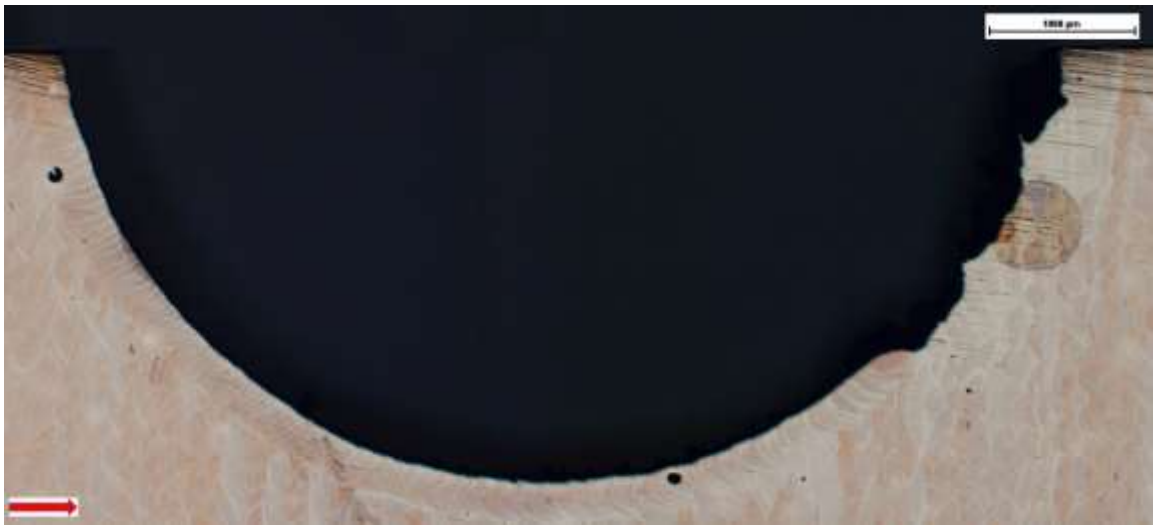

Figure 66: Porosity observed in AlSi10Mg, AB-35, 6.8 mm semi-circle, Printing Inclination 60°, Objective 2.5 X

Figure 67: Porosity observed in AlSi10Mg, AB-35, 6.8 mm semi-circle, Printing Inclination 90°, Objective 2.5 X

Discussion:

In case of vertical holes, i.e. 0° inclination, no significant porosity is seen. As printing angle increases, porosity appears mostly near the surface. From macrographs, a welded layer can be observed and mostly porosity was seen in this surface. Its width was estimated as 280-330 µm. To get rid of these porosities it is recommended to remove approx. 300 µm of material.

AlSi10Mg, AB-200, 5° recoater angle

Figures 68-72 represent macrographs of AlSi10Mg, AB-200 parts, printed in different inclinations indicated by red arrow.

Figure 68: Porosity observed in AlSi10Mg, AB-200, 6.8 mm semi-circle, Printing Inclination 0°, Objective 2.5 X

Figure 69: Porosity observed in AlSi10Mg, AB-200, 6.8 mm semi-circle, Printing Inclination 30°, Objective 2.5 X

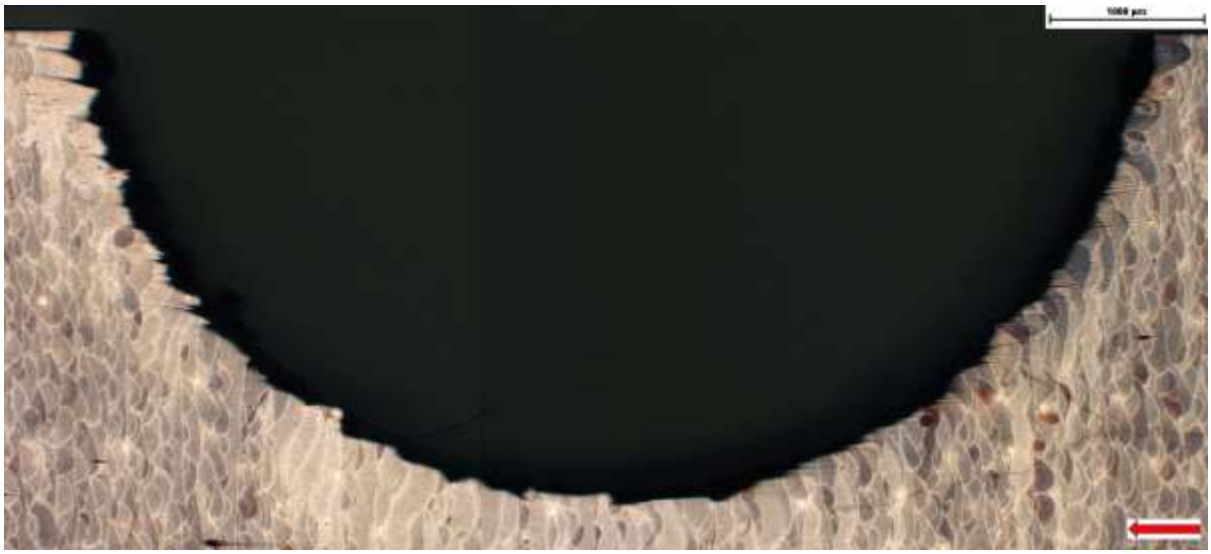

Figure 70: Porosity observed in AlSi10Mg, AB-200, 6.8 mm semi-circle, Printing Inclination 45°, Objective 2.5 X

Figure 71: Porosity observed in AlSi10Mg, AB-200, 6.8 mm semi-circle, Printing Inclination 60°, Objective 2.5 X

Figure 72: Porosity observed in AlSi10Mg, AB-200, 6.8 mm semi-circle, Printing Inclination 90°, Objective 2.5 X

Discussion

For macrographs of AB-200 parts, placed 5° to recoater, the same etchant is used but somehow quality of macrographs is slightly different. Here welded layer is missing, and less porosity is detected. Only small pores exist in dross formed in downskin surface as shown in Figure 72.

AlSi10Mg, AB-200, 45° recoater angle

Figure 73: Macrograph of AlSi10Mg, Solution Treated, 6.8 mm semi-circle, Printing Inclination 0°, Objective 2.5 X

Figure 74: Macrograph of AlSi10Mg, Solution Treated, 6.8 mm semi-circle, Printing Inclination 30°, Objective 2.5 X

Figure 75: Macrograph of AlSi10Mg, Solution Treated, 6.8 mm semi-circle, Printing Inclination 45°, Objective 2.5 X

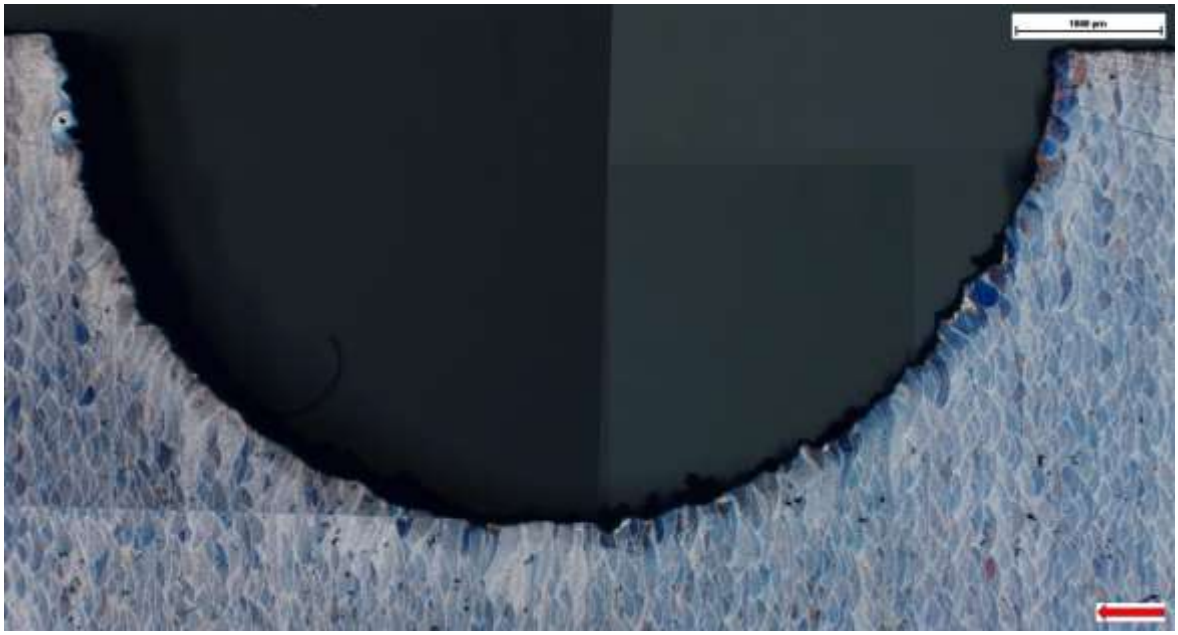

Figure 76: Macrograph of AlSi10Mg, Solution Treated, 6.8 mm semi-circle, Printing Inclination 60°, Objective 2.5 X

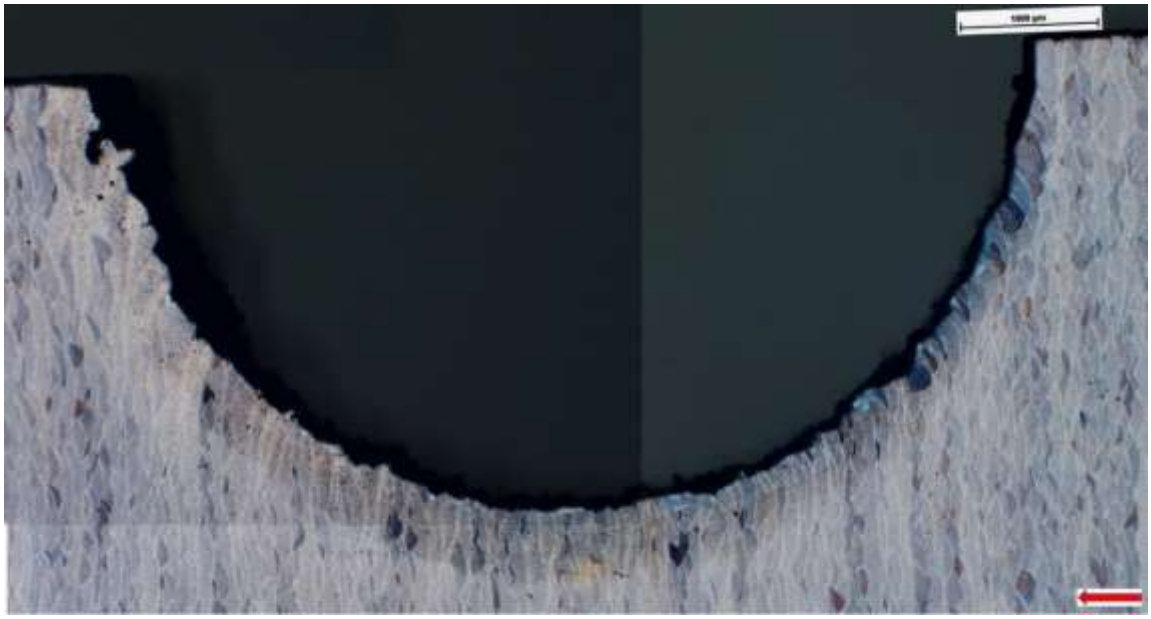

Figure 77: Macrograph of AlSi10Mg, Solution Treated, 6.8 mm semi-circle, Print Inclination 90°, Objective 2.5 X

Discussion

In Figures 73-77 macrographs of AlSi10Mg, AB-200, are laid out where recoater angle of 45° is used for printing. Same Keller's reagent is used as etchant. Weld layer, as was seen in AB-35 printed aluminium is not detected in these photographs. Some porosity is identified but that does not lie near surface.

Conclusion

To recapitulate the findings of porosity, it can be stated that though AB-35 material contains noticeable porosity near surface, AB-200 material is as sound as it could be. Parts placement to recoater have minimal influence on surface porosity. These macrographs also imply that quality of metal printing by EOS's printer is very good.

4.1.7 Thread stripping test

To further investigate influence of printing inclination and pre-hole diameter on hole/thread strength, an ISO standard 899-2 test [26] is employed. A mechanical system as demonstrated in Figure 78, is adopted to test thread stripping phenomena. Unlike guidance of this standard, internal threads made in metal printed parts were completely stripped off as delineated in Figure 78. Testing was executed on a custom-made tensile testing machine. This machine can exert a maximum force of 50 kN.

In setup, four bolts are used to clamp nut (internal threads made in printed aluminium) on a steel plate bolted on table of tensile tester. A mandrel (unused bolt) was clamped with a hard grip (52- HRC) as prescribed by standard. Total of 240 internal threads made in printed AlSi10Mg (both AB-35 parts and AB-200 parts, printed at 5° and 45° recoater angle) were tested with a new bolt every time. Test results are tabulated in Tables 12-14.

Figure 78: Axial tensile test setup for thread stripping and stripped threads on bolt

Internal threads made in aluminium 6082 were made in similar way, Figure 36, using 5-axis vertical milling centre. Threads were stripped on tensile testing machine and following results were obtained:

Table 11: Thread stripping force (kN) for M5 and M8 made in Al6082

Aluminium 6082	M5	M8
Thread stripping force (kN)	16.886	24.983

Tables 12-14 comprise stripping forces for internal threads made in metal printed parts, measured in kilo newton for M8 and M5 for AB-35 parts, AB-200 parts printed in two inclinations to recoater. Along columns, printing inclination is varied whereas pre-hole diameter (mm) is decreased in rows. Averages and differences (range) in kilo newton, are also specified along rows and columns. Average thread stripping forces are presented in Figures 79-84, to understand if the means are varying along rows and

columns. Colour formatting is used in following tables, where green highlights bigger values and red colour representing smaller figures.

AlSi10Mg, AB-35, 5° recoater angle

Table 12: Thread stripping force, AlSi10Mg, AB-35, 5° recoater angle

M8, AlSi10Mg, AB-35, 5°recoater angle							
pre-hole diameter (mm)	Printing Inclination					Average (kN)	Range (KN)
	0°	30°	45°	60°	90°		
	Thread breaking force (kN)						
6.9	--	25.73	29.19	32.6	32.85	30.09	7.12
6.8	30.05	24.64	27.44	33.52	32.57	29.64	8.88
6.7	32.09	24.74	28.56	--	33.54	29.73	8.80
6.4	--	26.48	26.86	30.68	33.39	29.35	6.91
6.1	--	25.09	30.71	32.95	29.52	29.57	7.86
5.8	29.38	25.98	28.06	31.28	34.79	29.90	8.81
3	32.66	24.93	27.87	33.72	--	29.80	8.79
0	32.18	26.51	30.53	31.99	34.01	31.04	7.50
Average (kN)	31.27	25.51	28.65	32.39	32.95		
Range(kN)	3.28	1.87	3.85	3.04	5.27		

M5, AlSi10Mg, AB-35, 5°recoater angle							
pre-hole diameter (mm)	Printing Inclination					Average (kN)	Range (KN)
	0°	30°	45°	60°	90°		
	Thread breaking force (kN)						
4.3	12.04	11.93	11.78	12.16	--	11.98	0.38
4.2	12.1	13.46	13.57	12.61	12.87	12.92	1.47
4.1	11.89	11.97	13.7	12.81	13.02	12.68	1.81
3.8	11.43	11.61	11.93	12.98	13.01	12.19	1.58
3.5	11.7	--	13.29	13.86	13.72	13.14	2.16
3.2	12.06	12.85	12.27	14.2	13.71	13.02	2.14
2	13	13.14	12.57	13.38	13.87	13.19	1.30
0	12.89	12.82	13.58	13.32	13.96	13.31	1.14
Average (kN)	12.14	12.54	12.836	13.17	13.45		
Range(kN)	1.57	1.85	1.92	2.04	1.09		

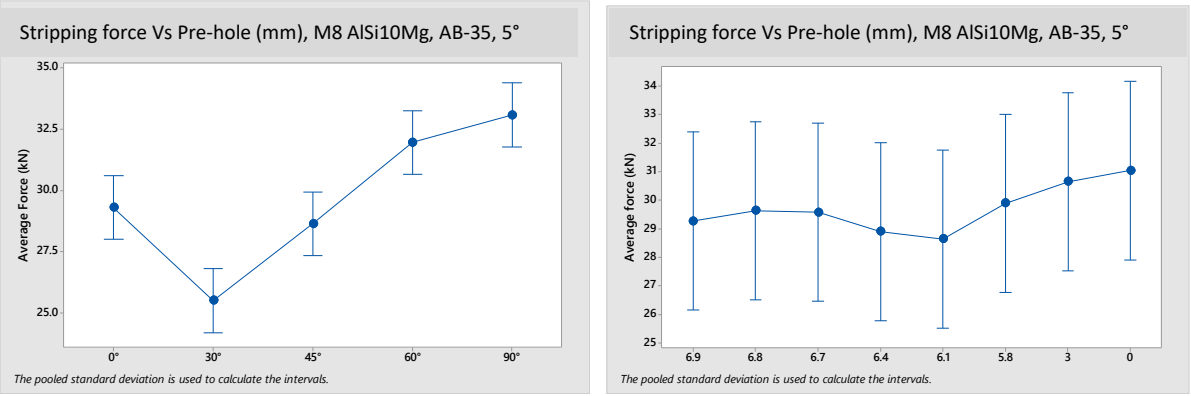

Figure 79: Mean thread stripping forces in AlSi10Mg, AB-35, M8, left (printing inclination), right (pre-hole diameter)

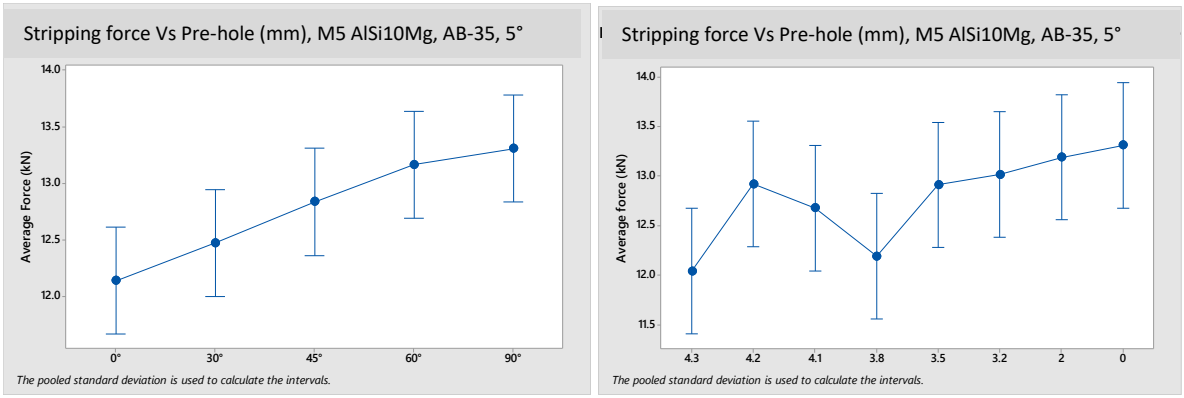

Figure 80: Mean thread stripping forces in AlSi10Mg, AB-35, M5, left (printing inclination), right (pre-hole diameter)

Discussion

M5 threads made in Al6082 (Table 11) have higher thread stripping forces than M5 made in AB-35, whereas M8 threads were stronger for AB-35 part. M8 threads made in AB-200, exhibited approximately same thread stripping force as were measured in aluminium 6082 Table 11.

M8 thread stripping force values in Table 12 clearly indicate that thread stripping forces in parts printed at 30° inclination are the lowest and 90° are the highest. This trend is slightly different for M5 threads.

Difference of forces is more evident in M8 than in M5. Average thread stripping forces are plotted against printing inclinations and pre-hole diameters separately in Figures 79 and 80, indicating that average forces are varying significantly along printing inclination and along pre-hole diameters. This trend is more visible for M5 in Figure 79. Pre-holes smaller than 6.1 mm and 3.5 mm for M8 and M5, respectively have resulted stronger holes for AB-35 components. This indicates that porosity is affecting material quality to some distance. Threads made in 90° appeared stronger than 0° printing inclination. This means material is behaving anisotropically.

AlSi10Mg, AB-200, 5° recoater angle

Table 13 presents thread stripping forces in M8 (left) and M5 (right) for AB-200, AlSi10Mg, built at 5° to recoater.

Table 13: Thread stripping force, AlSi10Mg, AB-200, 5° to recoater

M8, AlSi10Mg, AB-200, 5° recoater anglle							
pre-hole diameter (mm)	Printing Inclination					Average (kN)	Range (KN)
	0°	30°	45°	60°	90°		
	Thread breaking force (kN)						
6.9	26.33	26.43	26.97	28.17	27.26	27.03	1.84
6.8	27.16	27.22	26.67	26.79	27.87	27.14	1.20
6.7	25.79	26.92	26.82	27.16	28.34	27.01	2.55
6.4	27	24.47	27.23	26.84	26.68	26.44	2.76
6.1	26.6	26.58	26.77	27.68	26.35	26.80	1.33
5.8	25.74	26.99	27.82	27.62	26.04	26.84	2.08
3	27.87	27.8	27.55	27.7	27.93	27.77	0.38
0	25.68	27.19	25.99	26.52	26.24	26.32	1.51
Average (kN)	26.52	26.7	26.98	27.31	27.09		
Range(kN)	2.19	3.33	1.83	1.65	2.3		

M5, AlSi10Mg, AB-200, 5°recoater angle							
pre-hole diameter (mm)	Printing Inclination					Average (kN)	Range (KN)
	0°	30°	45°	60°	90°		
	Thread breaking force (kN)						
4.3	10.7	11.9	11.51	11.77	11.22	11.42	1.20
4.2	10.68	11.08	10.4	11	10.93	10.82	0.68
4.1	10.42	10.34	10.92	11.06	10.61	10.67	0.72
3.8	10.02	11.3	10.95	11.51	10.31	10.82	1.49
3.5	10.91	11.72	11.45	11.64	11.12	11.37	0.81
3.2	10.66	10.25	11.28	10.52	10.22	10.59	1.06
2	10.39	10.49	11.02	11.02	10.71	10.73	0.63
0	10.51	10.6	11.09	11.09	11.36	10.93	0.85
Average (kN)	10.54	10.96	11.078	11.2	10.81		
Range(kN)	0.89	1.65	1.11	1.25	1.14		

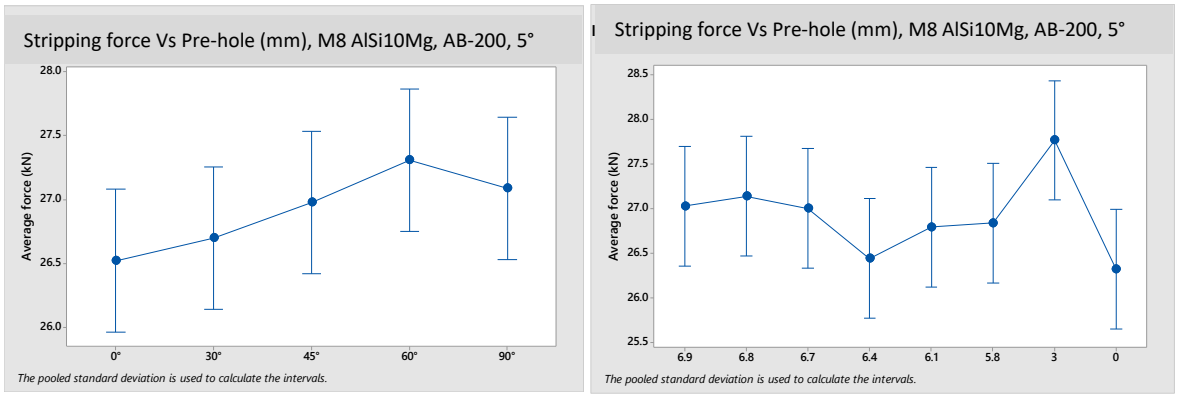

Figure 81: Mean thread stripping forces for AB-200, AlSi10Mg, 5° to recoater, M8, left (printing inclination), right (pre-hole diameter)

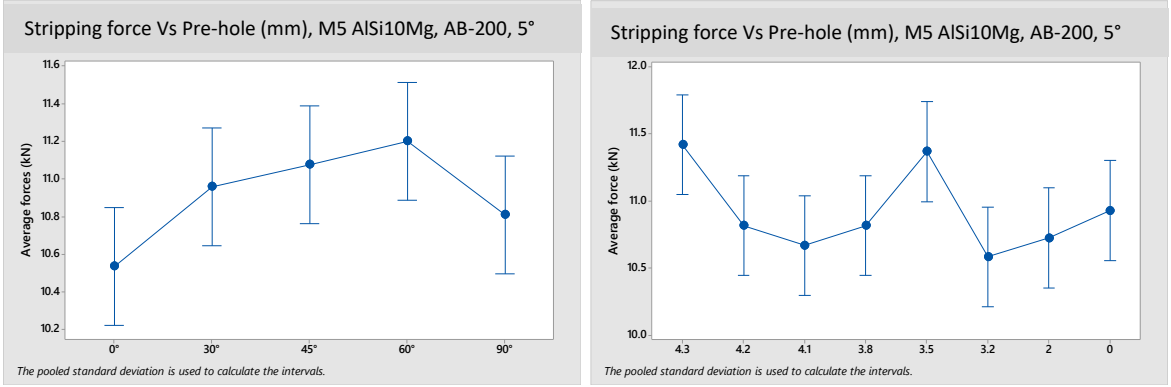

Figure 82: Mean thread stripping forces for AB-200, AlSi10Mg, 5° to recoater, M5, left (printing inclination), right (pre-hole diameter)

Discussion

Average thread stripping forces are lower in AB-200 components than AB-35 parts. Difference between thread stripping forces along rows and columns has reduced; indicating more uniform behaviour of material. Here too, material printed in 90° inclination is stronger than 0° (vertical holes) but difference in forces is not that much significant. Changing pre-hole diameter do not represent a clear trend in stripping forces. This infers that porosity is not affecting thread strength in printed material.

AlSi10Mg, AB-200, 45°

Thread stripping forces for AlSi10Mg, AB-200, and parts placed at 45° to recoater are provided in Table 14.

Table 14: Thread stripping force, AlSi10Mg, AB-200, 45° to recoater

M8, AlSi10Mg, AB-200, 45° recoater angle							
pre-hole diameter (mm)	Printing Inclination					Average (kN)	Range (KN)
	0°	30°	45°	60°	90°		
	Thread breaking force (kN)						
6.9	26.47	25.92	25.88	26.17	25.62	26.01	0.85
6.8	26.39	25.02	24.87	26.84	26.81	25.99	1.97
6.7	27.83	25.25	26.26	26.22	25.93	26.30	2.58
6.4	25.42	26.02	26.67	27.61	28.18	26.78	2.76
6.1	26.29	27.22	26.61	27.95	27.52	27.12	1.66
5.8	25.9	26.57	26.97	26.96	28.2	26.92	2.30
3	28.86	25.56	27.75	26.91	--	27.27	3.30
0	27.76	24.59	26.06	26.25	25.95	26.12	3.17
Average (kN)	26.87	25.77	26.38	26.86	26.89		
Range(kN)	3.44	2.63	2.88	1.78	2.58		

M8, AlSi10Mg, AB-200, 45° recoater angle							
pre-hole diameter (mm)	Printing Inclination					Average (kN)	Range (KN)
	0°	30°	45°	60°	90°		
	Thread breaking force (kN)						
4.3	10.83	11.57	10.83	11.41	11.78	11.28	0.95
4.2	11.75	11.04	11.51	11.19	11.33	11.36	0.71
4.1	10.54	11.28	11.07	11.08	11.4	11.07	0.86
3.8	10.76	10.83	11.32	11.09	11.13	11.03	0.56
3.5	10.7	11.45	11.29	11.27	12.06	11.35	1.36
3.2	10.84	10.4	11.06	11.55	11.18	11.01	1.15
2	11.23	11.62	10.959	11.37	11.04	11.24	0.66
0	10.86	11.53	11.25	11.38	11.39	11.28	0.67
Average (kN)	10.94	11.22	11.161	11.29	11.41		
Range(kN)	1.21	1.22	0.68	0.47	1.02		

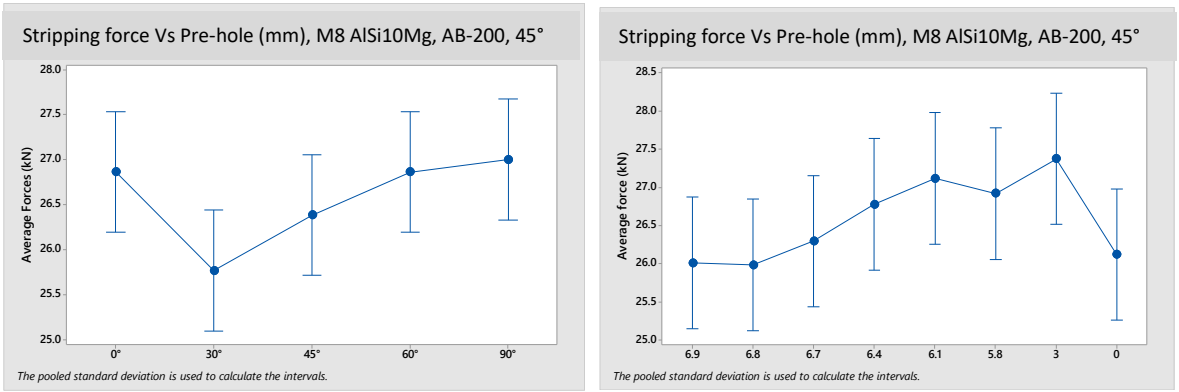

Figure 83: Mean thread stripping forces for AB-200, AlSi10Mg, 45° to recoater, M8, left (printing inclination), right (pre-hole diameter)

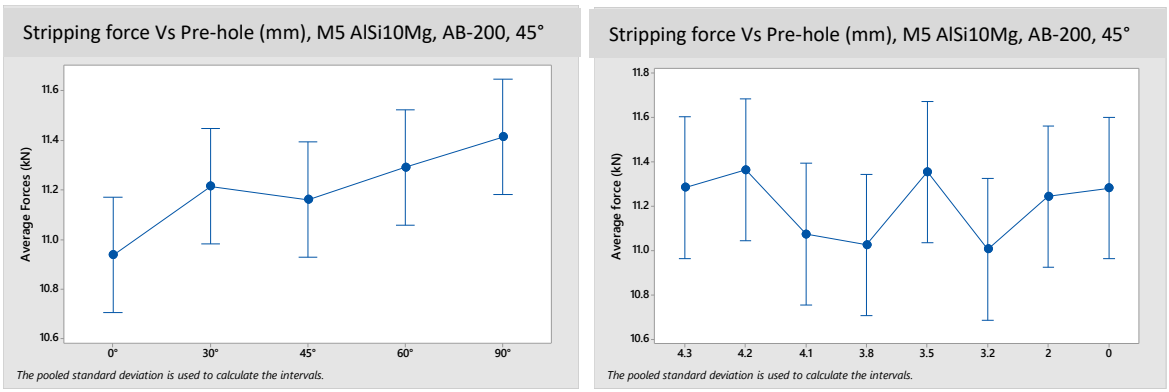

Figure 84: Mean thread stripping forces for AB-200, AlSi10Mg, 45° to recoater, M5, left (printing inclination), right (pre-hole diameter)

Discussion

Average thread stripping forces for AB-200, 45° recoater angle parts appear to be very close to AB-200, 5° recoater angle parts, given in Table 13, showing that parts placement does not affect thread strength and the material is more uniform.

Figures 83 & 84 show that printing inclination has effect on stripping forces, i.e. parallel (90°) holes are stronger than vertical (0°) ones. Pre-hole diameter influences thread stripping forces in case of M8, but that is not very evident in case of M5.

Conclusion

Based on observations related to thread stripping forces in AlSi10Mg for AB-35 and AB-200 components, it can be said that material is stronger in 90° printing orientation than along 0° inclination. Since there were less fluctuations in thread stripping forces along pre-hole diameters for AB-200 printed parts; pre-hole diameter is less likely to be key factor in determining thread strength. Printing inclination affects thread strength to some extent. Macrographs suggested that though porosity exists in AB-35 parts near surface and has affected thread strength, AB-200 components have shown less porosity and pre-hole diameter has minor effect on thread strength. This is mainly due to different printing strategies employed, i.e. build plate temperature was varied from 35 °C to 200 °C for as-built parts. With build plate temperature of 200 °C buildability of parts has improved but some other issues like aging/overaging resulted in variation in material properties (hardness). This is an iterative process of improvement where carefully selected printing parameters will produce uniform material properties.

4.2 Maraging steel

Maraging steel is high strength steel with high toughness. Word ‘maraging’ is combination of ‘Martensite’ and ‘Aging’. Owing to very minute amount of carbon, unlike other high strength steel, maraging steel is not brittle and has many useful applications like in tooling and aerospace industry. Primary alloying element is Nickel while other most important alloying elements are Cobalt, Molybdenum and Aluminium. Maraging steel MS1, printed on M 290, at EOS Finland, has chemical composition like US classification 18% Ni Maraging 300, European 1.2709 and German X3NiCoMoTi 18-9-5. EOS has powder maraging steel, MS1, which is most suitable for processing on EOSINT M systems. [24]

Material composition as given by EOS is listed in Table 15.

Table 15: Maraging steel, MS1 composition [24]

Element	Fe	Ni	Co	Mo	Ti	AL	Cr, Cu	C	Mn, SI	P,S
Weight %	balance	17-19	8.5-9.5	4.5-5.2	0.6-0.8	0.05-0.15	0.5 each	0.03	0.1 each	0.01 each

Figures 85 and 86 showing maraging steel components printed by EOS Finland. Printing inclination and pre-hole diameters are made with same nomenclatures and diameters as was done for aluminium in previous section. Here beside as-built parts, solution treatment is done for maraging steel components which are then drilled and tapped. Parts are placed at 5° and 45° to recoater to see the effect of recoater on parts placement on build plate.

Maraging steel properties are also determined in similar way. After having pre-holes printed at various inclinations, internal threads were made by drilling and tapping using the same equipment. Only difference was in determining thread strength. As strength class 12.9 bolts were not strong enough to strip threads made in maraging steel. Threads were cut with wire EDM for examining thread profile and porosity.

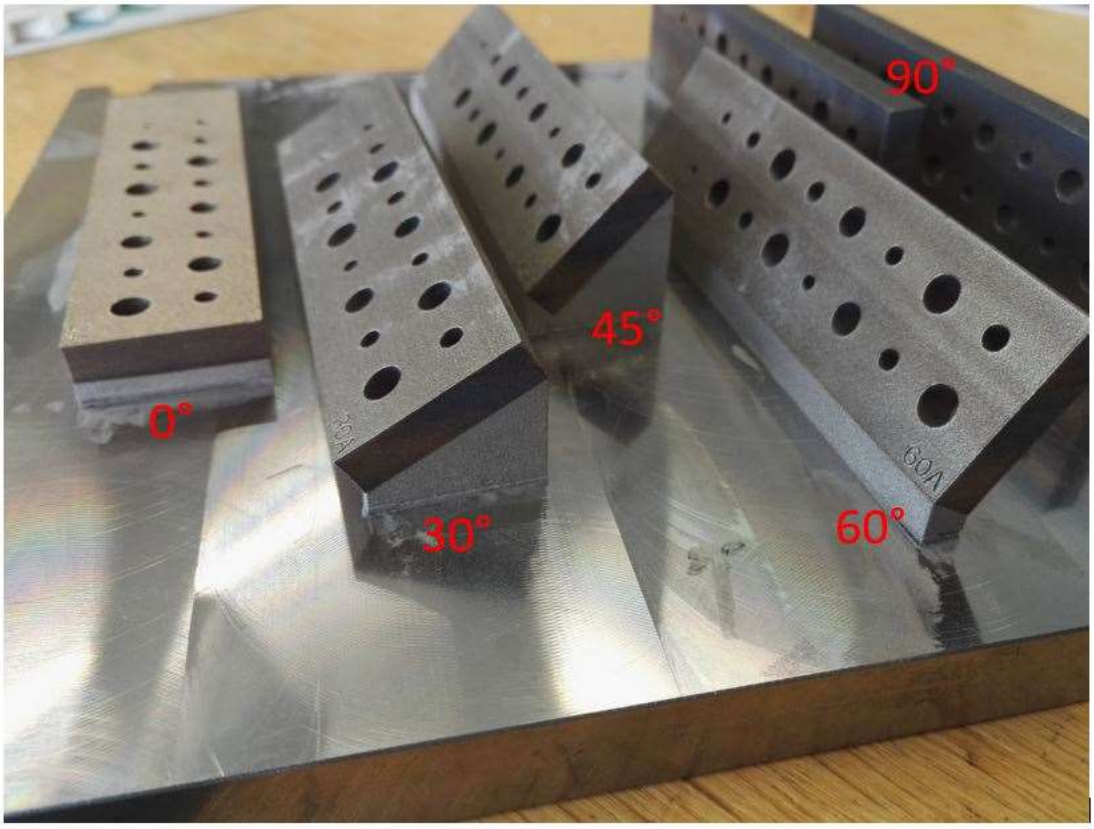

Figure 85: Maraging steel, as-built, parts placed 5° to recoater

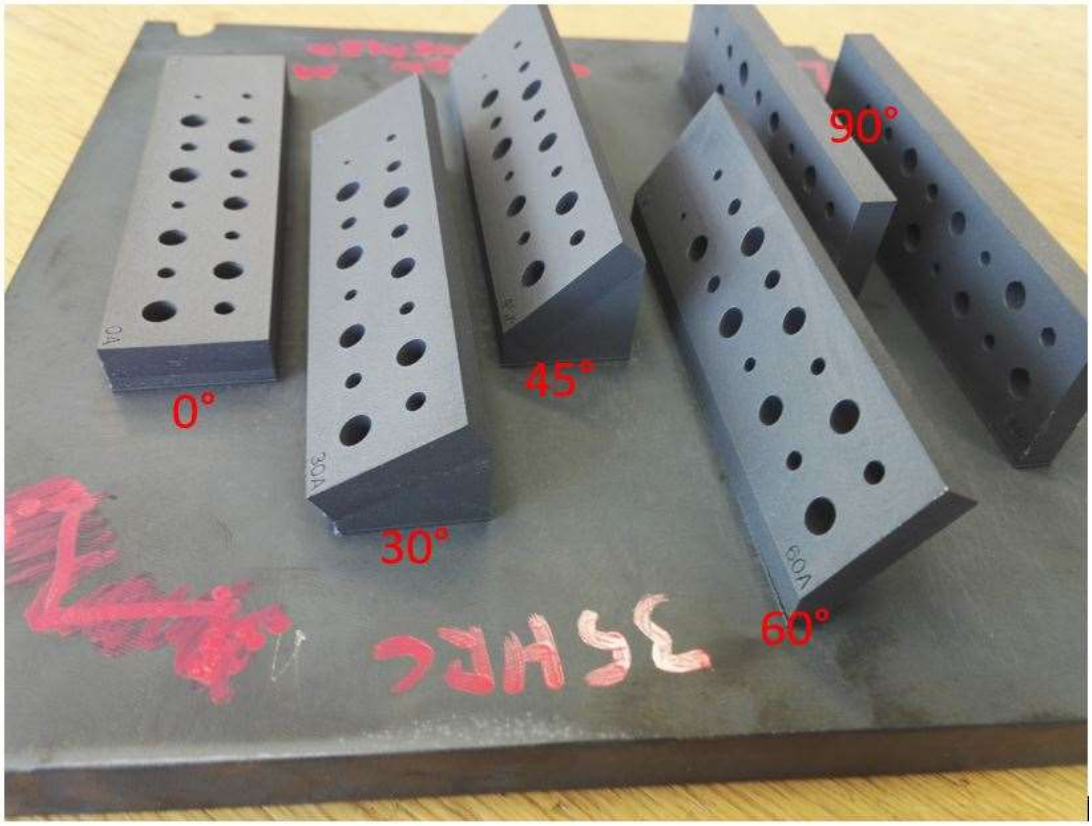

Figure 86: Maraging steel, solution treated, parts placed 5° to recoater

Heat treatment

In solution treatment (solution annealing), components are held at 940 °C for 2 hours. Rapid air-cooling cools down parts to 32 °C with a cooling rate of 20-60 °C/min. Solution treatment reduces amount of austinite in martensite matrix. This is done in inert environment. [24]

Components can also be age-hardened at 490 °C for 6 hours to get higher strength and hardness more than 50 HRC, by precipitation hardening. However, this treatment was not applied to the parts in this study.

4.2.1 Flatness

Flatness of maraging steel components is measured by CMM. These flatness values represent extent of unevenness. Smaller the flatness value, the more even the surface. When attached to build plate, the parts appeared to be more even, than being removed from build plate. Thermal stresses build up during printing process is probably the root cause for this curving.

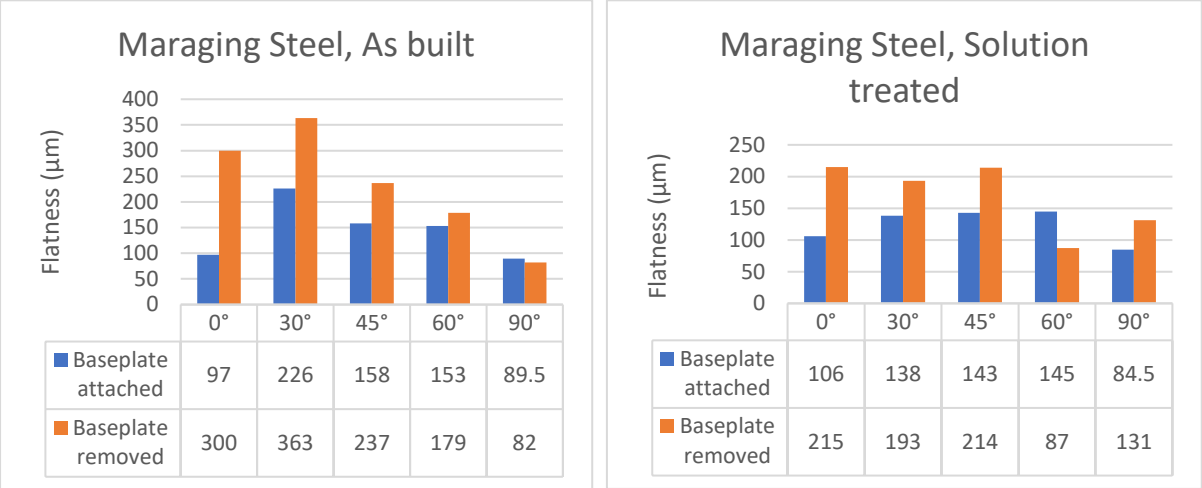

Figure 87: Flatness, MS1, as-built, 5° recoater angle (Left) and Flatness, MS1, Solution Treated, 5° recoater angle (Right)

Discussion

Figure 87 shows flatness of parts has reduced after being removed from build pate. This kind of behaviour is expected for as-built material having more internal stresses build up during printing process. Difference of flatness before and after removal from baseplate is higher for 0°, 30° and 45°, where supports used are having more contact area to build plate. For 60° and 90° printing inclinations, support's contact area is reduced and so does flatness value.

For solution treated parts, flatness value has slightly improved compared to as-built components. These flatness values are higher compared to solution treated aluminium components.

4.2.2 Surface Roughness

Surface roughness of maraging steel is measured with Taylor Hobson equipment and shown in Figure 88.

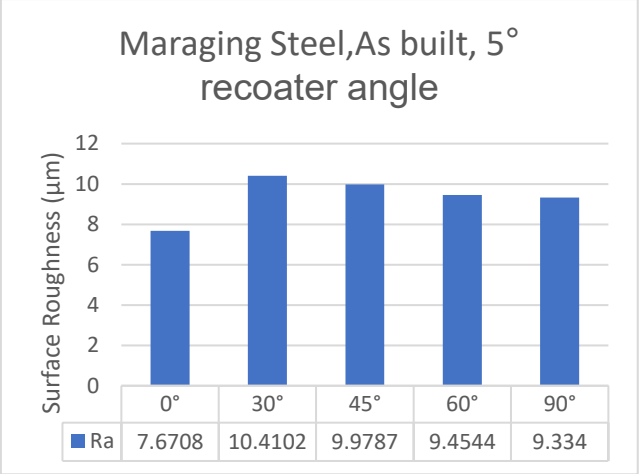

Figure 88: Surface roughness of Maraging steel

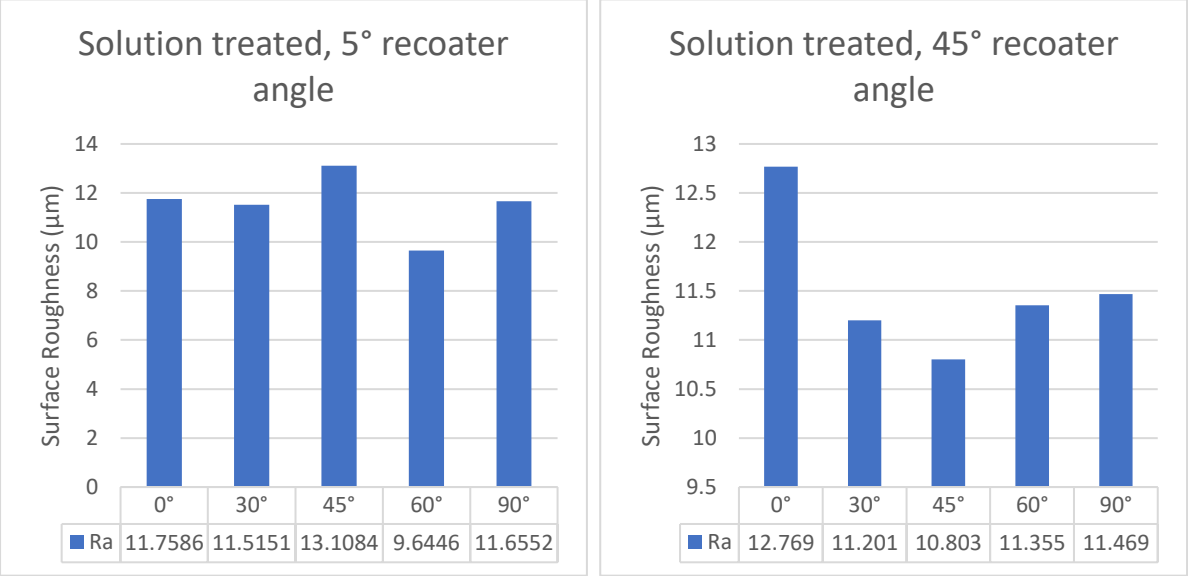

Figure 89: comparison of surface roughness of Maraging steel, solution treated, 5° and 45° to recoater

Discussion

Surface roughness of as built maraging steel is better than that of solution treated maraging steel. Roughness value for as-built parts is smaller for 0° printing inclination and then remains consistent for other inclinations.

Surface roughness of solution treated samples does not seem to be a function of printing inclination for maraging steel, or no visible trend can be identified. Printed surface is rougher as compared to a milled surface so appropriate machining process should follow, if higher surface properties are required. Maraging steel components showed better surface properties than solution treated aluminium components.

4.2.3 Hardness

Figure 90 shows Rockwell hardness, measured for printed maraging steel components, in three different states. As-built maraging steel work pieces are not annealed, and so thermal stresses originated from

printing process remained in material. Stress reliving is done in solution treated components, placed at 5° and 45° to recoater direction on build plate.

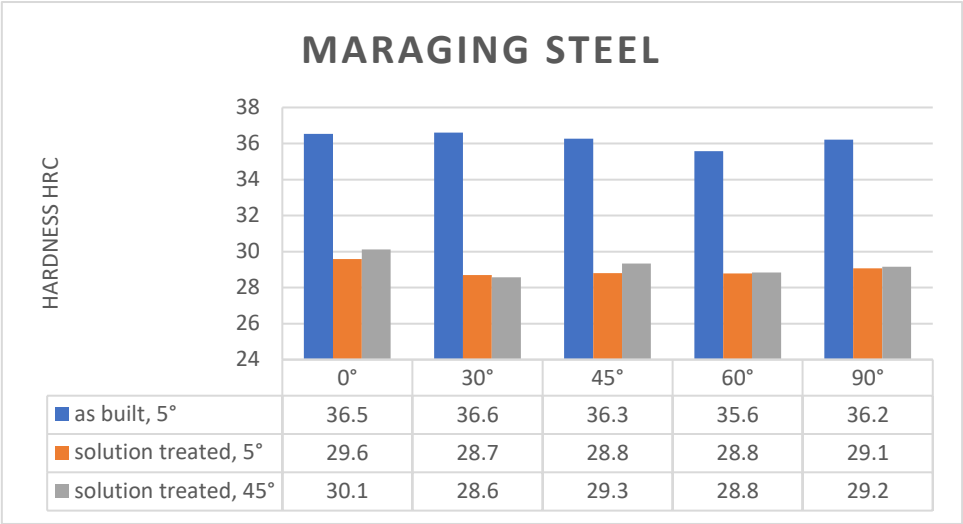

Figure 90: Hardness (Rockwell C) comparison of Maraging steel

Discussion

Hardness is measured along face A as shown in Figure 51, but instead of Vickers, Rockwell C scale is used. Hardness of as-built maraging steel is higher than solution treated components. Variation is not significant along different printing inclinations for as-built and solution treated components, implying uniform hardness of material. On other hand, hardness is not changed significantly for solution treated parts printed at 5° and 45° on build plate. Based on data acquired from hardness measurements, it can be inferred that height and position of parts on build plate do not affect hardness of components in maraging steel.

4.2.4 Hole Diameter

Figure 89 shows a comparison of hole diameters measured with hole gauge and micrometre. These holes are studied for as-built maraging steel.

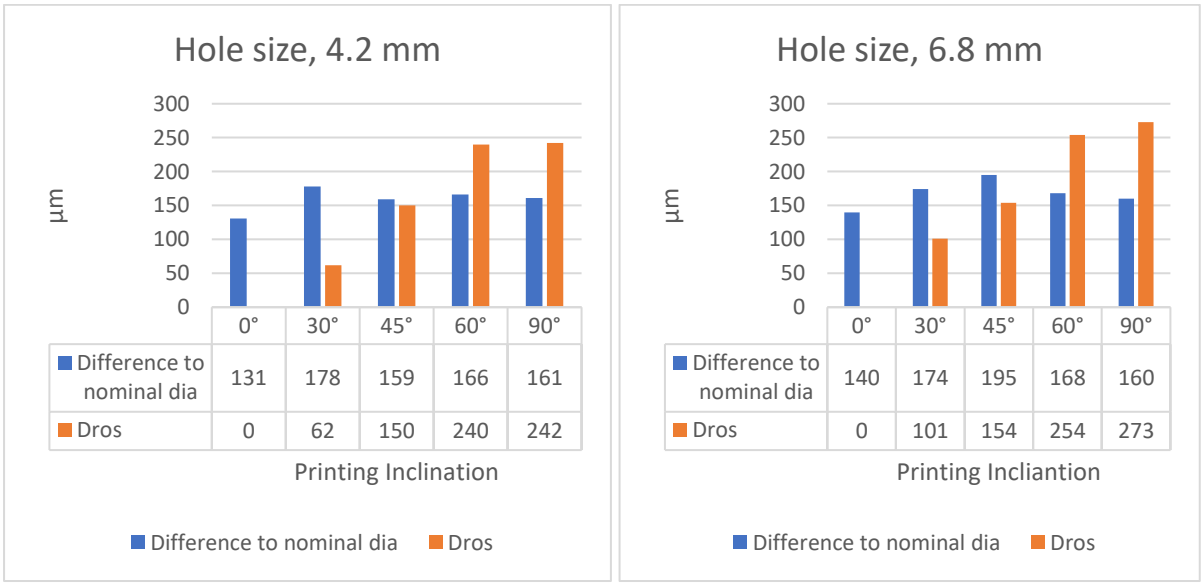

Figure 91: Hole size comparison of 4.2 mm and 6.8 mm holes printed in Maraging steel, As-built, 5° to recoater

Discussion

Printed pre-hole diameter is smaller than required dimensions and it remains constant with increase in printing inclination, but dross increases exponentially. Similar guidelines hold true for hole-printing in maraging steel as the recommended for aluminium in previous discussion. When holes are to be made to nominal diameter by drilling, dross will be removed. Detailed information of printed holes diameter in maraging steel is attached in appendix B.

4.2.5 Cutting Forces

Pre-holes made in maraging steel components, shown in Figures 85 and 86, are drilled and tapped with similar process as was used for aluminium. Kistler sensor was used to measured axial drilling force and torque. Torque measured was too small and it was not included in results. Table 16 enlists axial thrust forces (in newtons), measured during drilling for various pre-holes and along different printing inclinations for as-built maraging steel components. Colour formatting is applied to visualise any trend in drilling forces.

As-built Maraging steel, 5° recoater angle

Table 16: Axial drilling forces (N) for as-built maraging steel for 4.2 mm and 6.8 mm drills

Printing inclination	0°	30°	45°	60°	90°			Printing inclination	0°	30°	45°	60°	90°		
pre-hole diameter (mm)	Force (N) for drilling 4.2 mm hole					Mean force (N)	Range (N)	pre-hole diameter (mm)	Force (N) for drilling 6.8 mm hole					Mean force (N)	Range (N)
0	477	493	483	481	482	483	16	0	1043	1068	1051	1051	1050	1053	24
2	193	201	201	201	196	198	9	2	472	503	484	482	490	486	31
3.2	87	90	90	90	91	90	4	5.8	122	159	157	157	152	149	37
3.5	67	75	76	76	77	74	10	6.1	91	123	119	119	123	115	32
3.8	46	50	50	49	49	49	4	6.4	66	101	89	89	101	89	35
Mean Force (N)	174	182	180	179	179			Mean Force (N)	359	391	380	380	383		

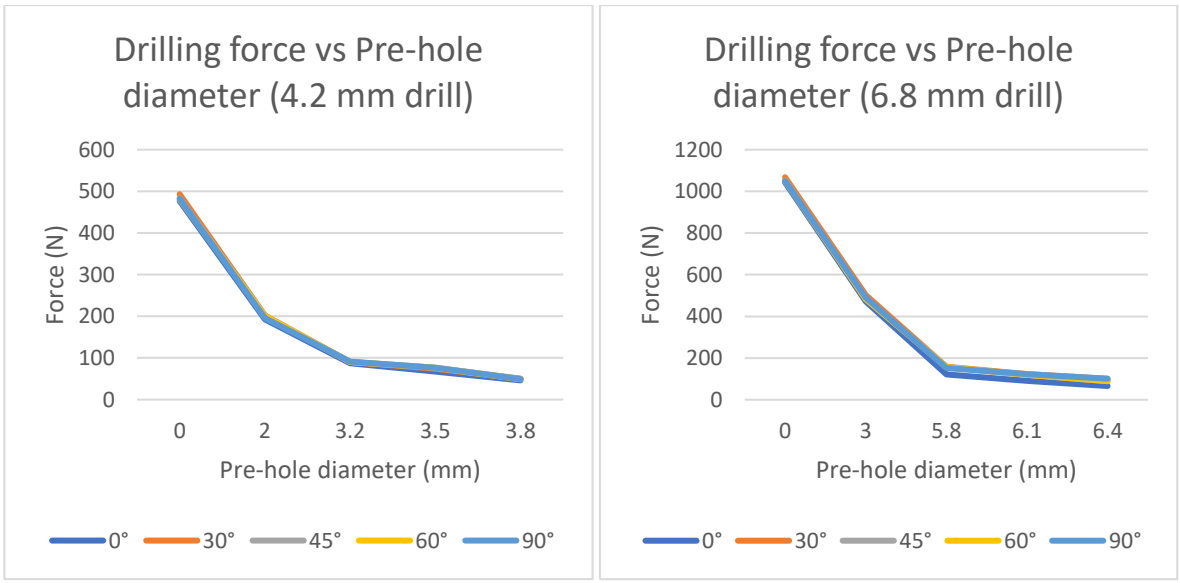

Figure 92: Axial drilling force variation with pre-hole sizes in as-built, MS1 (5° to recoater)

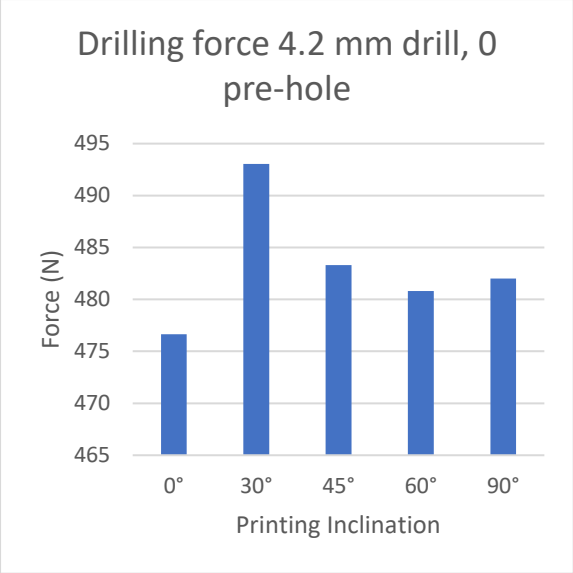

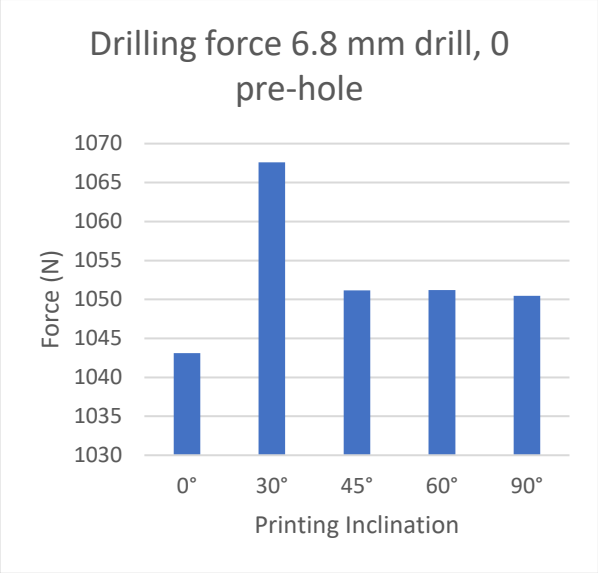

Figure 93: Drilling force variation with printing inclination in 0 pre-hole for As-built, MS1 (5° recoater angle)

Discussion

Horizontal (0°) components showed lowest forces while 30° components gave highest forces. From 45° onward to 90° printing inclination, force then remained constant. Figure 93 visually present this fact for drilling in solid material i.e. without any pre-hole. Both drills 4.2 mm and 6.8 mm showed similar results but difference of forces among printing inclination was more evident for 6.8 mm drill.

When axial drilling forces are plotted against various pre-hole diameter, results obtained are presented in Figure 92. This is in accordance with already known fact that with reduction in pre-hole diameter, drilling forces can be minimised [30, page 220]. For 2 mm and 3 mm pre-holes for 4.2 mm and 6.8 mm drill, axial forces are halved.

Maraging steel, Solution treated (ST), 5° recoater angle

Table 17 contains drilling forces for ST, maraging steels components printed 5° to recoater.

Table 17: Axial drilling forces(N) for solution treated maraging steel for 4.2 mm and 6.8 mm drills, 5° to recoater

Printing Inclination	0°	30°	45°	60°	90°			Printing Inclination	0°	30°	45°	60°	90°		
pre-hole diameter (mm)	Force (N) for drilling 4.2 mm hole					Mean Force (N)	Range (N)	pre-hole diameter (mm)	Force (N) for drilling 6.8 mm hole					Mean Force (N)	Range (N)
0	451	458	456	461	463	458	12	0	1077	1098	1040	909	1069	1039	189
2	158	158	163	167	159	161	9	2	429	453	460	490	485	464	61
3.2	72	75	74	77	75	75	5	5.8	138	137	142	207	200	165	70
3.5	62	58	61	63	60	61	6	6.1	111	110	115	179	170	137	69
3.8	56	38	37	39	42	42	18	6.4	88	87	91	150	125	108	63
Mean Force (N)	304	308	310	314	311			Mean Force (N)	753	776	750	700	777		

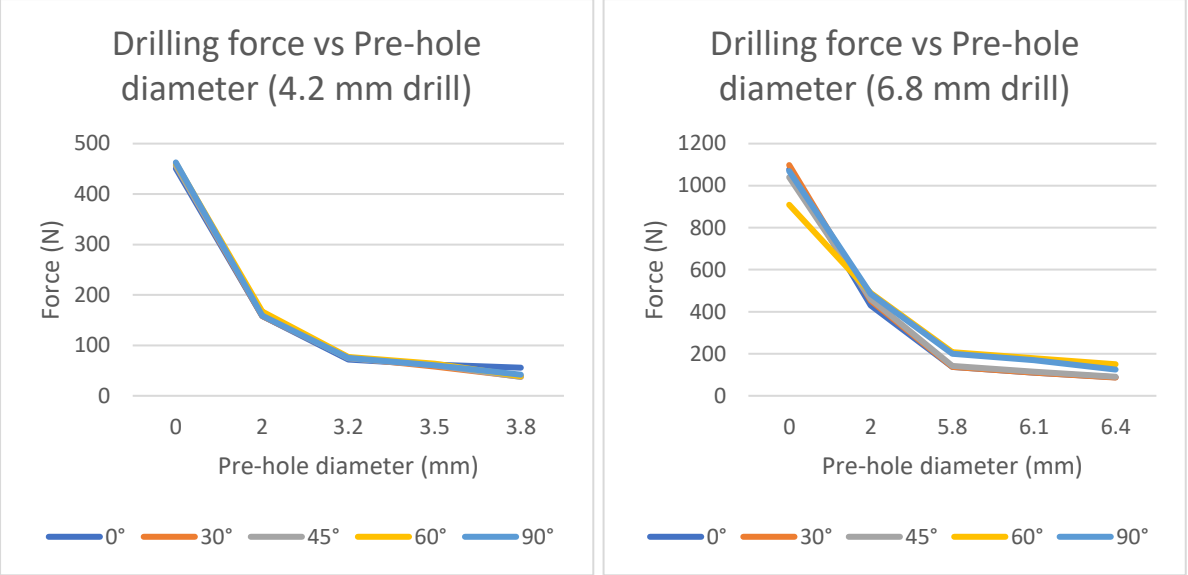

Figure 94: Axial drilling force variation with pre-hole sizes in Solution treated, MS1 (5° to recoater)

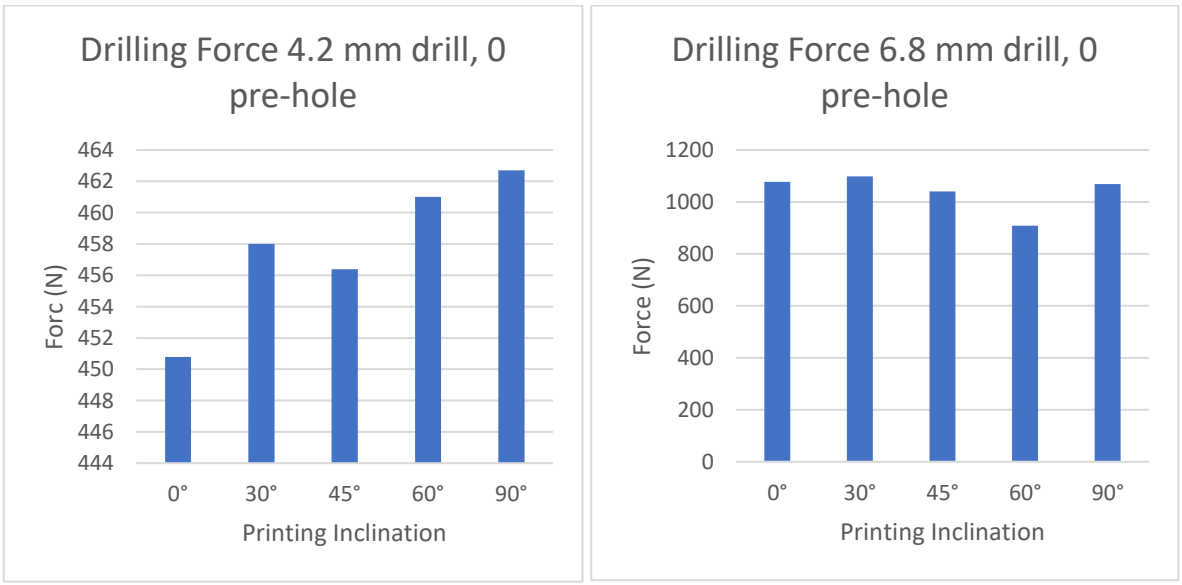

Figure 95: Drilling force variation with printing inclination in 0 pre-hole for Solution treated, MS1 (5° recoater angle)

Discussion

Drilling forces are reduced a bit for ST components compared to as-built condition for 4.2 mm drill, but values remained same for 6.8 mm drill. Here it appears that for both drills, (vertical) 90° components are stronger than horizontal (0°) components. Range of forces along printing inclinations is much smaller with 6.8 mm drill.

Reduction in drilling forces with decreasing pre-hole diameters is illustrated in Figure 94. Greater difference in forces can be easily distinguished in 6.8 mm drill. Figure 95 shows this trend for direct drilling i.e. 0 pre-hole.

Maraging steel, Solution treated (ST), 45° recoater angle

ST, maraging steel components printed at 45° to recoater are drilled and tapped too. Drilling forces (newton) are listed in Table 18

Table 18: Axial drilling forces (N) for solution treated maraging steel for 4.2 mm and 6.8 mm drills, 45° to recoater

Printing Inclination	0°	30°	45°	60°	90°		
pre-hole diameter (mm)	Force (N) for drilling 4.2 mm hole					Mean Force (N)	Range (N)
0	444	455	461	468	464	458	24
2	153	151	158	156	158	155	7
3.2	69	70	73	67	73	70	6
3.5	58	55	57	55	54	56	4
3.8	37	37	39	37	37	38	3
Mean Force (N)	152	154	158	157	157		

Printing Inclination	0°	30°	45°	60°	90°		
pre-hole diameter (mm)	Force (N) for drilling 6.8 mm hole					Mean Force (N)	Range (N)
0	956	925	949	996	1012	968	87
3	385	385	386	394	367	383	27
5.8	90	94	93	90	86	91	8
6.1	67	68	71	64	64	67	7
6.4	47	51	54	49	47	50	7
	309	305	311	319	315		

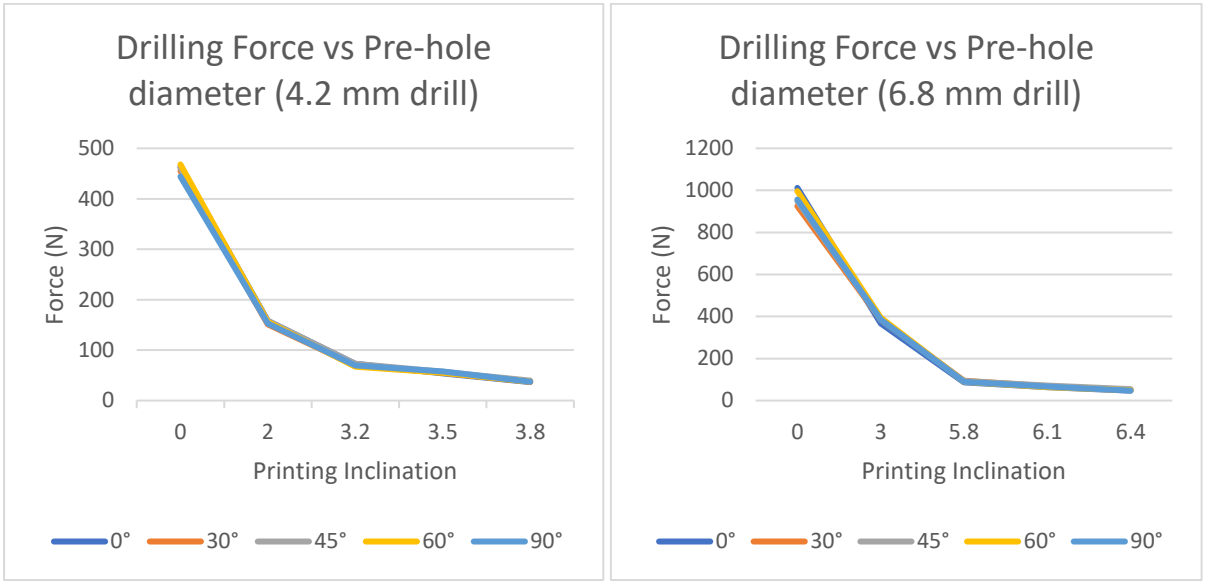

Figure 96: Axial drilling force variation with pre-hole sizes in Solution treated, MS1 (45° to recoater)

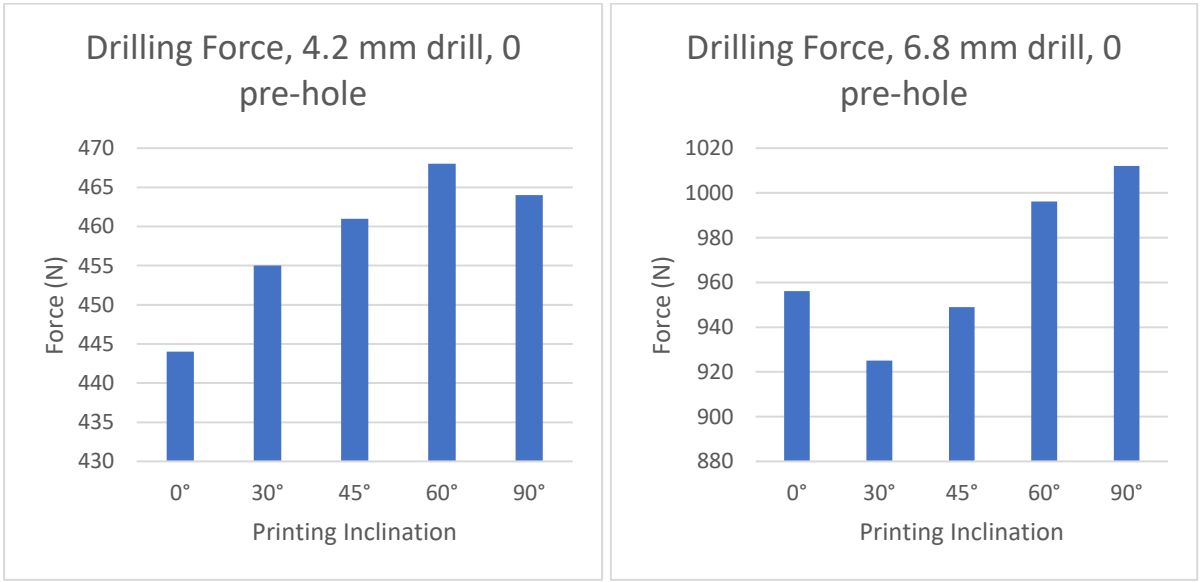

Figure 97: Drilling force variation with printing inclination in 0 pre-hole for Solution treated, MS1 (45° recoater angle)

Discussion

It is observed again that vertically oriented components are stronger than horizontal ones as shown in Figure 97. Drilling forces have reduced slightly with 4.2 mm drill in ST components compared to as-built condition, but reduction of forces is significant for 6.8 mm drill. Drilling forces are reducing the same way with reduction in pre-hole diameter (Figure 96).

Concluding remarks for drilling forces in Maraging steel

Drilling forces appeared to be reduced in solution treated components compared to as-built maraging steel. This trend was opposite in case of aluminium.

4.2.6 Machining issues

Carbide drills and HSS taps used for drilling and tapping of maraging steel grade 300, experienced tool wear. To avoid this, it is recommended to use tungsten carbide tools and lower cutting speeds.

4.2.7 Microstructure

Microstructures of printed, solution treated, maraging steel are shown in Figures 98 and 99 at 50X and 100X magnification.

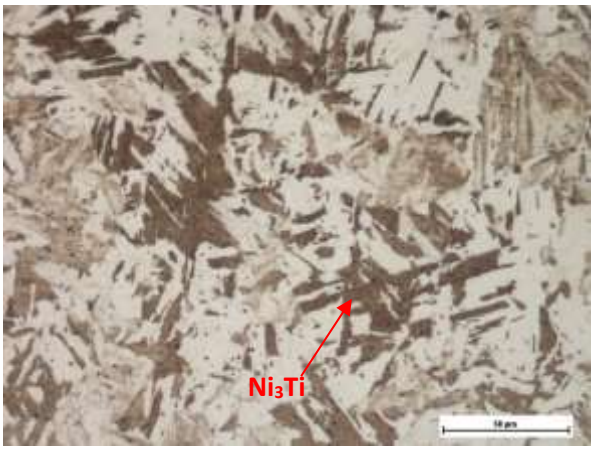

Figure 98: Maraging steel, ST, 5°, objective 50X

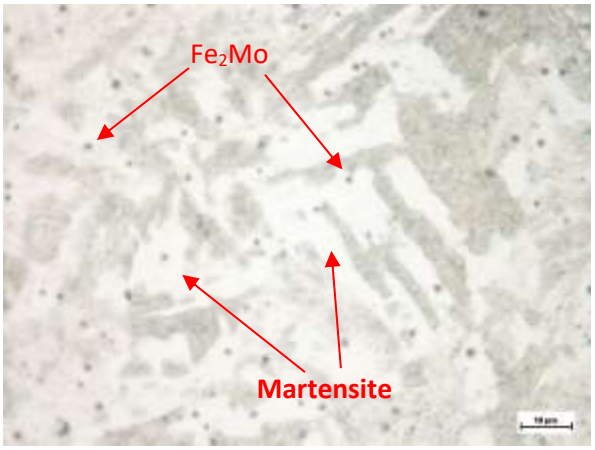

Figure 99: Maraging steel, ST, 5°, objective 100X

In microstructure, needle shaped structure is supposed to be Ni_3Ti and Fe_3Mo which are main strengthening elements in white martensitic matrix [28].

4.2.8 Macrographs

Optical microscope is used to observe presence of porosity in maraging steel components made by DLMS process. Holes printed at various inclinations were observed under optical microscope at 2.5X magnification and presented in Figures 100-102. Etchant specified in Table 5 is employed for this study.

Figure 100: 4.2 mm hole Maraging steel, 0° printing inclination, 5° to recoater

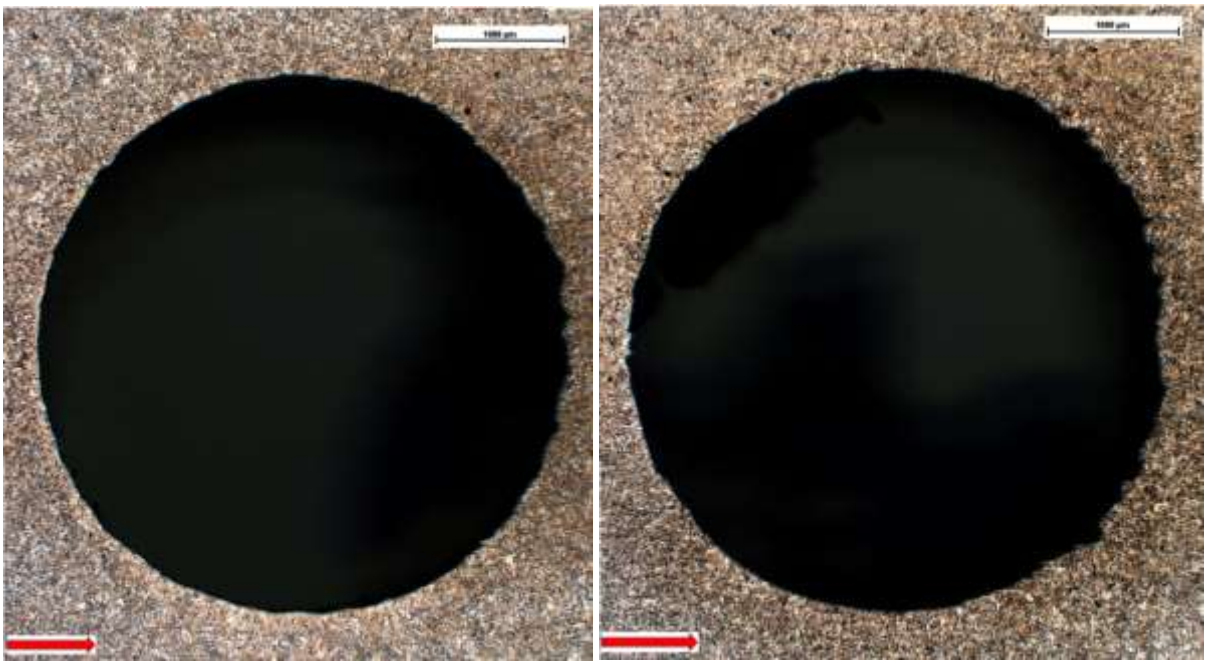

Figure 101: 4.2 mm hole Maraging steel, (left) 30° printing inclination (right) 45° printing inclination

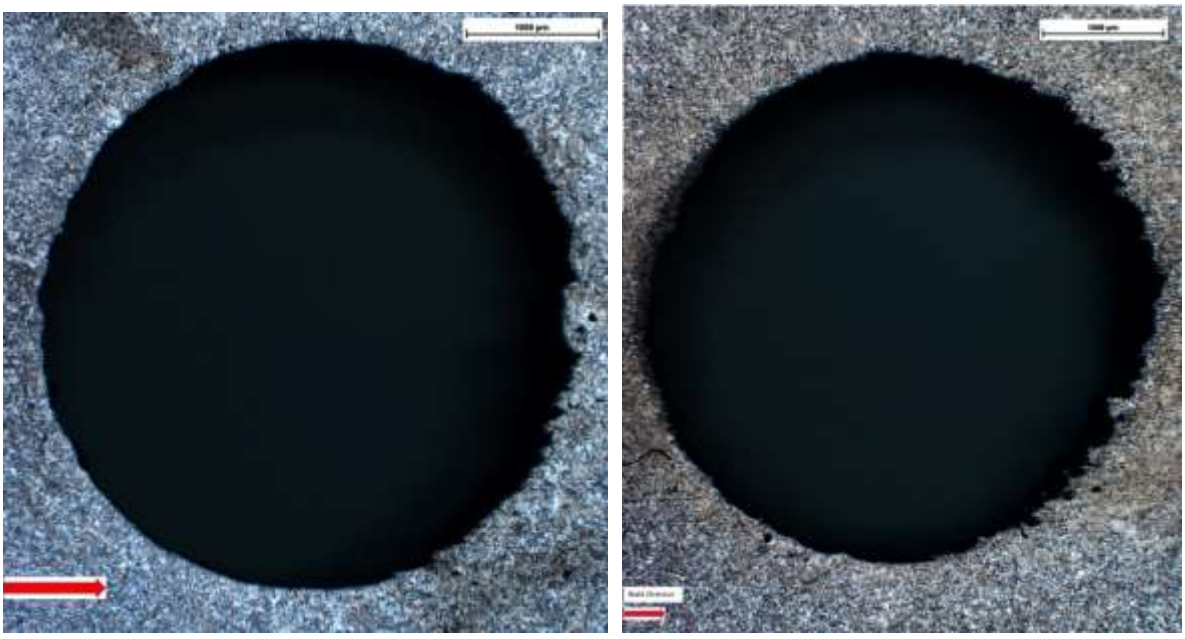

Figure 102: 4.2 mm hole Maraging steel, (left)60° printing inclination (right) 90° printing inclination

Discussion

We did not see any significant porosity in maraging steel prints in both as-built and solution treated components. Here too it was observed that horizontally printed holes i.e. 0° do not contain any dross. Dross increases as printing inclination increases. Dross contains some pores and must be removed. Shape of holes is identical to Figure 53 scheme.

4.2.9 Thread Profile

To investigate effect of porosity, threads were stripped using Figure 78 equipment. 12.9 strength class bolts failed during this test and threads remained intact. Broken bolts are shown in Figure 103. Threads

made in maraging steel components easily withstand 46 kN force. Special HSS bolt, stronger than 12.9 strength class bolts, was employed but it failed too.

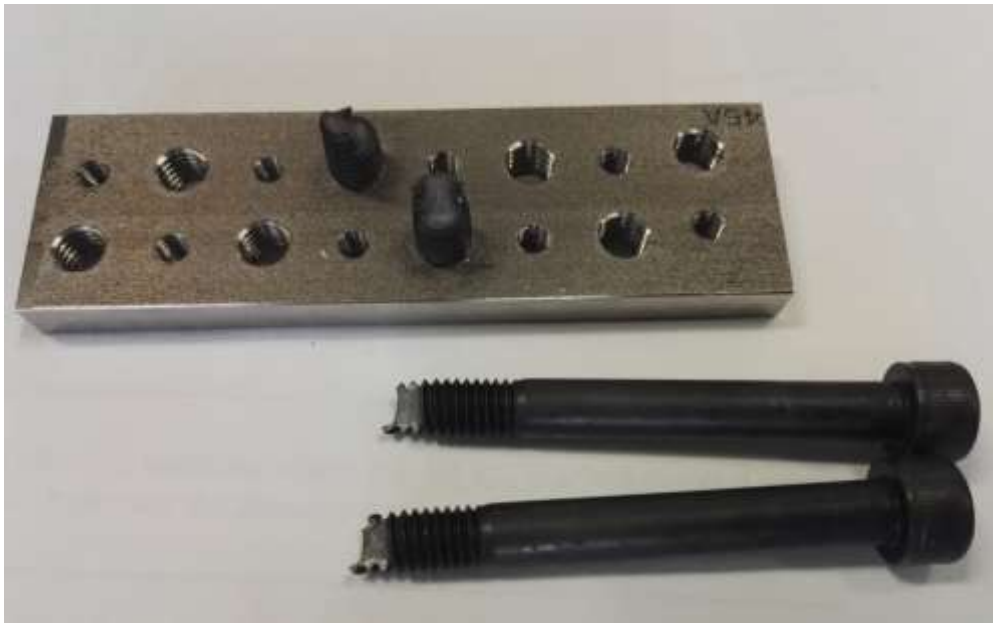

Figure 103: 12.9 strength class bolts broken; maraging steel threads remained intact

Figure 104 shows internal threads made in maraging steel. A section was cut from maraging steel specimen and shown in Figure 105. Optical microscope was used to observe threads profile manufactured in maraging steel. Walter TITEX's tools, as listed in Table 1 and 2, were used to make these threads and manufacturer's recommended machining parameters (feed and cutting speed) were used.

Figure 104: Internal threads, M5 & M8 made in Maraging steel

Figure 105: section cut from maraging steel for thread profile

Using optical microscope, thread profile was observed at magnification of 10X. Here term lower thread means threads made in downskin surface and upper thread means threads made in up-skin surfaces as illustrated in Figure 106.

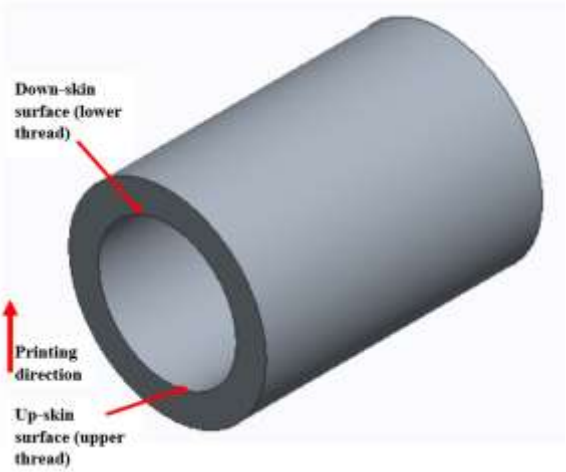

Figure 106: Schematic used for upper and lower thread

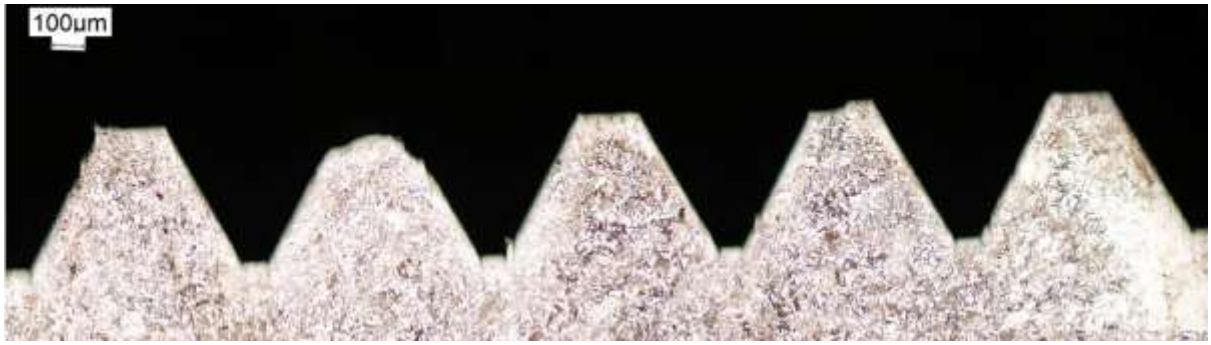

Figure 107: M5, pre-hole diameter 4.3 mm, lower thread profile, objective 10X, 45° printing inclination

Figure 108: M5, pre-hole diameter 4.3 mm, upper thread profile, objective 10X, 45° printing inclination

Figure 109: M8, pre-hole diameter 6.9 mm, lower thread profile, Objective 10X, 45° printing inclination

Figure 110: M8, pre-hole diameter 6.9 mm, upper thread profile, objective 10X, 45° printing inclination

Figure 111: M5, pre-hole diameter 4.3 mm, lower thread profile, Objective 10X, 90° printing inclination

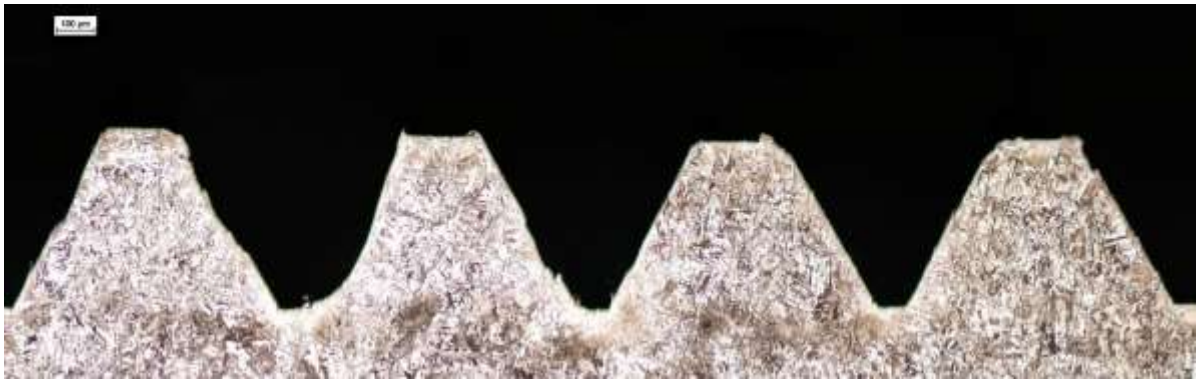

Figure 112: M5, pre-hole diameter 4.3 mm, upper thread profile, Objective 10X, 90° printing inclination

Figure 113: M8, pre-hole diameter 6.9 mm, lower thread profile, Objective 10X, 90° printing inclination

Figure 114: M8, pre-hole diameter 6.9 mm, upper thread profile, Objective 10X, 90° printing inclination

Discussion

It was observed that with recommended tools the machining parameters were not adequate and need to be adjusted for tool wear. Tool was wearing a lot during drilling and tapping and resulted threads were not completed along depth, as can be seen in Figures 107...110 and 113,114. Thread profiles seem to be more affected as tool penetrates more into the material.

Thread profiles presented here were made in biggest pre-holes, i.e. 4.3 mm and 6.9 mm. If there is likelihood of porosity, then this size is more suitable for observing porosity. Unlike aluminium, we did not detect ample porosity, neither in pre-holes nor in thread profiles. Off-centering can cause lack of material and will result in bad thread profile as can be observed in Figure 111. Thread profile depicted the impression of very sturdy threads in maraging steel.

We were not successful to quantify strength of threads made in maraging steel. Analysis was based on optical microscope results of thread profiles observed for biggest pre-holes, i.e. 4.3 mm and 6.9 mm for M5 and M8 respectively and at 90° inclination. It can be inferred that threads are of high quality and high strength, irrespective of printing inclination and pre-hole diameter. Yet it is recommended to avoid making threads directly into printed material due to presence of dross. Pre-holes very close to nominal diameter must be avoided to prevent off-centering effect and thereby undermining thread strength.

5 Conclusions

This chapter outlines conclusions drawn from experimentation and observations made on MDLS components. It can be stated that printing inclination does not affect too much material properties. It was observed for aluminium that build plate temperature played important role in determining parts accuracy. So, some parameters are material specific and must be optimized. For maraging steel, solution treatment has yielded better results than as-built material.

5.1 Specific conclusions

1. **Recoater angle**
   It is observed that material properties remain consistent in all part orientations to the recoater.

2. **Flatness**
   As-built components inherit stresses built up during DLMS process, irrespective of printing material used. For aluminium, build plate temperature of 200 °C has resulted in better part accuracy than 35 °C. For maraging steel, solution treatment (ST) of printed parts retains the flatness after removal from build plate. Flatness of aluminium was better in AB-200 state than for solution treated maraging steel.

3. **Surface roughness**
   Based on DLMS process parameters, surface roughness can vary. For EOS's surface 1.0 mode, smoother surface can be achieved at cost of longer printing time. Similarly printing with EOS's speed 1.0 mode will reduce printing time but surface produced will be comparatively rough. Printing parameters can significantly affect surface of printed parts.

4. **Hardness**
   For aluminium, hardness varies with printing inclination, but variations are small. For AB-200 parts, vertically printed (90°) components are softer than horizontally (0°) printed components, indicating anisotropy.
   As-built maraging steel is harder than ST maraging steel. Printing inclination does not affect hardness significantly.

5. **Hole sizes**
   Printing pre-holes will save ample printing material and time. Printed holes were undersized from required nominal diameter. This difference to nominal size is unaffected with printing inclination but dross grows exponentially from 0° to 90° printing inclination. Dross only appears on downskin surfaces. All dross is removed once holes are drilled to their nominal size.

6. **Machining allowances**
   For internal holes, machining allowances are not required as holes are undersized after printing process due to shrinkage.

7. **Axial drilling forces**
   Increasing pre-hole diameter reduces axial drilling forces. So, making pre-holes is beneficial as it will reduce axial forces experienced by printed material.

8. **Thread strength (Aluminium)**
   Internal threads made in vertically printed components are somewhat stronger than horizontally printed ones. So, in this way printing inclination affects thread strength.

Maraging steel
Internal thread made in maraging steel did not show porosity and survived 46kN axial stripping force for M8. Qualitatively, it can be stated that these were high quality threads.

5.2 Practical guidelines

1. **Machining allowances**
   Dross is typically present in inclined holes and affects material properties up to 0.2 mm. Additionally if it is considered that no shrinkage occurs during printing process at all and for keeping on safe side, machining allowance of 0.2 mm for aluminium and 0.1 mm for maraging steel are recommended.

2. **Drilling forces**
   For fragile 3D printed structures, large pre-holes cut down axial forces by 75-80%.

3. **Thread strength**
   Although not all the data acquired from thread stripping experiments suggest that variation of pre-hole diameter has substantial effect on thread strength, nonetheless it is recommended to keep at least 0.2 mm difference from nominal size to avoid surface porosity. To be on safe side it is also recommended to keep pre-hole diameter around 1 mm smaller than nominal size to avoid lacking material in threads due to off-centering problems.

5.3 Evaluation of Reliability

In this study, as most of the results were obtained experimentally, so human error might have influenced. This was minimised by taking multiple readings (for hardness, surface roughness and hole size measurement) and using different experimental methods. In discussion section, results of experiments are explained which are subjective.

During experimentation, only one set of parameters of pre-hole sizes and printing inclinations were tested, i.e. all combinations were unique, no repetition was made. This can reduce reliability of results.

Also, it can be noted that a lot of peaks are observed in results, indicating variations in the property to be measured, so a careful interpretation is required.

5.4 Recommendations for further research

For further research following questions are put forth:

- In case of aluminium, effect of solution treatment on material properties must be investigated. How printing inclination affects physical properties like flatness, hardness, porosity and surface roughness for solution treated parts. Drilling forces and thread strength should be compared with as-built samples.
- For maraging steel, machinability in hardened state, i.e. after aging, must be investigated.
- What are appropriate machining parameters and cutting tools employed for machining of maraging steel?
- Does aging affect thread profile and dimensions?

6 References

[1] Additively Ltd., 2017 [Online] Overview over 3D printing technologies.

Retrieved from additively: https://www.additively.com/en/learn-about/3d-printing-technologies. Accessed at 2018, November 20

[2] Customerpart.net. [Online] Laminated Object Manufacturing. Retrieved from Customerpart.net: http://www.custompartnet.com/wu/laminated-object-manufacturing; Accessed at 2018, November 18

[3] Robles Hernandez F.C., Herrera Ramírez J.M., Mackay R., 2017, Al-Si Alloys, Minor, Major, and Impurity Elements. Pages 1-15, Springer, Cham

[4] Takata, N., Kodaira, H., Sekizawa, K., Suzuki, A., Kobashi, A., 2017, Change in Microstructure of Selectively Laser Melted AlSi10Mg Alloy with Heat Treatments. Materials Science and Engineering, Vol 704, pp 218-228

[5] Mouritz, Adrian P., 2012, Steels for aircraft structures, Chapter: Introduction to Aerospace Materials, pp 232-250, Woodhead Publishing Limited

[6] Kruth, J-P., Yasa, E., Badrossamay, M., Deckers, J., Thijs, L., & Humbeeck, Jv., 2010, Part and material properties in selective laser melting of metals. 16th International Symposium on Electromachining

[7] Du, W., Bai, Q., & Zhang, B., 2017, Machining characteristics of 18Ni-300 steel in additive/subtractive hybrid manufacturing. The International Journal of Advanced Manufacturing Technology. Vol 95, pp 2509–2519

[8] Saint John, D., Joshi, S., Simpson, T., Qu, M., Rowatt, J., & Lou, Y., 2016, A Preliminary Examination of Variability Due to Build Location and Powder Feedstock in Additive Manufacture of Inconel 718 using Laser-Based Powder Bed Fusion. Proceedings of the 27th Annual International Solid Freeform Fabrication Symposium, 542

[9] Gibson, I., Rosen, D. & Stucker, B., 2015. Additive Manufacturing Technologies. New York, Springer

[10] Paschotta, D., 2008, [Online], Encyclopedia of Laser Physics and Technology - high-power lasers, high-powered, solid-state, rod, slab, thin-disk, fiber laser. Retrieved from https://www.rp-photonics.com/high_power_lasers.html

[11] Paschotta, D., 2008, [Online], Encyclopedia of Laser Physics and Technology - YAG lasers, Nd:YAG laser, Yb:YAG, yttrium aluminum garnet. Retrieved from https://www.rp-photonics.com/yag_lasers.html

[12] Paschotta, D., 2008, [Online], Encyclopedia of Laser Physics and Technology - CO2 lasers, carbon dioxide laser. Retrieved from https://www.rp-photonics.com/co2_lasers.html

[13] Rosenthal, I., Stern, A., & Frage, N., 2014, Microstructure and Mechanical Properties of AlSi10Mg Parts Produced by the Laser Beam Additive Manufacturing (AM) Technology. Metallography, Microstructure, And Analysis, 3(6), pp 448-453

[14] Su, X., & Yang, Y., 2012, Research on track overlapping during Selective Laser Melting of powders. Journal of Materials Processing Technology, Vol 212, pp 2074-2079

[16] Fortunato, A., Lulaj, A., Melkote, S., Liverani E., Ascari A., & Umbrello D., 2018, Milling of maraging steel components produced by selective laser melting. The International Journal of Advanced Manufacturing Technology, Vol 94, pp 1895–1902.

[17] Kranz, J., Herzog, D., & Emmelmann C., 2015, Design guidelines for laser additive manufacturing of lightweight structures in TiAl6V4. Journal of Laser Applications, 27(S1)

[18] Moylan, S., Slotwinski, J., Cooke, A., Jurrens, K., & Donmez, M., 2019, [Online] Lessons Learned in Establishing the NIST Metal Additive Manufacturing Laboratory. Retrieved from https://www.nist.gov/publications/lessons-learned-establishing-nist-metal-additive-manufacturing-laboratory

[19] Li, W., Li, S., Liu, J., Zhang, A., Zhou, Y., & Wei, Q. et al, 2016, Effect of heat treatment on AlSi10Mg alloy fabricated by selective laser melting: Microstructure evolution, mechanical properties and fracture mechanism. Materials Science and Engineering: A, Vol 663, 116-125.

[20] Mondolfo, L. F.,1976, Aluminium alloys: Structure and properties. London: Butterworths.

[21] Gu, D., & Shen, Y., 2009, Balling phenomena in direct laser sintering of stainless-steel powder: Metallurgical mechanisms and control methods. Materials & Design, Vol 30, pp 2903-2910

[22] Kurzynowski, T., Chlebus, E., & Kuźnicka, B., & Reiner, J., 2012, Parameters in Selective Laser Melting for processing metallic powders. Proceedings of SPIE. 8239. 823914

[23] Sandvik Coromant [Online], Downloads. Retrieved from: http://sandvik.ecbook.se/se/en/training_handbook/; Accessed on 20 May 2018

[24] EOS. Systems and Solutions for Metal Additive Manufacturing. Retrieved from: https://www.eos.info/material-m; Accessed on 18 November 2018

[25]VTT Technical Research Centre of Finland Ltd. Publications. [Online], Retrieved from: www.vttresearch.com/services/smart-industry/factory-of-the-future-(2)/materials-and-manufacturing/3d-printing ; Accessed on 20 May 2018

[26] Mechanical properties of fasteners made of carbon steel and alloy steel -- Part 2: Nuts with specified property classes, Coarse thread and fine pitch thread. ISO 898-2 (2012) test. Retrieved from: https://www.iso.org/standard/46228.html

[27] Watler TITEX. [Online], Retrieved from: https://www.walter-tools.com/en-gb/pages/default.aspx

[28] Montevecchi, F., Grossi, N., Takagi, H., Scippa, A., Sasahara, H., & Gianni Campatelli, 2016, Cutting Forces Analysis in Additive Manufactured AISI H13 Alloy. Procedia CIRP, Vol 46, pp 476-479

[28] Zhu, F., Yin, Y.F., & Faulkner, R.G., 2011, Microstructural control of maraging steel C300. Materials Science and Technology. Vol 27, pp 395-405

[29] Mathers, G., 2002, The Welding of Aluminium and its Alloys. Woodhead Publishing.

[30] Viktor P, A., 2010, Geometry of Single-point Turning Tools and Drills.

[31] Vander, V. G. F.,1999, Metallography, principles and practice. Materials Park, OH: ASM International.

[32] Shunmugavel, M., Goldberg, M., Polishetty, A., Nomani, J., Sun, S., & Littlefair, G., 2017, Chip formation characteristics of selective laser melted Ti–6Al–4V. Australian Journal of Mechanical Engineering, 1-18.

[33] Le Coz, G., Fischer, M., Piquard, R., D'Acunto, A., Laheurte, P., & Dudzinski, D. (2017). Micro Cutting of Ti-6Al-4V Parts Produced by SLM Process. Procedia CIRP, Vol 58, 228-232

Appendices

Appendix A: Hole diameters of printed pre-holes

Appendix B: Drilling forces for various pre-holes and printing inclinations

Appendix: A

Hole diameter variation, AB-35 AlSi10Mg, 5° recoater angle

Printing Inclination	0°		30°				45°			
Nominal diameter (mm)	Major Diameter d1 (mm)	Difference to nominal dia (µm)	Major Diameter d1 (mm)	Difference to nominal dia (µm)	Minor dia d2 (mm)	Dross (µm)	Major Diameter d1 (mm)	Difference to nominal dia (µm)	Minor dia d2 (mm)	Dross (µm)
3.2	3.133	67	3.043	157	3	43	3.06	140	3.02	40
3.5	3.435	65	3.38	120	3.252	128	3.395	105	3.31	85
3.8	3.71	90	3.64	160	3.528	112	3.608	192	3.532	76
4.1	4	100	3.923	177	3.805	118	3.963	137	3.935	28
4.2	4.122	78	4.065	135	3.925	140	4.045	155	3.965	80
4.3	4.23	70	4.18	120	4.105	75	4.16	140	4.123	37
Average		78		145		103		145		58
5.8	5.669	131	5.66	140	5.552	108	5.69	110	5.617	73
6.1	5.977	123	5.857	243	5.715	142	5.95	150	5.89	60
6.4	6.27	130	6.25	150	6.143	107	6.29	110	6.215	75
6.7	6.558	142	6.553	147	6.335	218	6.6	100	6.492	108
6.8	6.672	128	6.635	165	6.573	62	6.672	128	6.543	129
6.9	6.76	140	6.693	207	6.582	111	6.785	115	6.677	108
Average		132		175		125		119		92

Printing Inclination	60°				90°			
Nominal diameter (mm)	Major Diameter d1 (mm)	Difference to nominal dia (µm)	Minor dia d2 (mm)	Dross (µm)	Major Diameter d1 (mm)	Difference to nominal dia (µm)	Minor dia d2 (mm)	Dross (µm)
3.2	3	200	2.9	100	2.98	220	2.65	330
3.5	3.35	150	3.2	150	3.31	190	3.17	140
3.8	3.66	140	3.58	80	3.638	162	3.335	303
4.1	3.923	177	3.89	33	3.939	161	3.76	179
4.2	4.055	145	3.925	130	4.041	159	3.673	368
4.3	4.2	100	4.13	70	4.185	115	3.819	366
Average		152		94		168		281
5.8	5.64	160	5.41	230	5.603	197	5.02	583
6.1	5.94	160	5.87	70	5.95	150	5.368	582
6.4	6.26	140	6.025	235	6.182	218	5.873	309
6.7	6.55	150	6.47	80	6.557	143	6.255	302
6.8	6.64	160	6.5	140	6.65	150	6.258	392
6.9	6.75	150	6.51	240	6.735	165	6.255	480
Average		153		166		171		441

Hole diameter variation, AB-200, AlSi10Mg, 5° recoater angle

Printing Inclination	0°		30°				45°			
Nominal diameter (mm)	Major Diameter d1 (mm)	Difference to nominal dia (µm)	Major Diameter d1 (mm)	Difference to nominal dia (µm)	Minor dia d2 (mm)	Dross (µm)	Major Diameter d1 (mm)	Difference to nominal dia (µm)	Minor dia d2 (mm)	Dross (µm)
3.2	3.12	80	3.12	80	3.055	65	3.132	68	3.03	102
3.5	3.42	80	3.413	87	3.358	55	3.435	65	3.315	120
3.8	3.695	105	3.7	100	3.6	100	3.735	65	3.6	135
4.1	4.08	20	4.025	75	3.925	100	4.073	27	3.905	168
4.2	4.12	80	4.1	100	4.045	55	4.165	35	4.05	115
4.3	4.21	90	4.268	32	4.125	143	4.268	32	4.06	208
Average		76		79		86		49		141
5.8	5.67	130	5.71	90	5.595	115	5.683	117	5.54	143
6.1	5.967	133	6.005	95	5.88	125	6.015	85	5.81	205
6.4	6.303	97	6.308	92	6.167	141	6.27	130	6.145	125
6.7	6.638	62	6.57	130	6.465	105	6.583	117	6.42	163
6.8	6.7	100	6.665	135	6.583	82	6.704	96	6.59	114
6.9	6.81	90	6.78	120	6.7	80	6.785	115	6.46	325
Average		102		110		108		110		179

Printing Inclination	60°				90°			
Nominal diameter (mm)	Major Diameter d1 (mm)	Difference to nominal dia (µm)	Minor dia d2 (mm)	Dross (µm)	Major Diameter d1 (mm)	Difference to nominal dia (µm)	Minor dia d2 (mm)	Dross (µm)
3.2	3.03	170	2.82	210	3.15	50	2.7	450
3.5	3.4	100	3.205	195	3.43	70	3.02	410
3.8	3.78	20	3.48	300	3.74	60	3.29	450
4.1	4.06	40	3.83	230	4.015	85	3.73	285
4.2	4.175	25	3.865	310	4.115	85	3.8	315
4.3	4.22	80	3.96	260	4.24	60	3.74	500
Average		73		251		68		402
5.8	5.69	110	5.37	320	5.69	110	5.27	420
6.1	6.03	70	5.775	255	5.98	120	5.63	350
6.4	6.303	97	5.98	323	6.32	80	5.8	520
6.7	6.59	110	6.32	270	6.58	120	6.1	480
6.8	6.665	135	6.4	265	6.705	95	6.35	355
6.9	6.75	150	6.53	220	6.78	120	6.47	310
Average		112		276		108		406

Hole diameter variation, AB-200, AlSi10Mg, 45° recoater angle

Printing Inclination	0°		45°				60°				90°			
Nominal diameter (mm)	Major Diameter d1 (mm)	Difference to nominal dia (µm)	Major Diameter d1 (mm)	Difference to nominal dia (µm)	Minor dia d2 (mm)	Dross (µm)	Major Diameter d1 (mm)	Difference to nominal dia (µm)	Minor dia d2 (mm)	Dross (µm)	Major Diameter d1 (mm)	Difference to nominal dia (µm)	Minor dia d2 (mm)	Dross (µm)
3.2	3.18	20	3.07	130	3	70	3.05	150	3	50	3	200	2.775	225
3.5	3.475	25	3.46	40	3.35	110	3.44	60	3.21	230	3.245	255	2.875	370
3.8	3.75	50	3.73	70	3.635	95	3.75	50	3.57	180	3.715	85	3.335	380
4.1	4.065	35	4.05	50	3.89	160	4.01	90	3.795	215	4	100	3.595	405
4.2	4.152	48	4.12	80	4.04	80	4.135	65	3.905	230	4.1	100	3.69	410
4.3	4.235	65	4.23	70	4.12	110	4.225	75	3.935	290	4.22	80	3.73	490
Average		40		73		104		82		199		137		380
5.8	5.72	80	5.675	125	5.56	115	5.715	85	5.46	255	5.66	140	5.28	380
6.1	5.995	105	5.985	115	5.855	130	5.97	130	5.73	240	5.98	120	5.59	390
6.4	6.35	50	6.3	100	6.17	130	6.27	130	6.11	160	6.24	160	5.87	370
6.7	6.615	85	6.6	100	6.36	240	6.6	100	6.31	290	6.59	110	6.17	420
6.8	6.69	110	6.725	75	6.5	225	6.65	150	6.425	225	6.65	150	6.3	350
6.9	6.795	105	6.75	150	6.56	190	6.81	90	6.515	295	6.795	105	6.32	475
Average		89		111		172		114		244		131		398

Hole diameter variation for As-built, Maraging steel, 5° recoater angle

Printing Inclination	0°		30°				45°			
Nominal diameter (mm)	Major Diameter d1 (mm)	Difference to nominal dia (µm)	Major Diameter d1 (mm)	Difference to nominal dia (µm)	Minor dia d2 (mm)	Dross (µm)	Major Diameter d1 (mm)	Difference to nominal dia (µm)	Minor dia d2 (mm)	Dross (µm)
3,2	3,08	120	3,01	190	2,97	40	3	200	2,92	80
3,5	3,387	113	3,32	180	3,27	50	3,355	145	3,2	155
3,8	3,655	145	3,6	200	3,535	65	3,66	140	3,5	160
4,1	3,97	130	3,92	180	3,86	60	3,94	160	3,79	150
4,2	4,05	150	4,06	140	3,96	100	4,055	145	3,89	165
4,3	4,17	130	4,12	180	4,06	60	4,137	163	3,95	187
Average		131		178		62		159		150
5,8	5,68	120	5,62	180	5,52	100	5,523	277	5,387	136
6,1	5,925	175	5,93	170	5,85	80	5,9	200	5,77	130
6,4	6,26	140	6,21	190	6,14	70	6,23	170	6,05	180
6,7	6,56	140	6,53	170	6,43	100	6,535	165	6,355	180
6,8	6,655	145	6,61	190	6,48	130	6,6	200	6,465	135
6,9	6,783	117	6,755	145	6,63	125	6,74	160	6,58	160
Average		140		174		101		195		154

Printing Inclination	60°				90°			
Nominal diameter (mm)	Major Diameter d1 (mm)	Difference to nominal dia (µm)	Minor dia d2 (mm)	Dross (µm)	Major Diameter d1 (mm)	Difference to nominal dia (µm)	Minor dia d2 (mm)	Dross(µm)
3,2	2,95	250	2,8	150	2,95	250	2,7	250
3,5	3,33	170	3,04	290	3,375	125	3,1	275
3,8	3,665	135	3,39	275	3,68	120	3,485	195
4,1	3,97	130	3,718	252	3,96	140	3,7	260
4,2	4,04	160	3,84	200	4,04	160	3,8	240
4,3	4,15	150	3,88	270	4,13	170	3,9	230
Average		166		240		161		242
5,8	5,635	165	5,42	215	5,63	170	5,33	300
6,1	5,94	160	5,73	210	5,95	150	5,7	250
6,4	6,19	210	5,89	300	6,225	175	5,9	325
6,7	6,555	145	6,3	255	6,52	180	6,265	255
6,8	6,63	170	6,35	280	6,675	125	6,4	275
6,9	6,745	155	6,48	265	6,74	160	6,51	230
Average		168		254		160		273

Appendix B: Drilling Forces

AlSi10Mg, AB-35, 5° recoater angle

Axial drilling force for various pre-holes, 0° printing inclination

4.2 mm drill

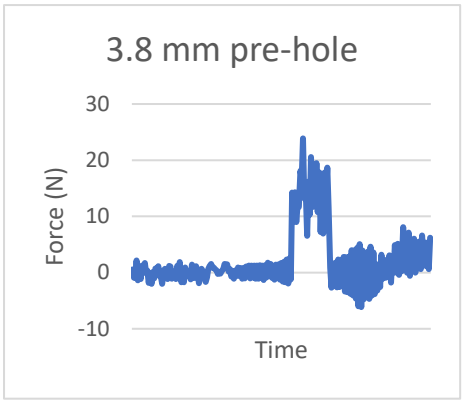

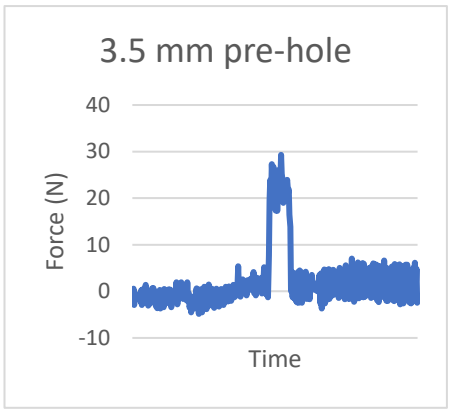

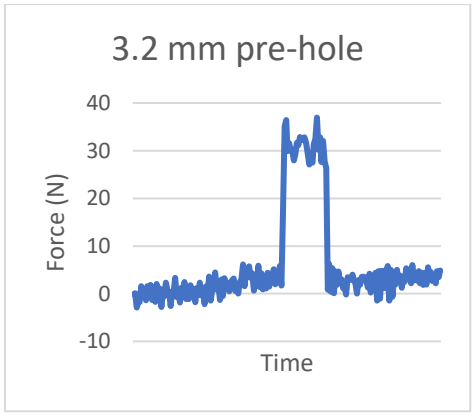

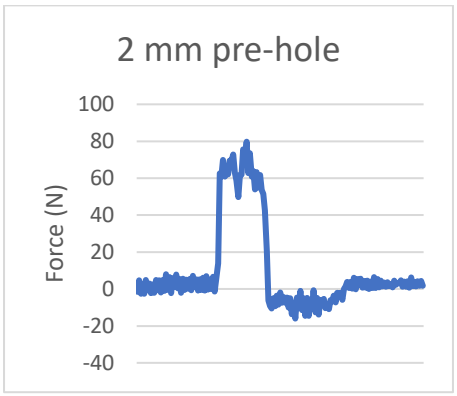

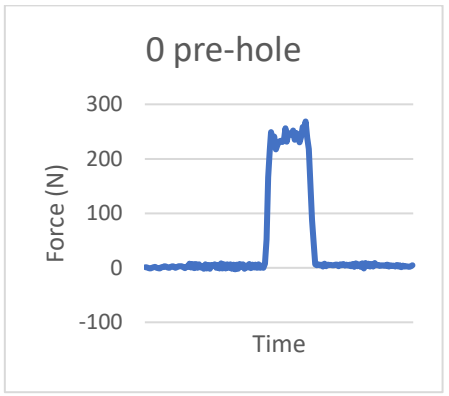

6.8 mm drill

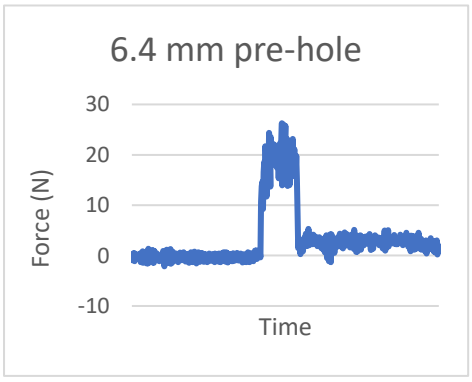

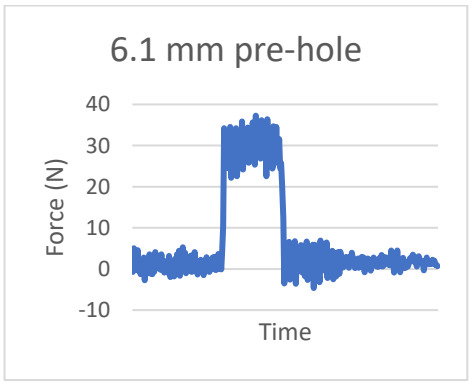

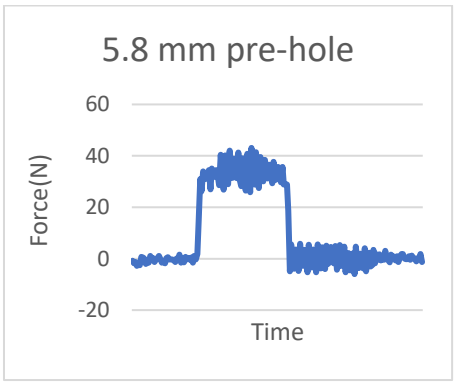

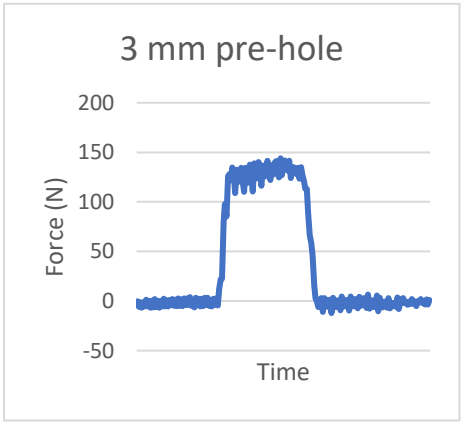

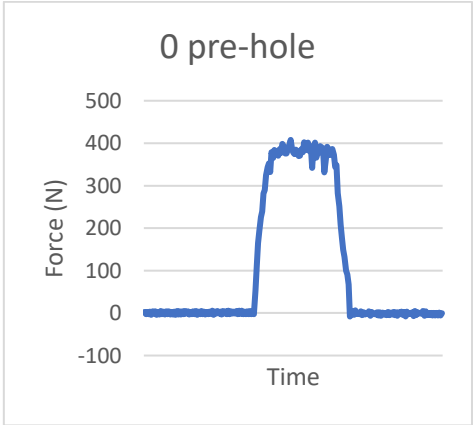

AlSi10Mg, AB-35, 5° recoater angle

Axial drilling force for various pre-holes, 30° printing inclination

4.2 mm drill

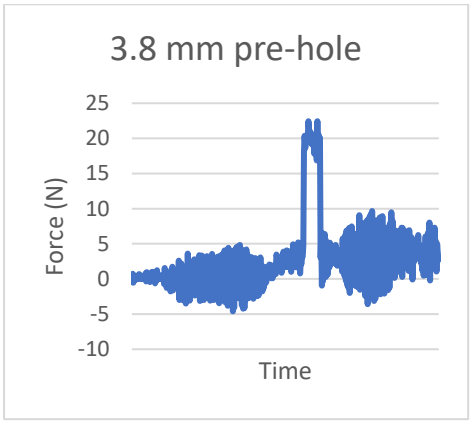

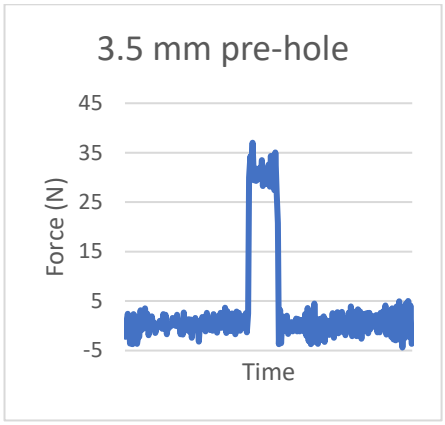

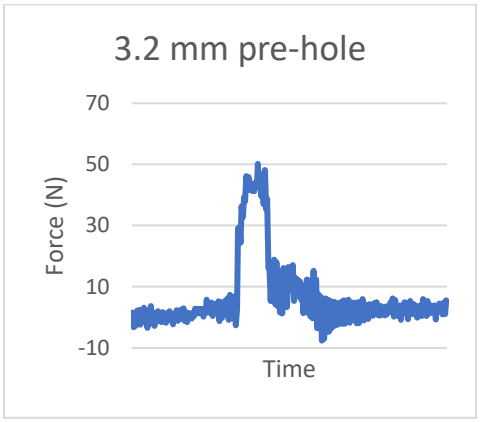

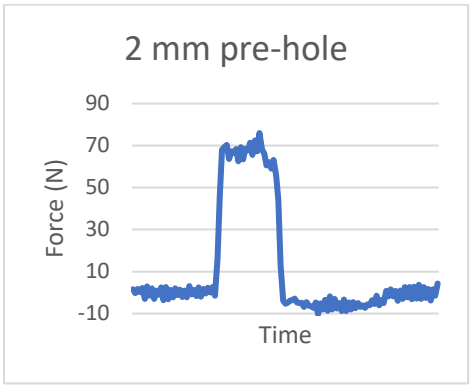

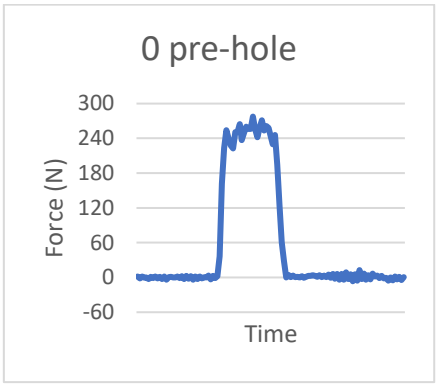

6.8 mm drill

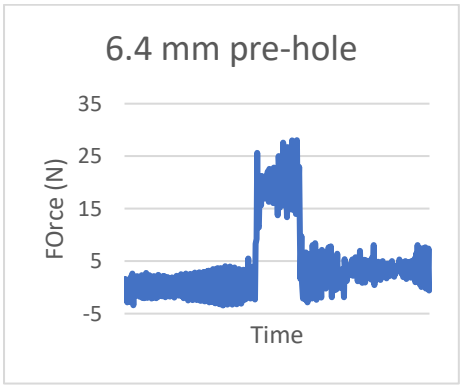

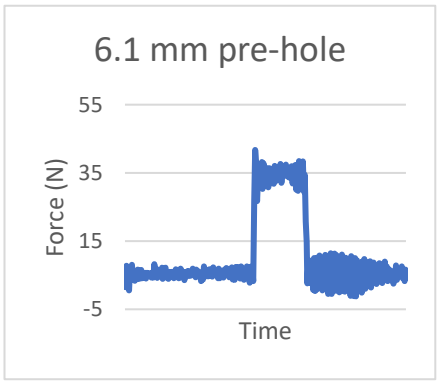

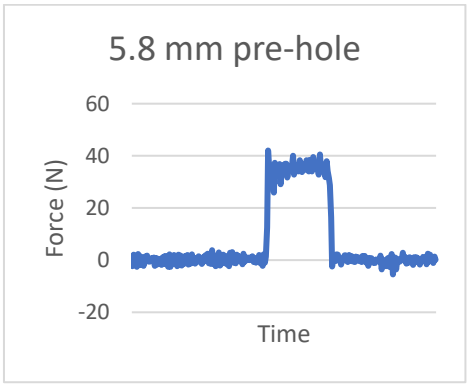

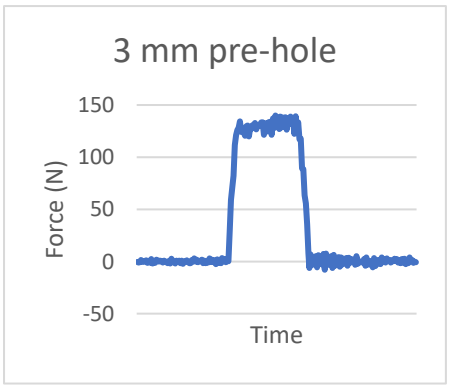

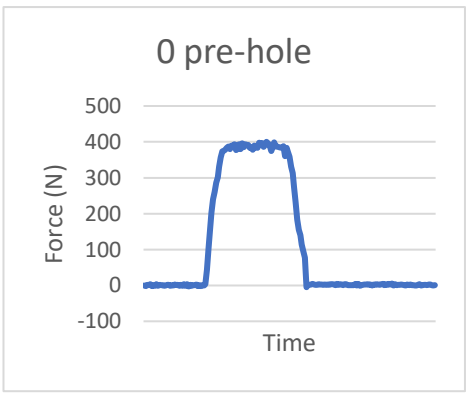

AlSi10Mg, AB-35, 5° recoater angle

Axial drilling force for various pre-holes, 45° printing inclination

4.2 mm drill

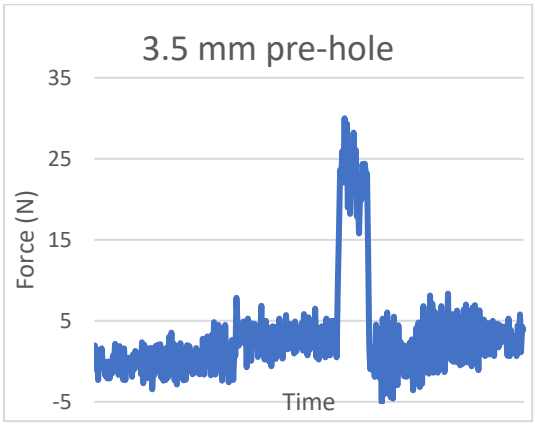

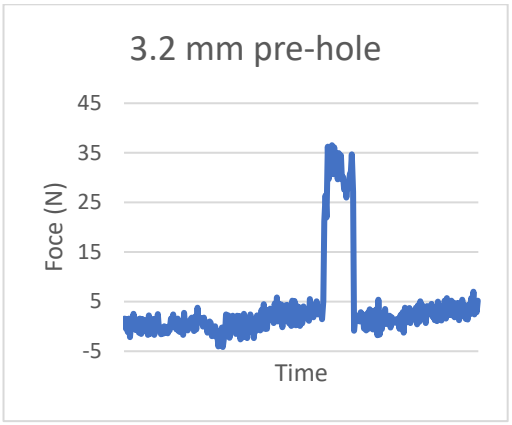

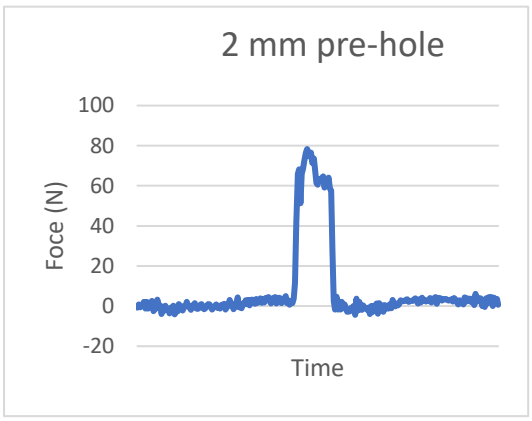

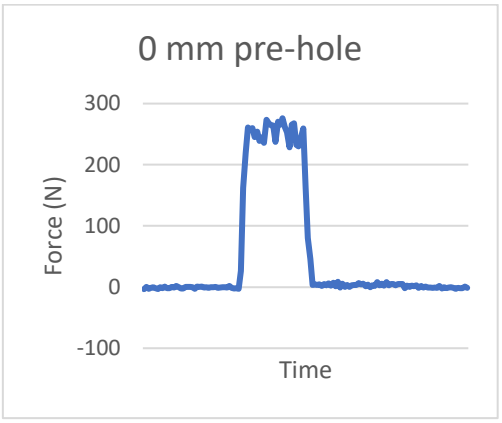

6.8 mm drill

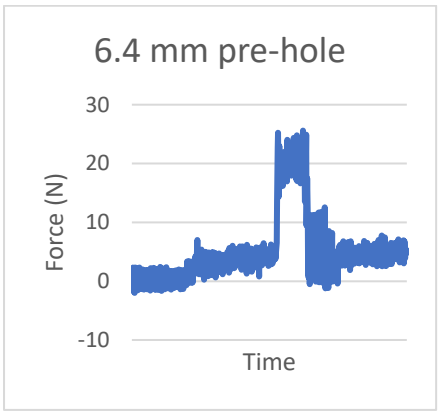

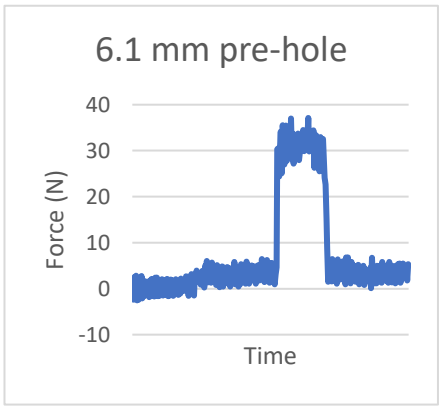

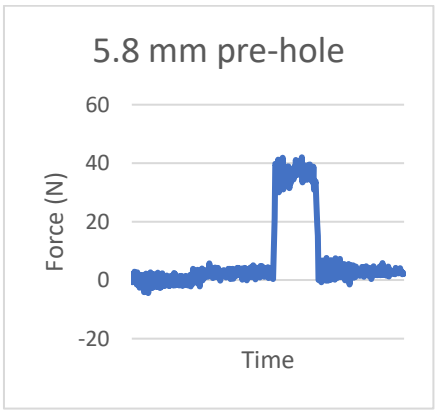

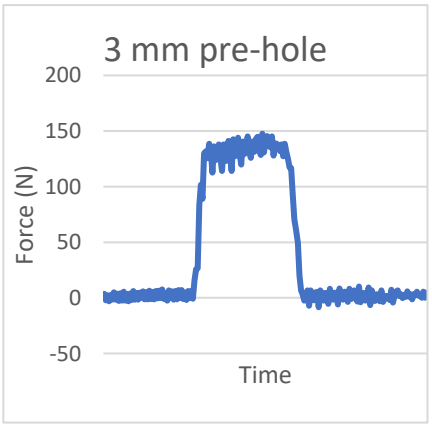

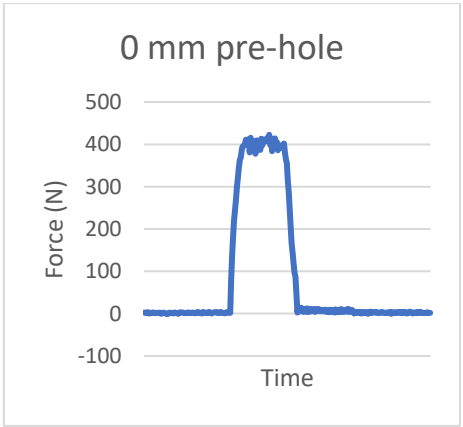

AlSi10Mg, AB-35, 5° recoater angle

Axial drilling force for various pre-holes, 60° printing inclination

4.2 mm drill

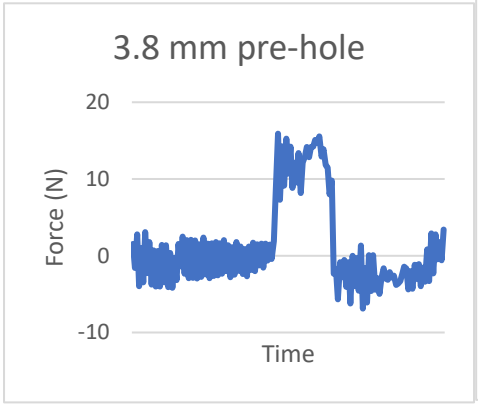

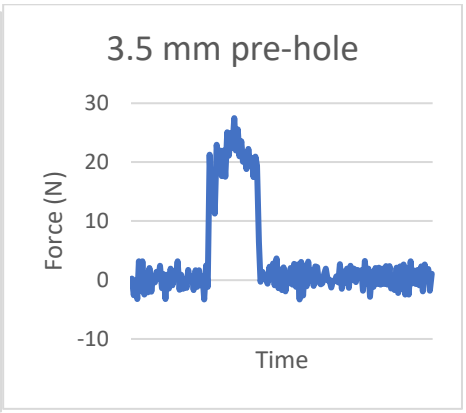

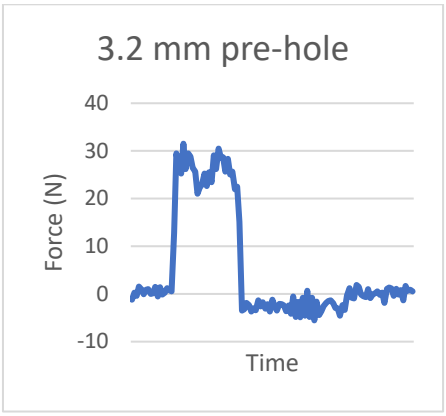

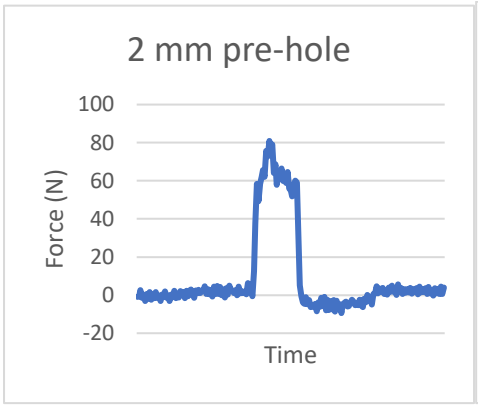

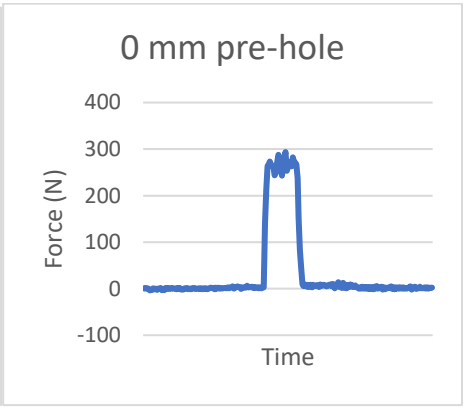

6.8 mm drill

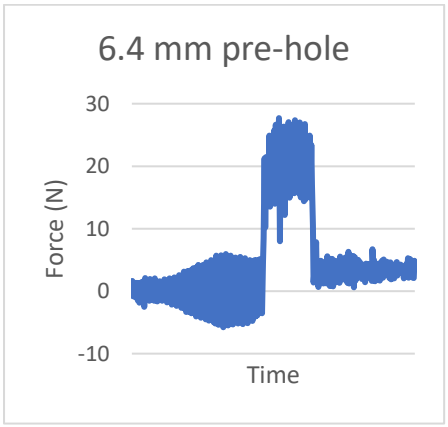

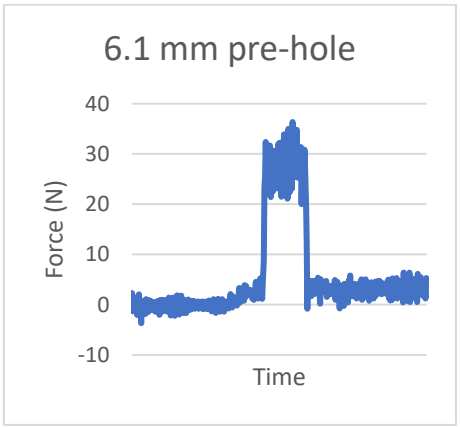

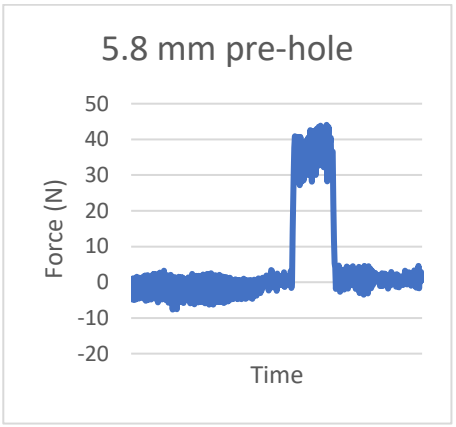

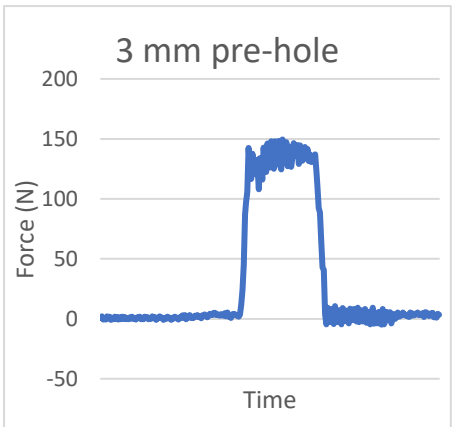

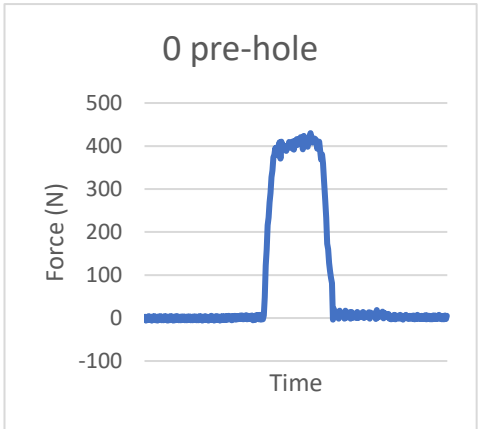

AlSi10Mg, AB-35, 5° recoater angle

Axial drilling force for various pre-holes, 90° printing inclination

4.2 mm drill

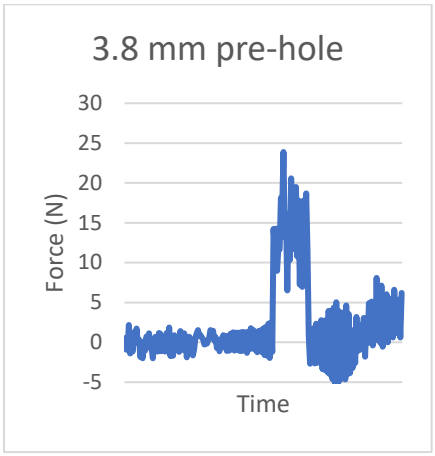

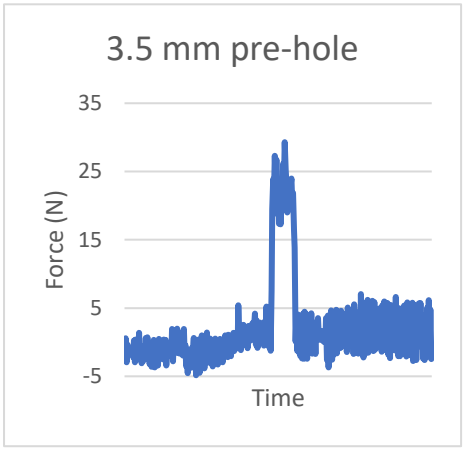

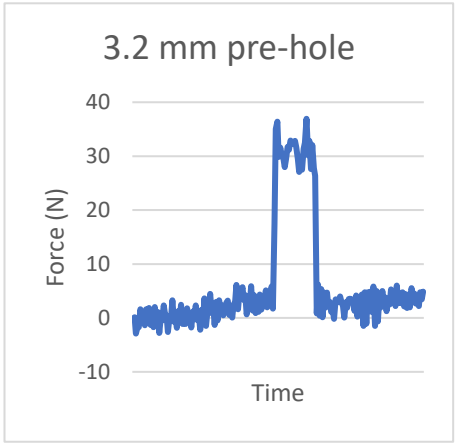

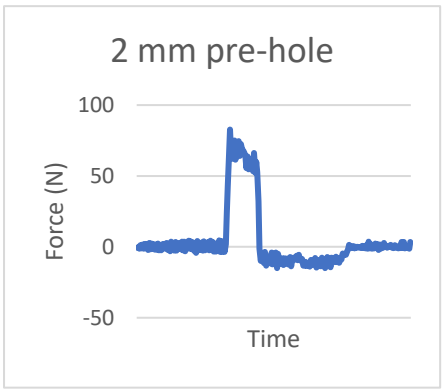

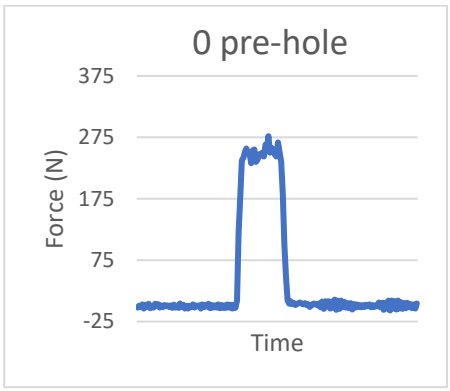

6.8 mm drill

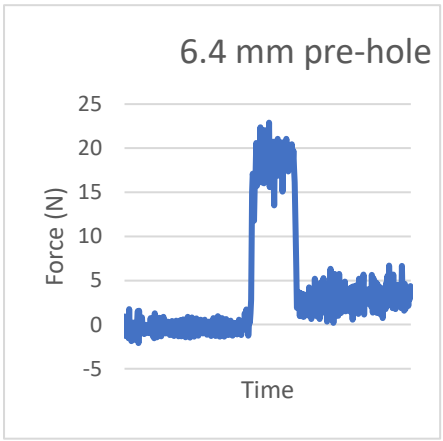

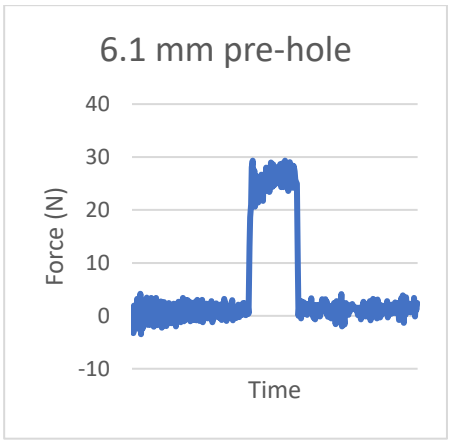

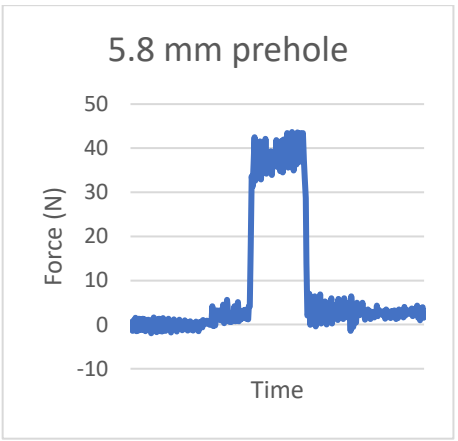

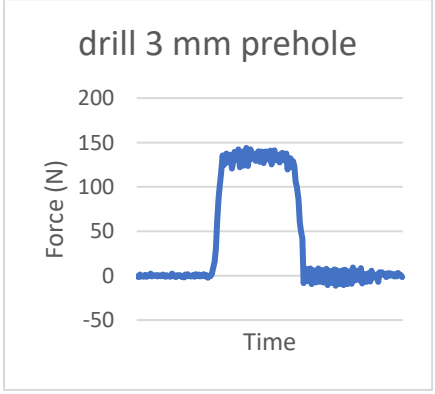

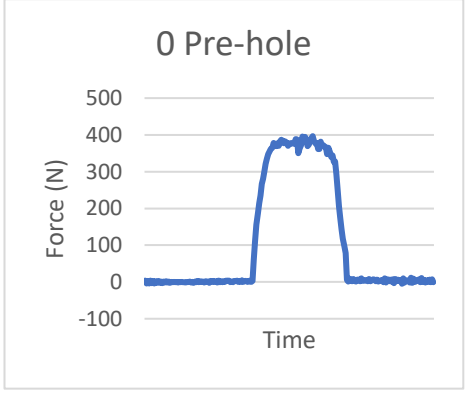

AlSi10Mg, AB-200, 5° recoater angle

Axial drilling force for various pre-holes, Printing inclination 0°

4.2 mm drill

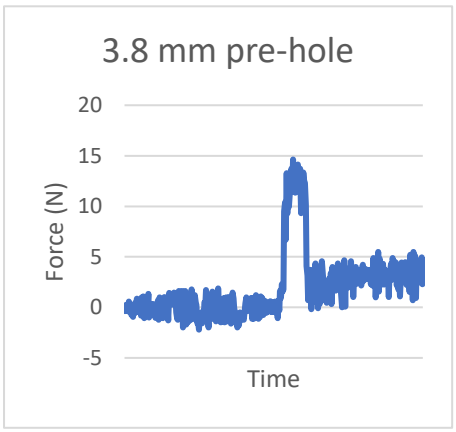

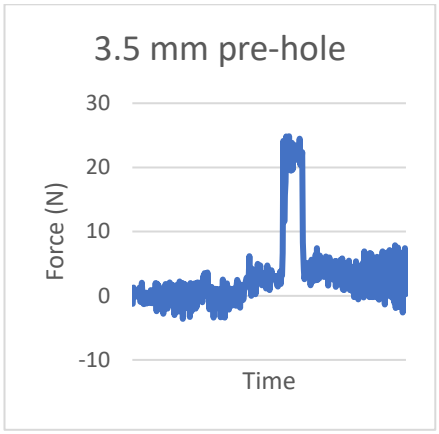

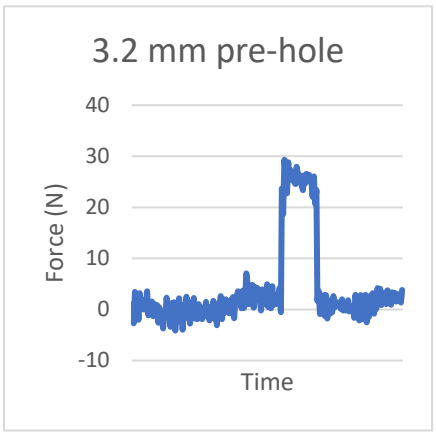

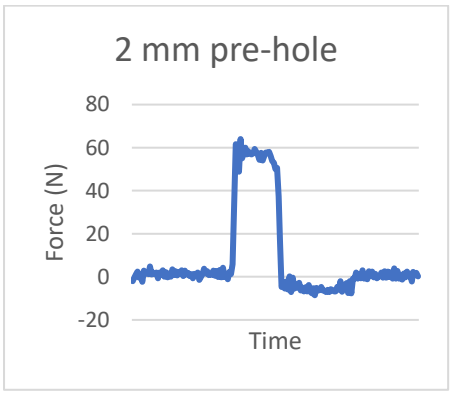

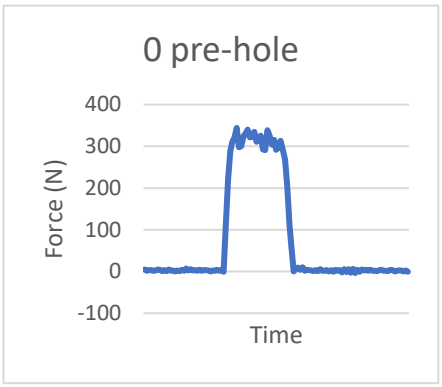

6.8 mm drill

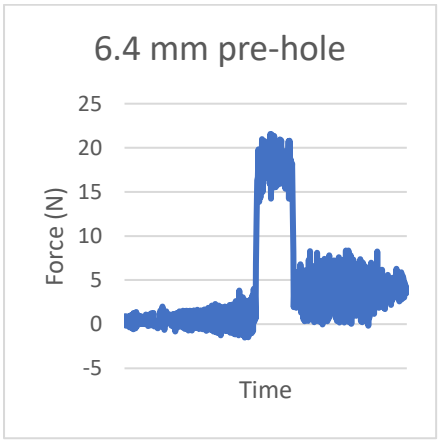

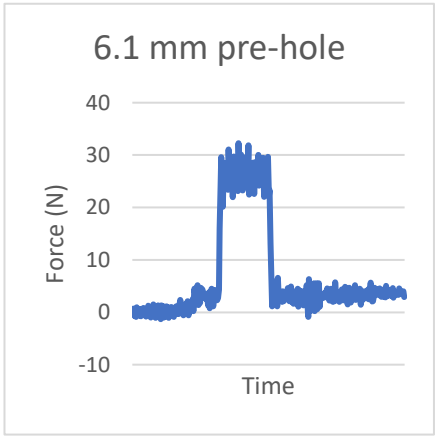

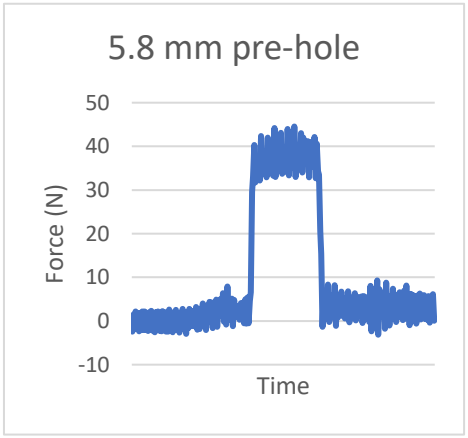

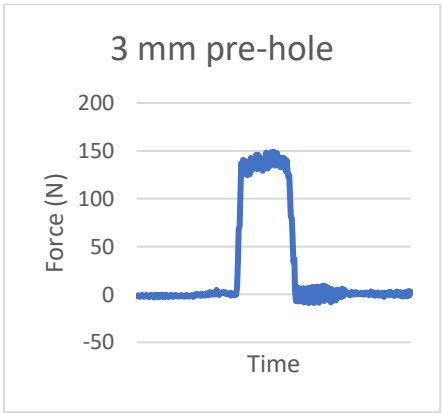

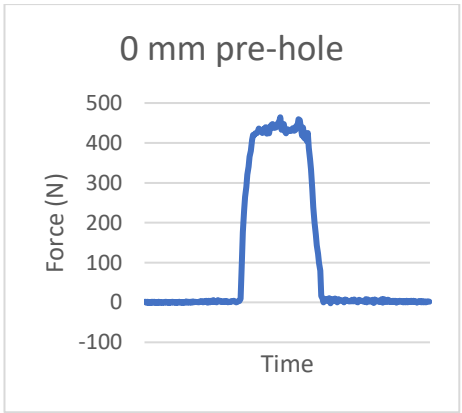

AlSi10Mg, AB-200, 5° recoater angle

Axial drilling force for various pre-holes, Printing inclination 30°

4.2 mm drill

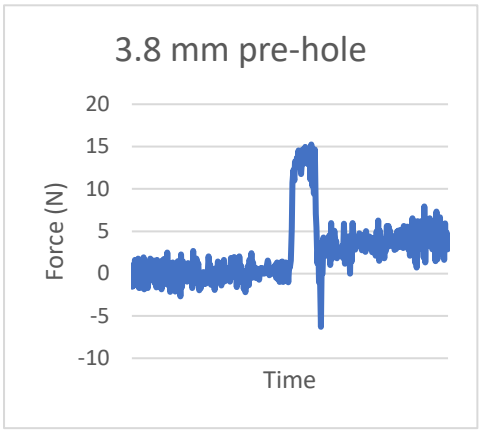

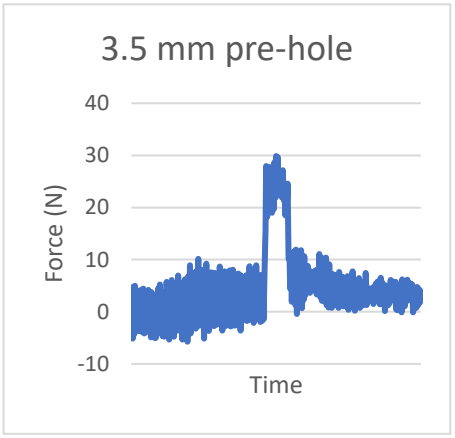

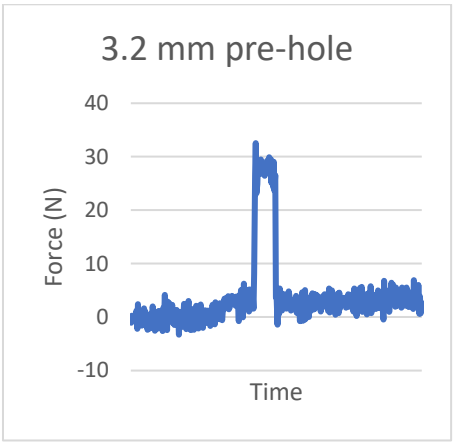

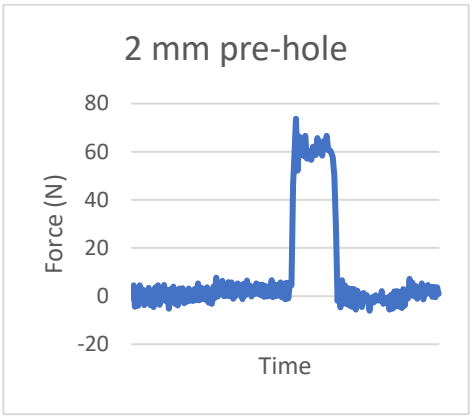

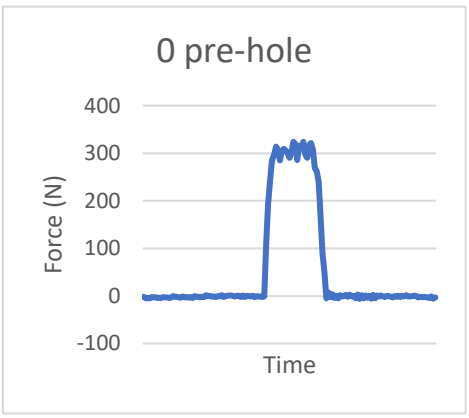

6.8 mm drill

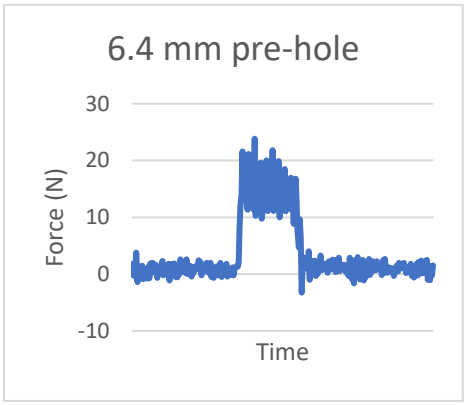

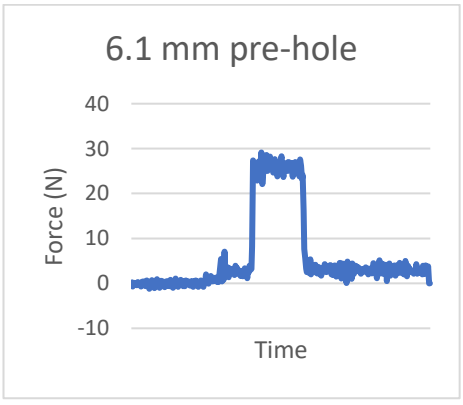

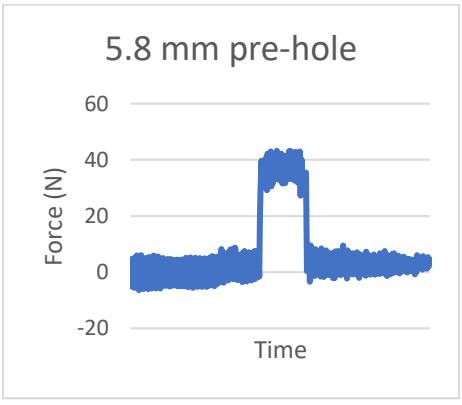

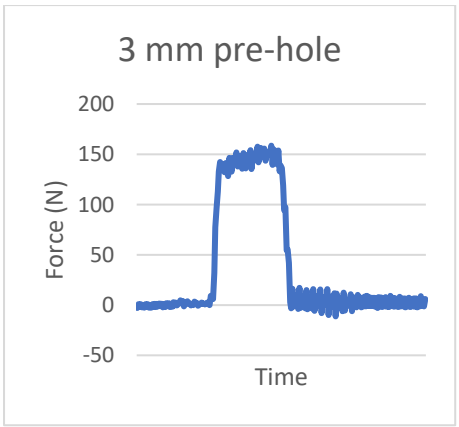

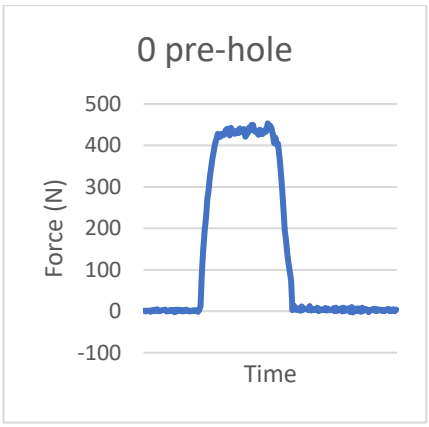

AlSi10Mg, AB-200, 5° recoater angle

Axial drilling force for various pre-holes, Printing inclination 45°

4.2 mm drill

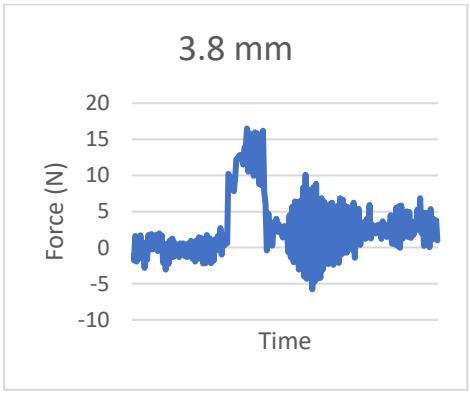

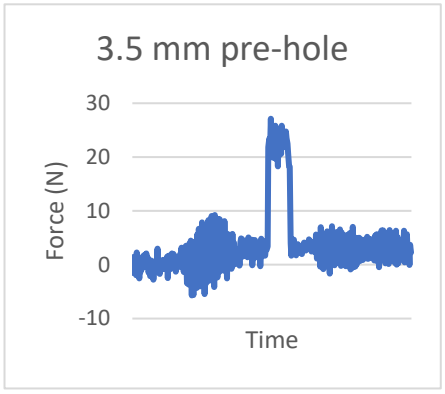

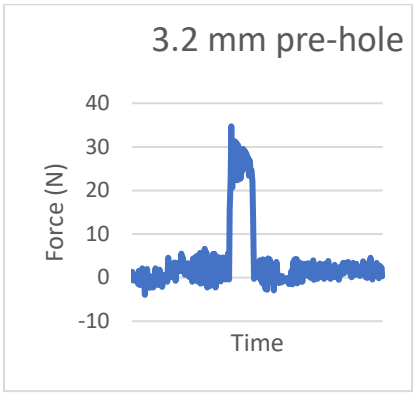

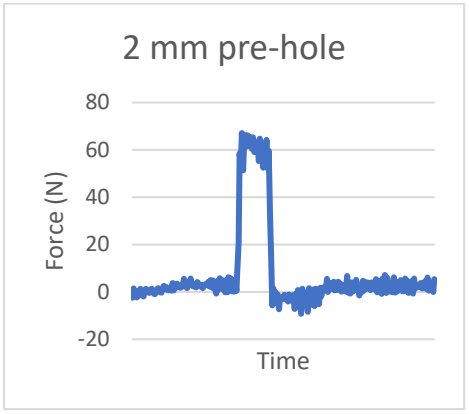

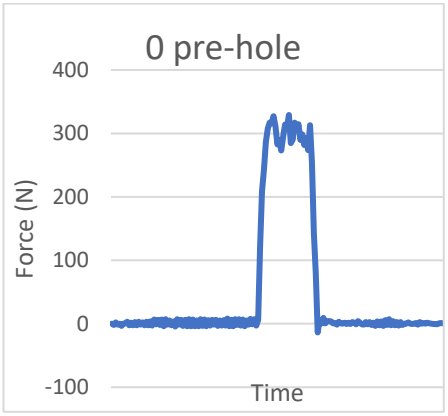

6.8 mm drill

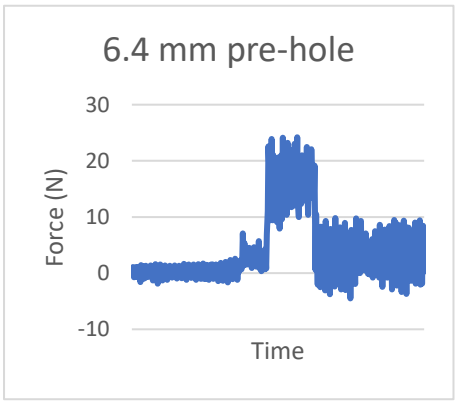

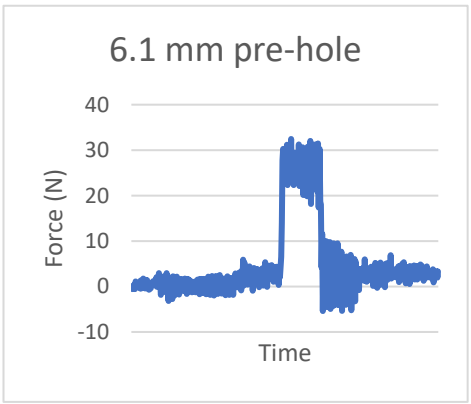

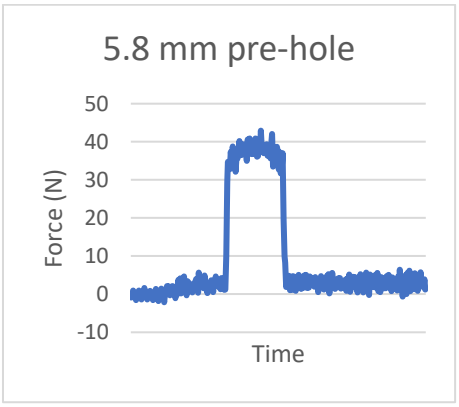

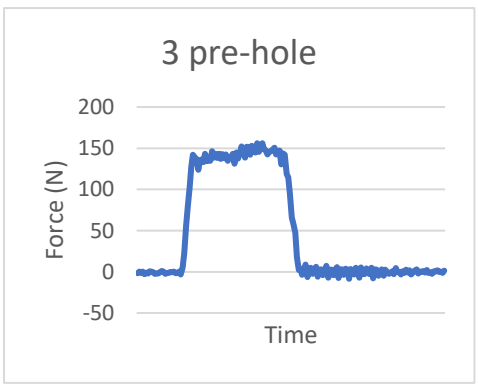

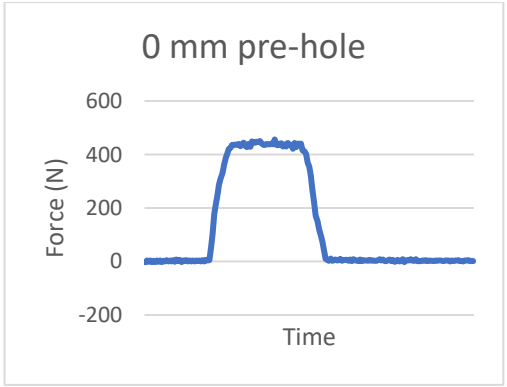

AlSi10Mg, AB-200, 5° recoater angle

Axial drilling force for various pre-holes, Printing inclination 60°

4.2 mm drill

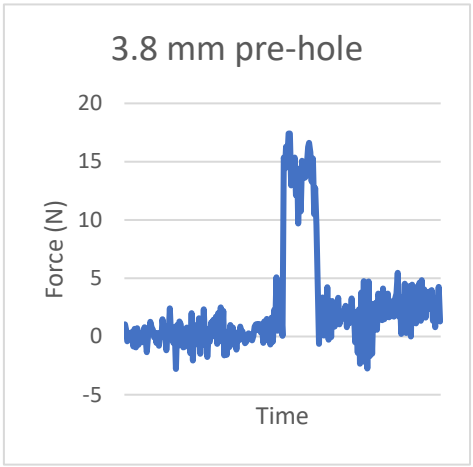

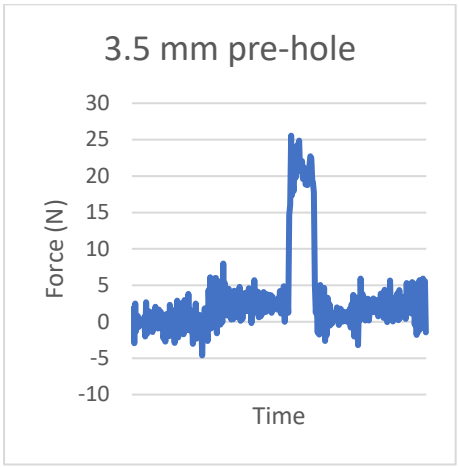

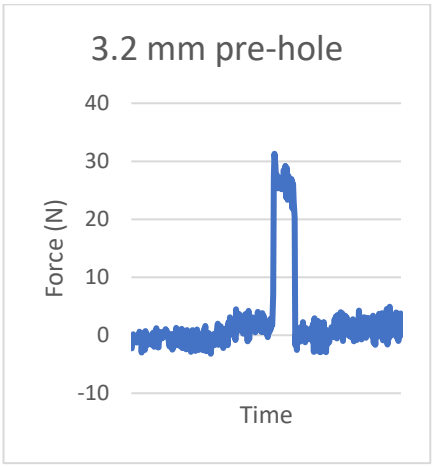

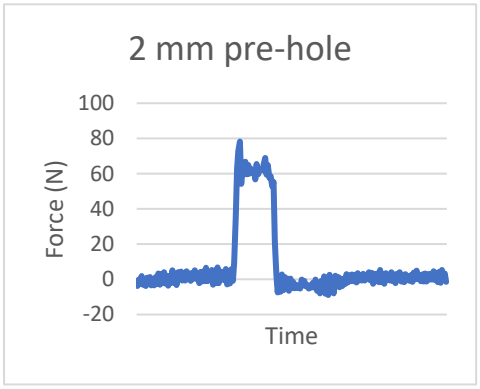

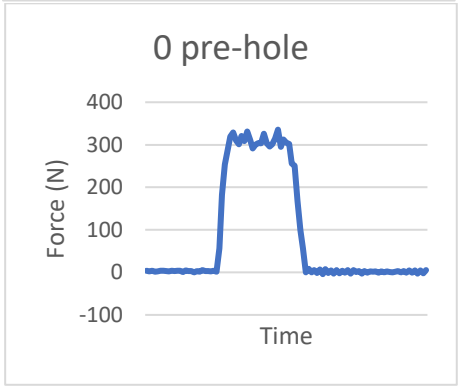

6.8 mm drill

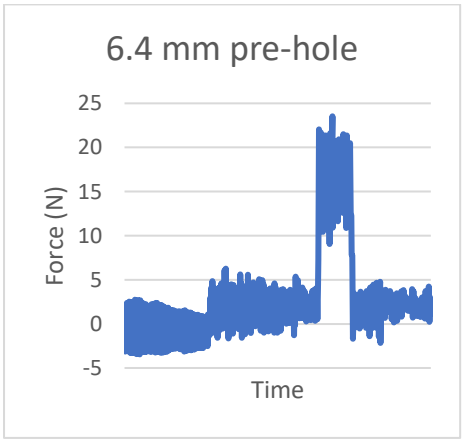

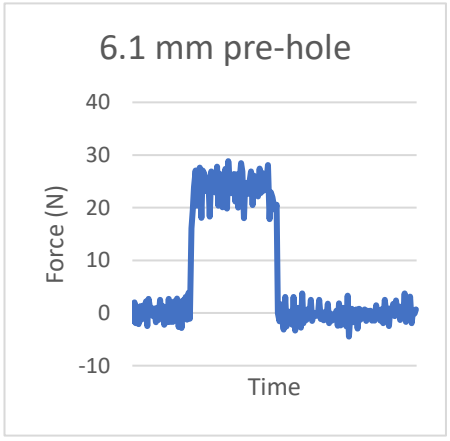

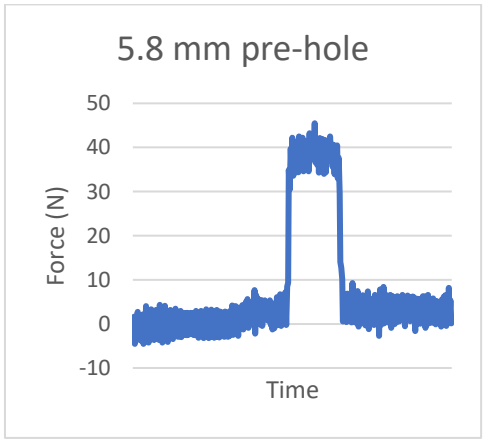

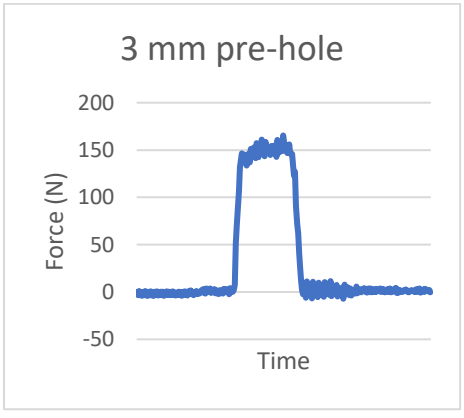

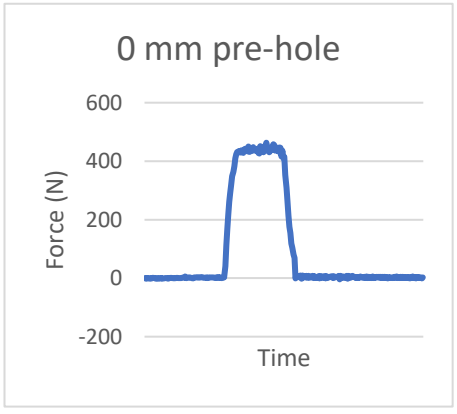

AlSi10Mg, AB-200, 5° recoater angle

Axial drilling force for various pre-holes, Printing inclination 90°

4.2 mm drill

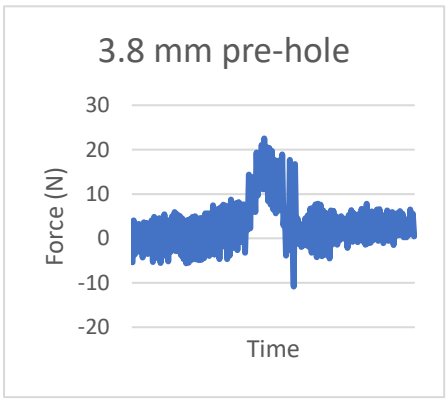

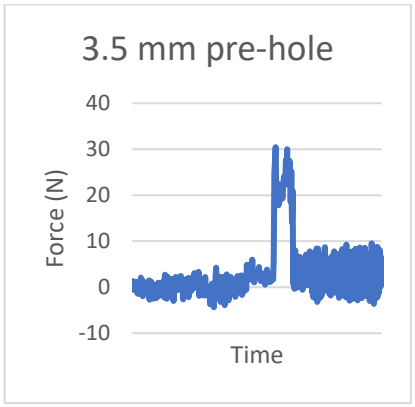

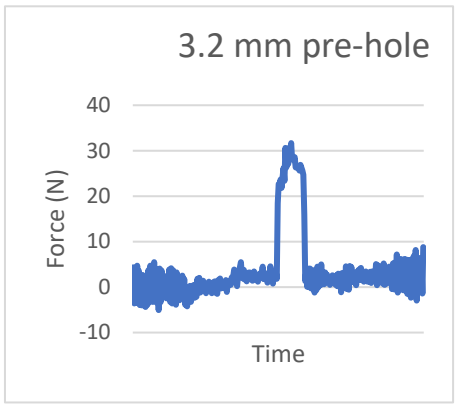

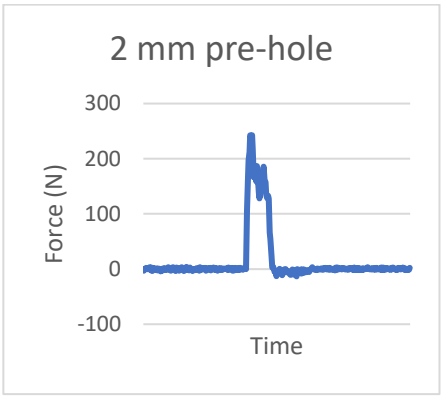

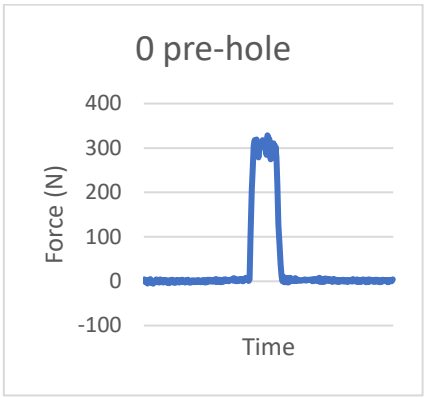

6.8 mm drill

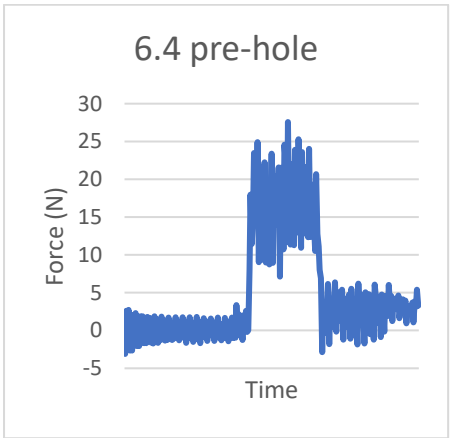

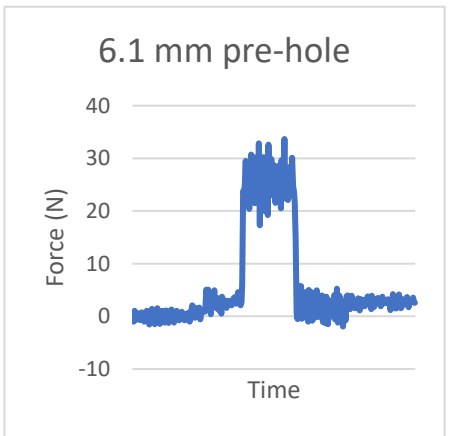

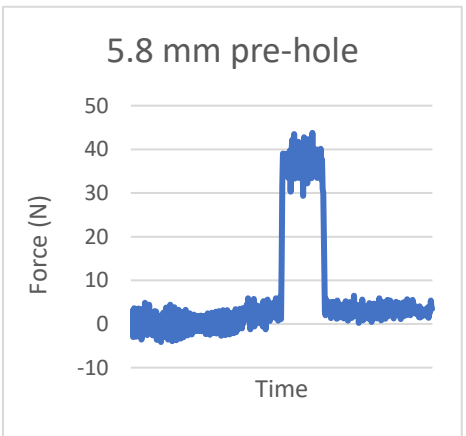

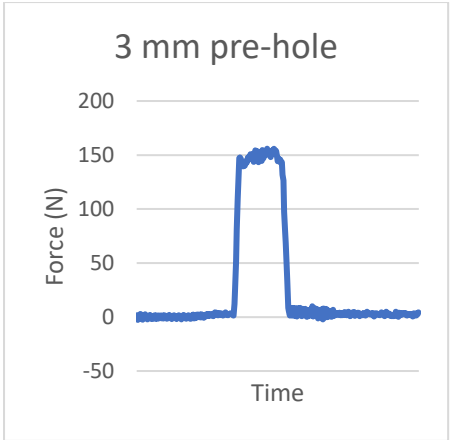

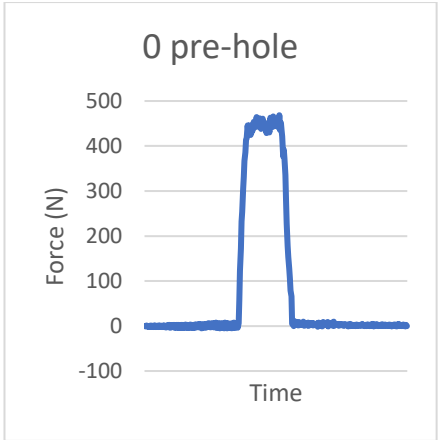

AlSi10Mg, AB-200, 45° recoater angle

Axial drilling force for various pre-holes, Printing inclination 0°

6.8 mm drill

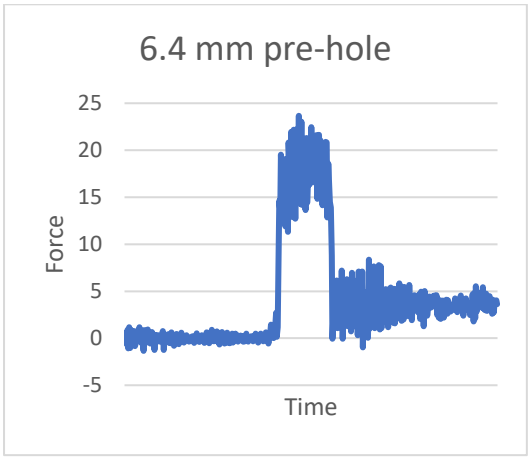

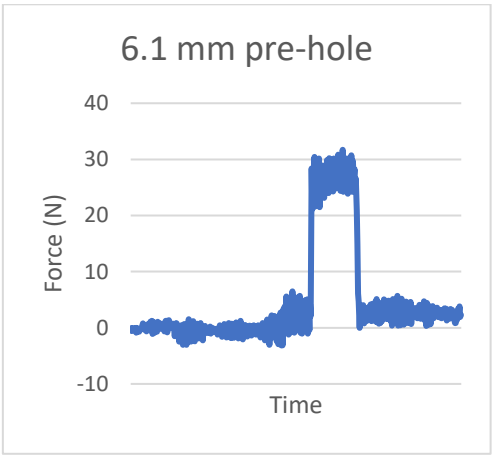

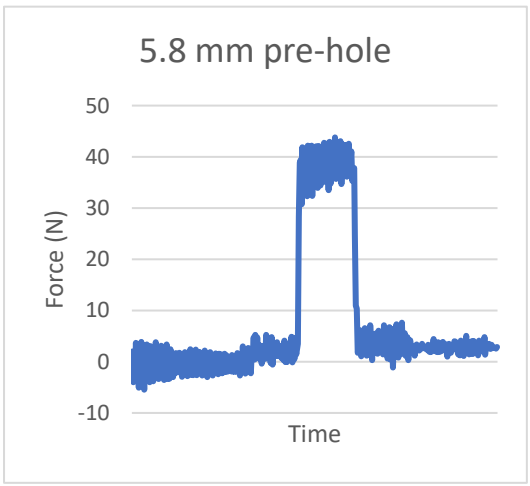

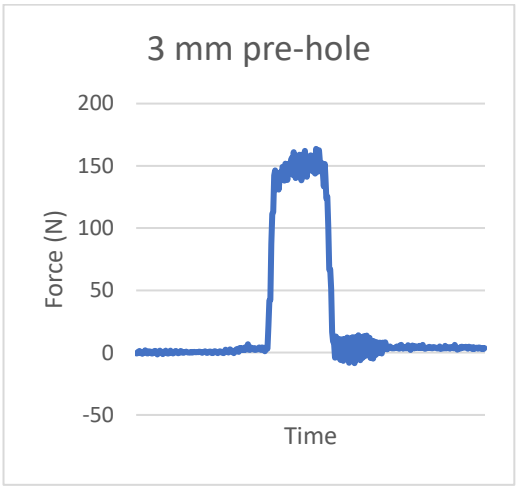

AlSi10Mg, AB-200 45° recoater angle

Axial drilling force for various pre-holes, Printing inclination 30°

4.2 mm drill

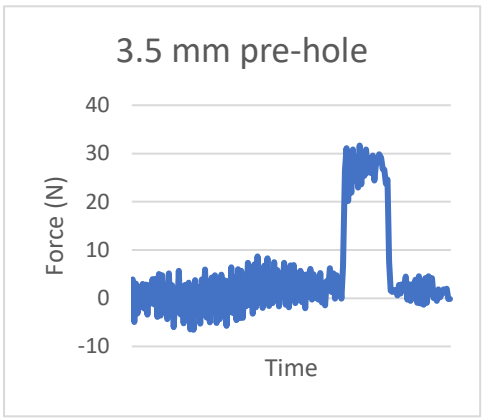

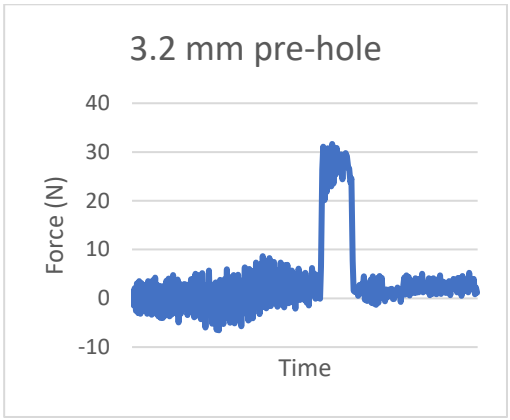

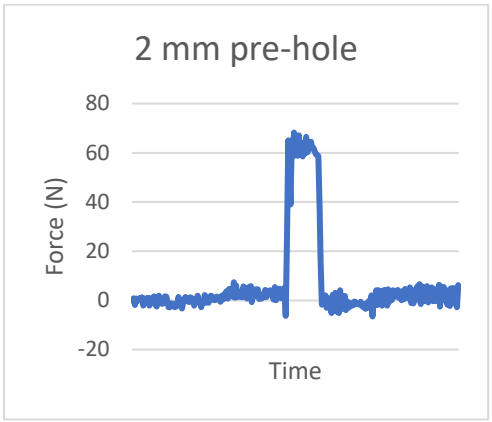

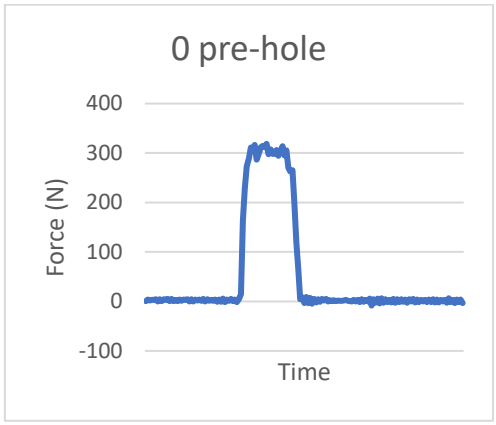

6.8 mm drill

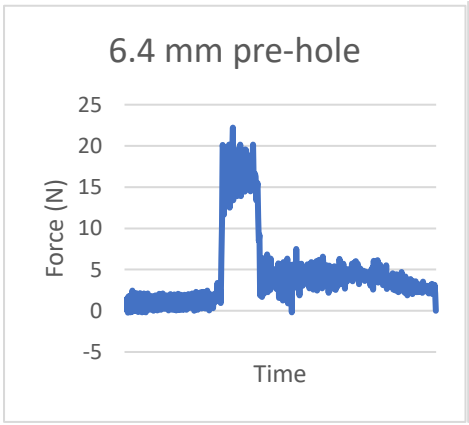

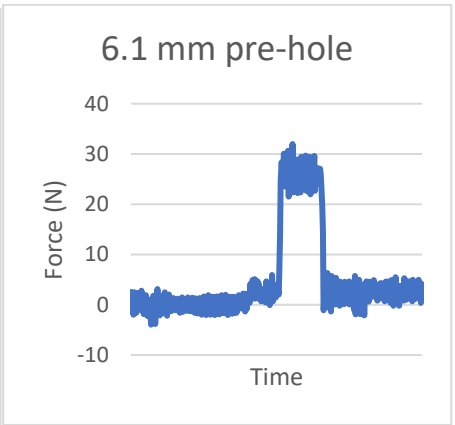

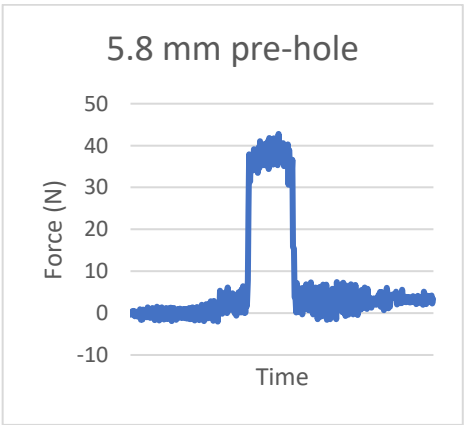

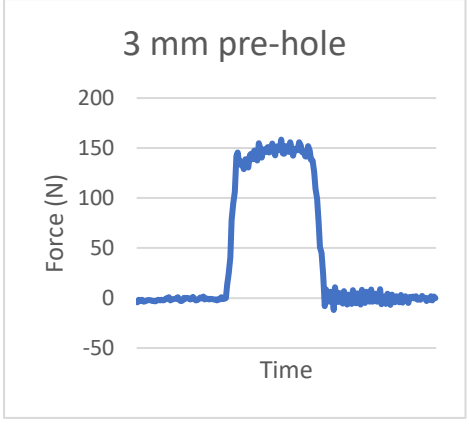

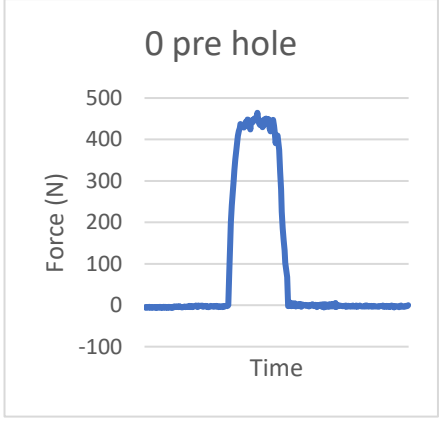

AlSi10Mg, AB-200, 45° recoater angle

Axial drilling force for various pre-holes, Printing inclination 45°

4.2 mm drill

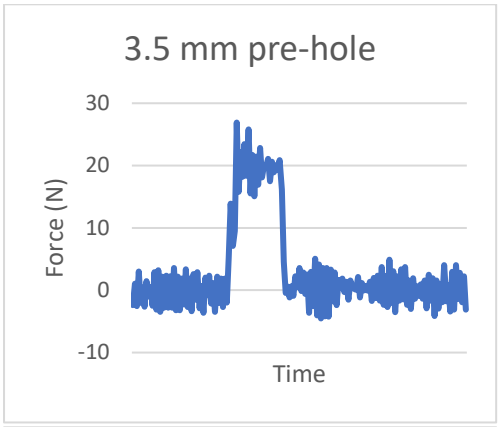

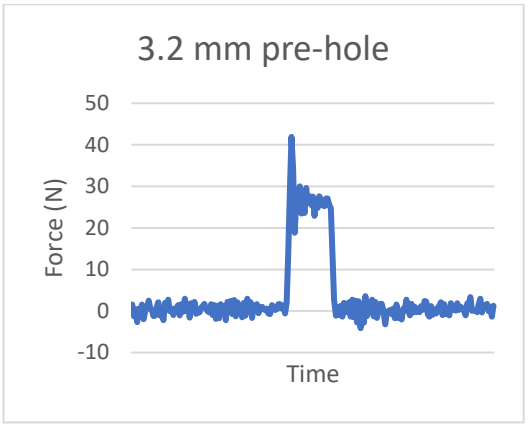

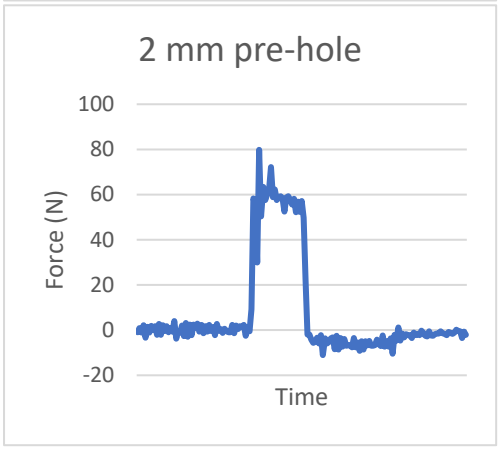

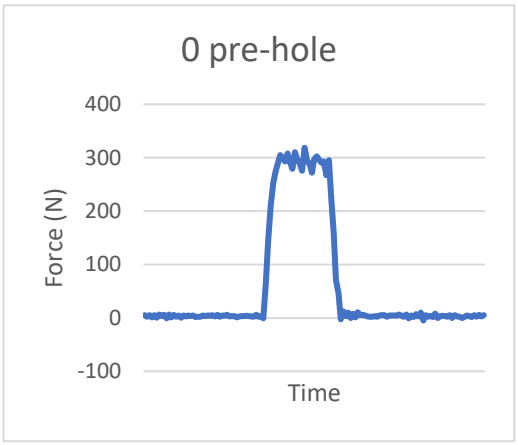

6.8 mm drill

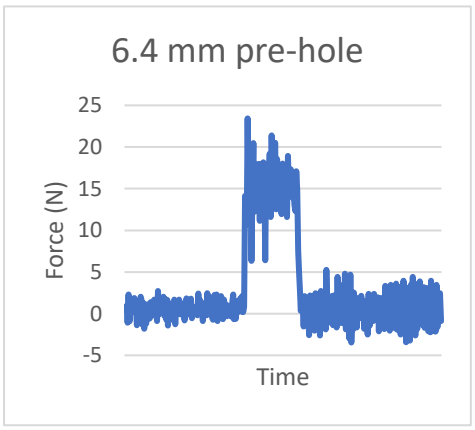

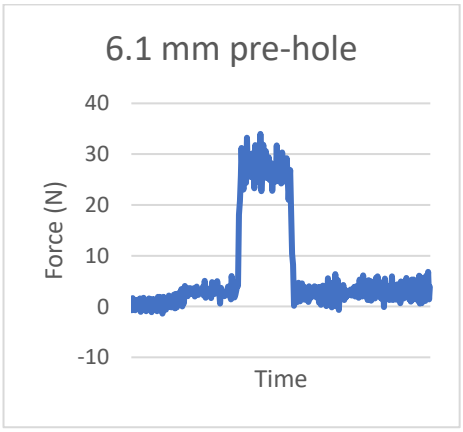

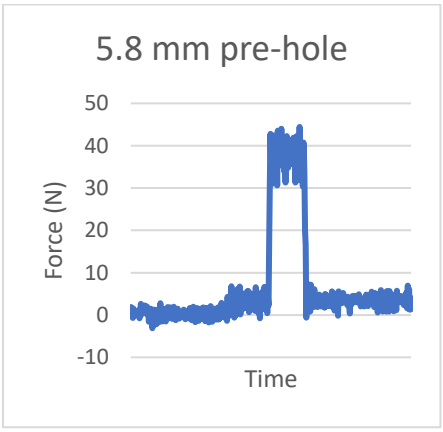

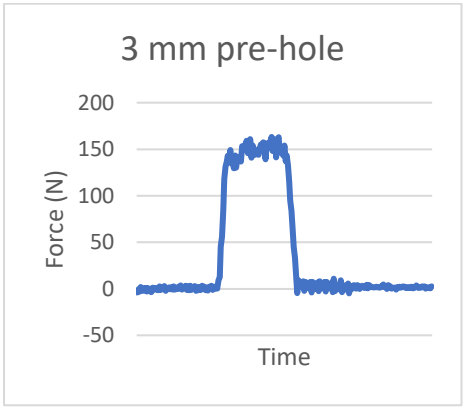

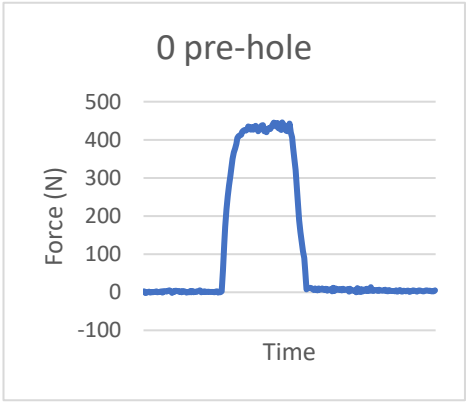

AlSi10Mg, AB-200, 45° recoater angle

Axial drilling force for various pre-holes, Printing inclination 60°

4.2 mm drill

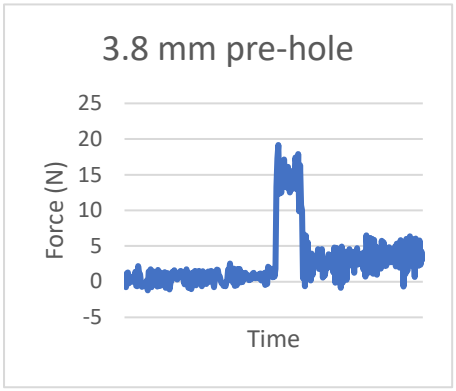

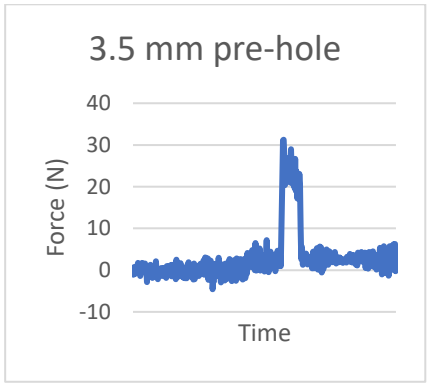

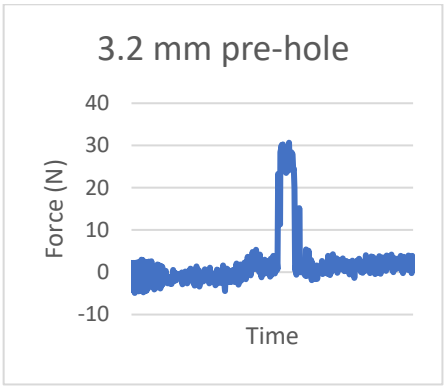

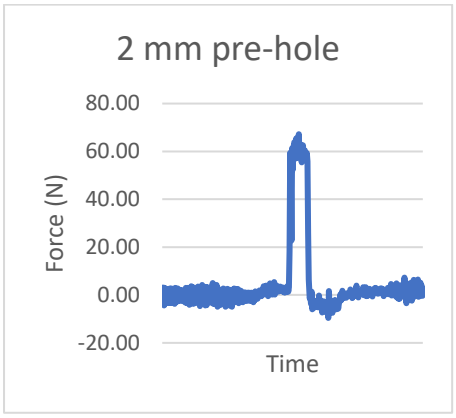

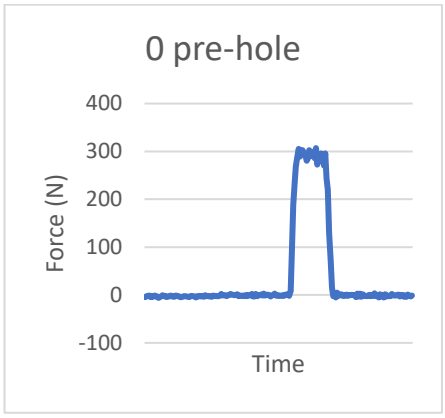

6.8 mm drill

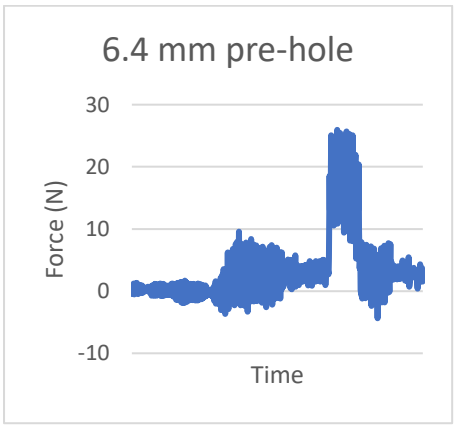

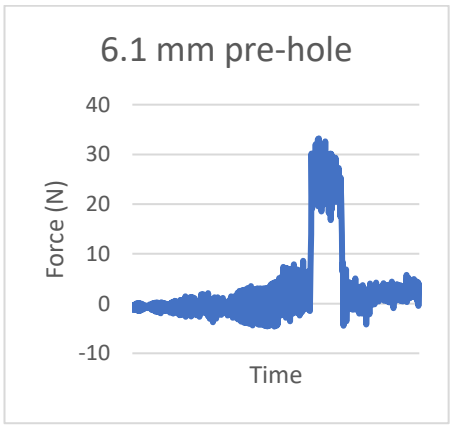

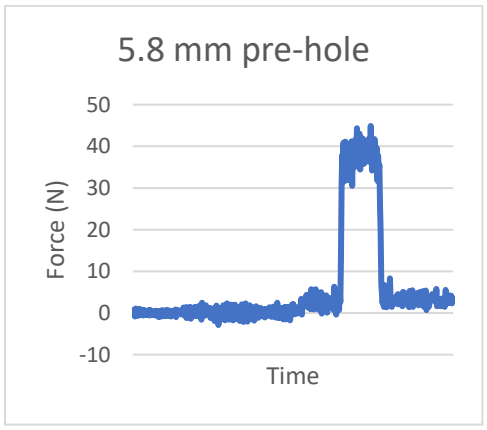

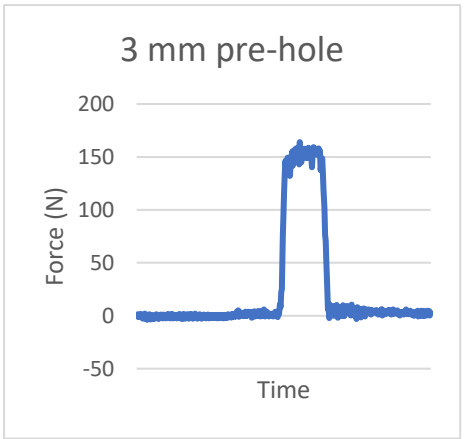

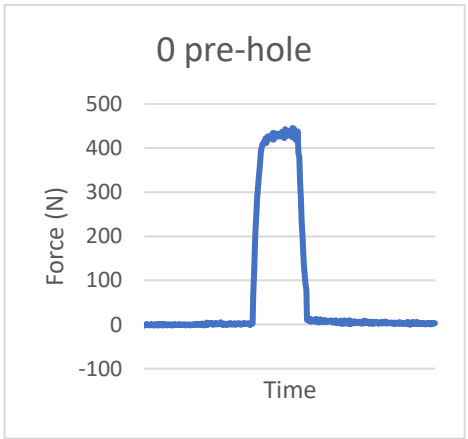

AlSi10Mg, AB-200, 45° recoater angle

Axial drilling force for various pre-holes, Printing inclination 90°

4.2 mm drill

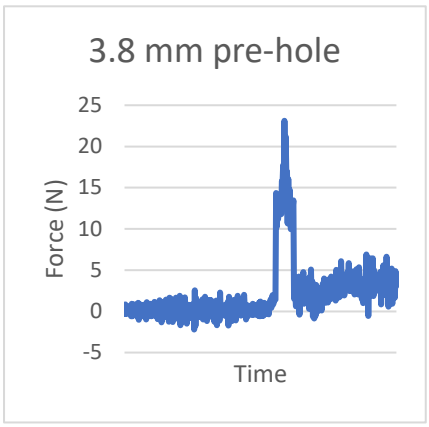

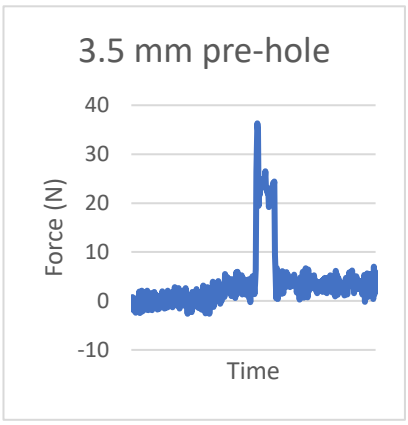

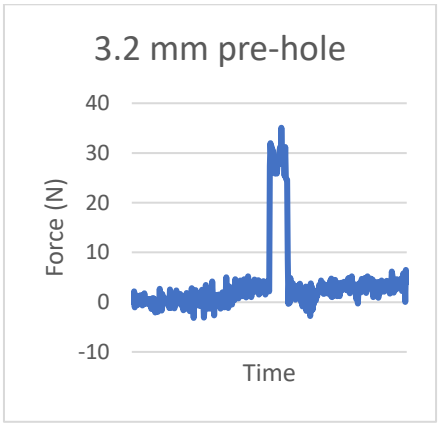

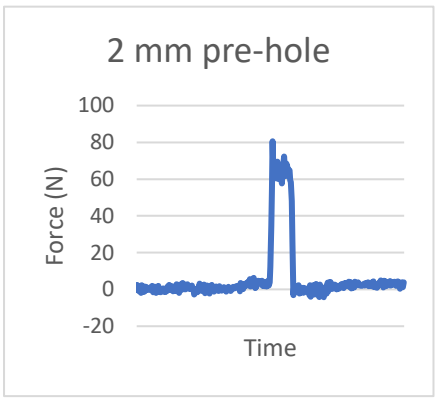

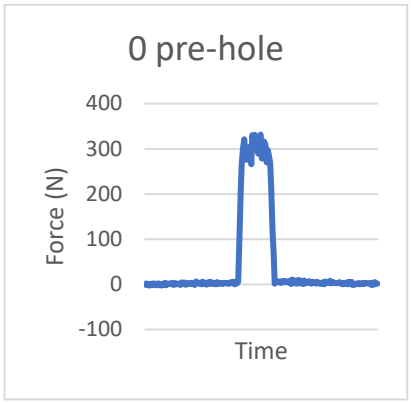

6.8 mm drill

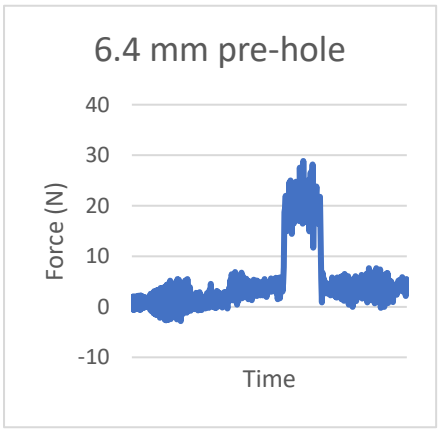

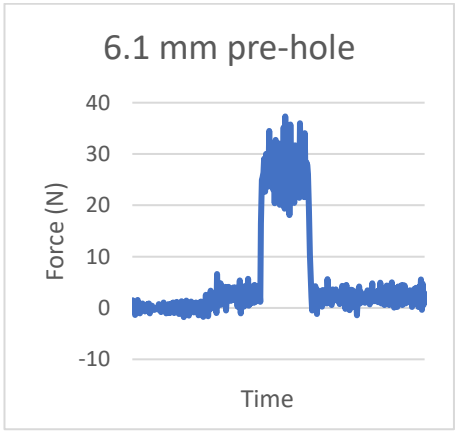

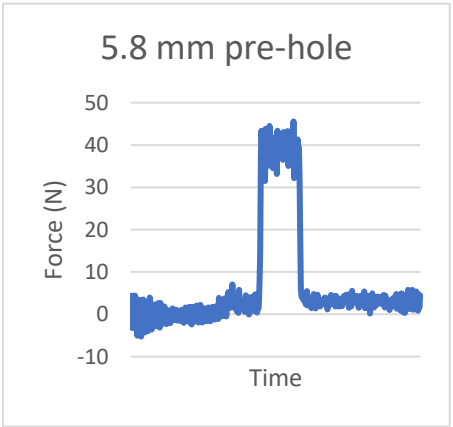

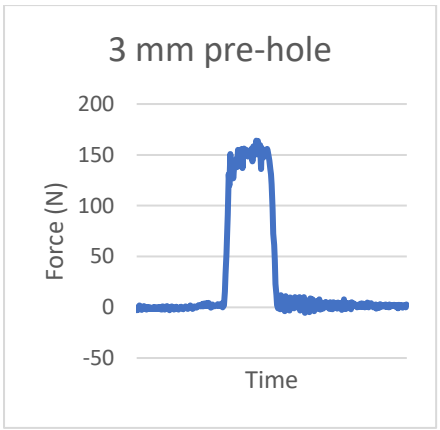

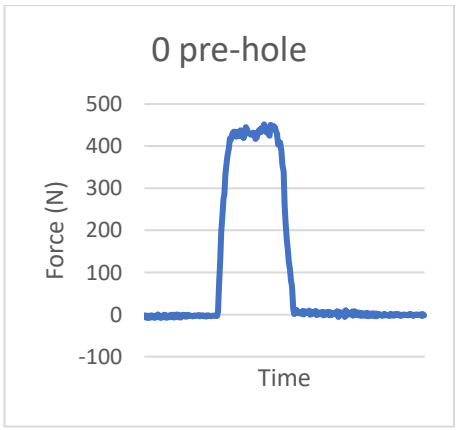

Maraging steel, As-built, 5° recoater angle

Axial drilling force for various pre-holes, Printing inclination 0°

4.2 mm drill

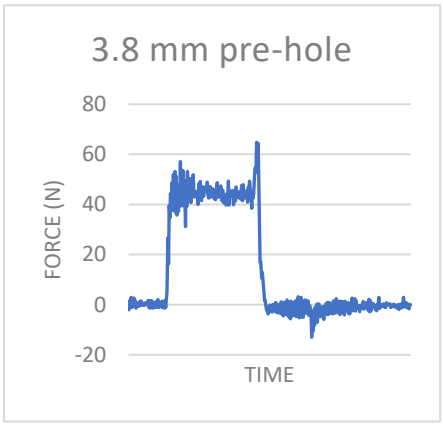

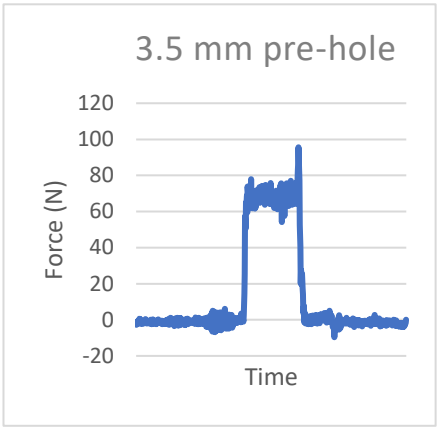

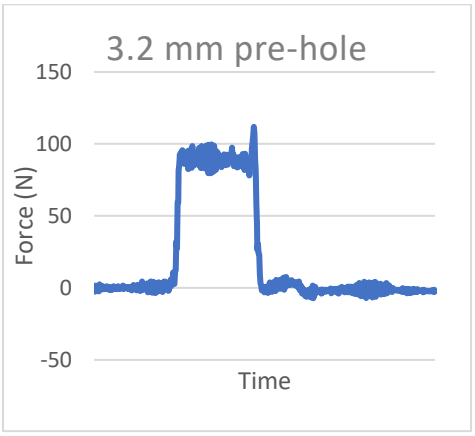

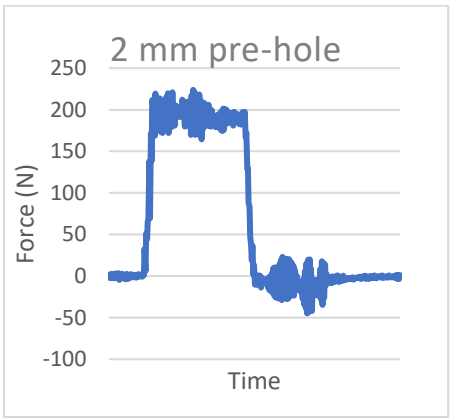

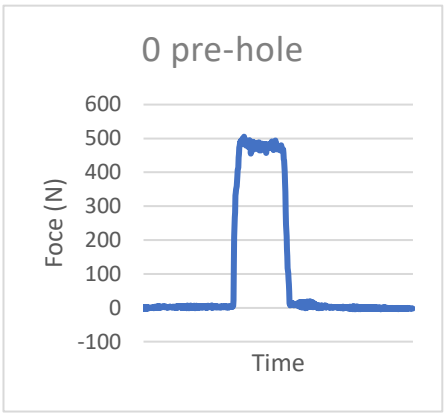

6.8 mm drill

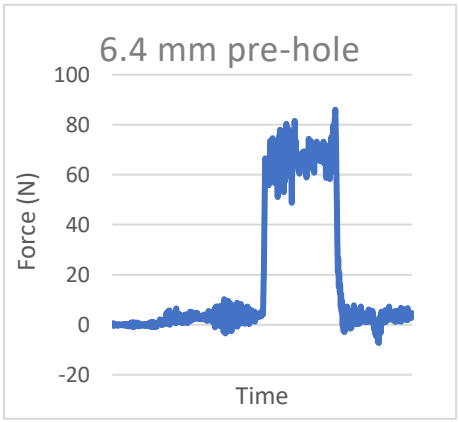

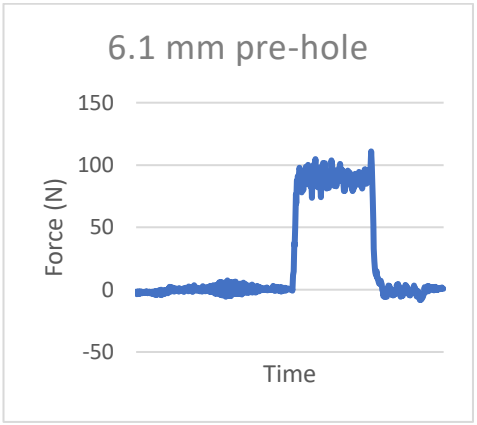

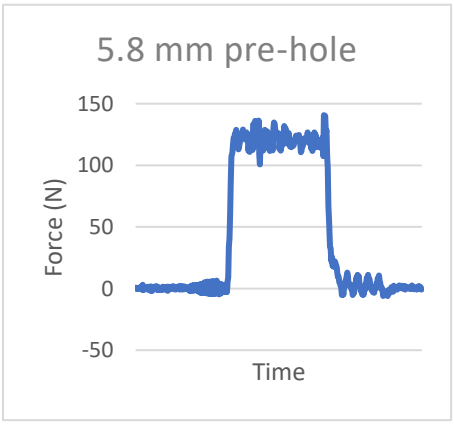

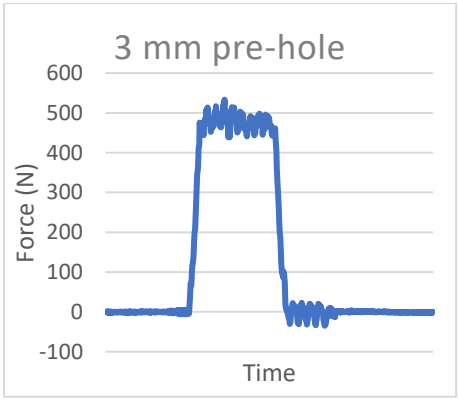

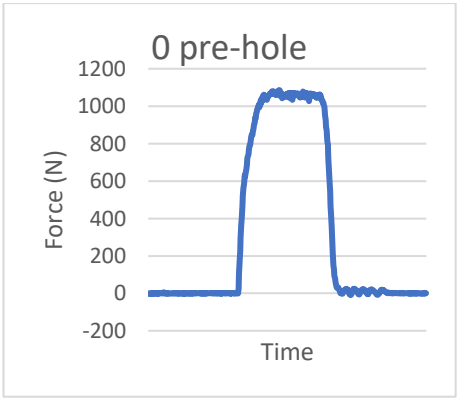

Maraging steel, As-built, 5° recoater angle

Axial drilling force for various pre-holes, Printing inclination 30°

4.2 mm drill

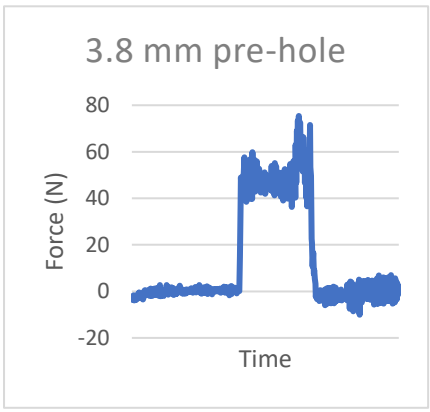

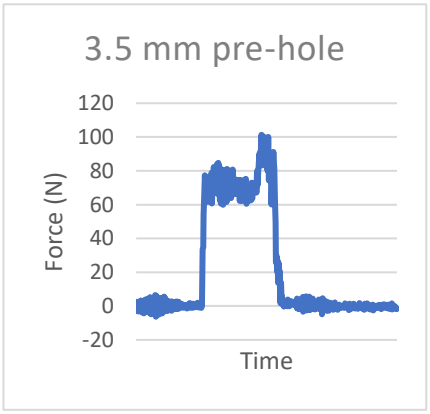

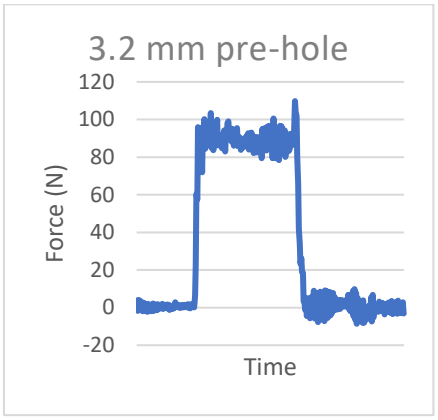

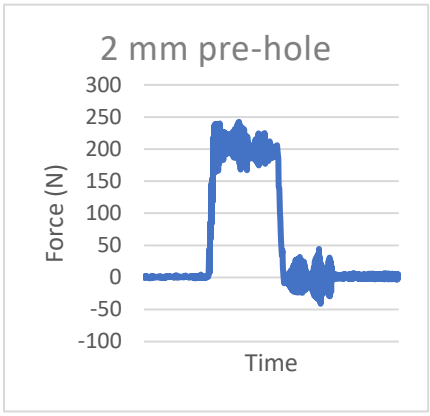

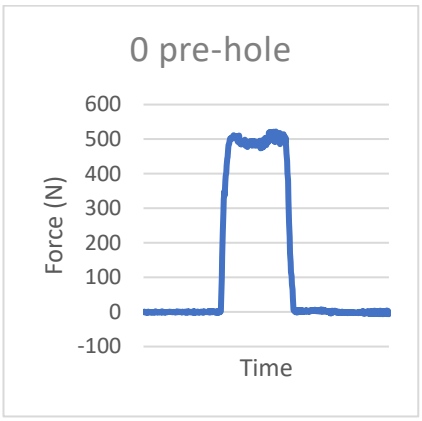

6.8 mm drill

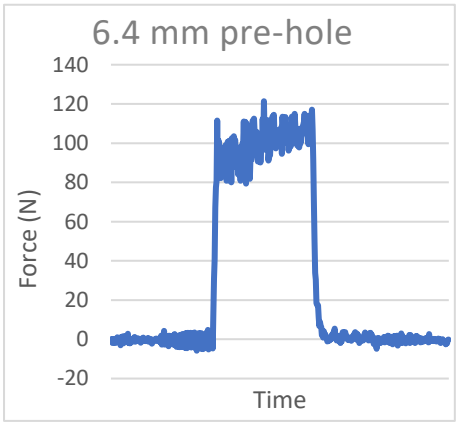

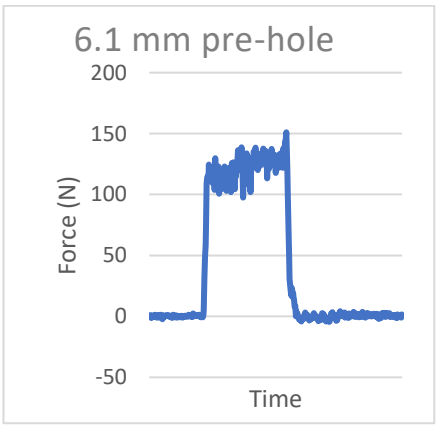

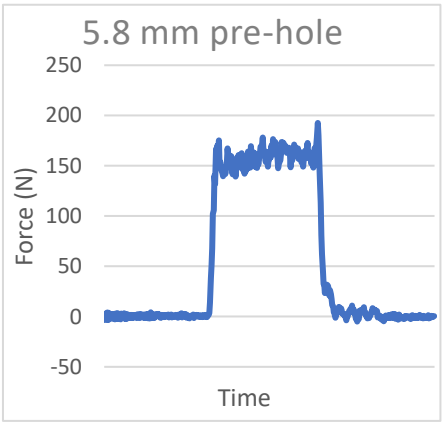

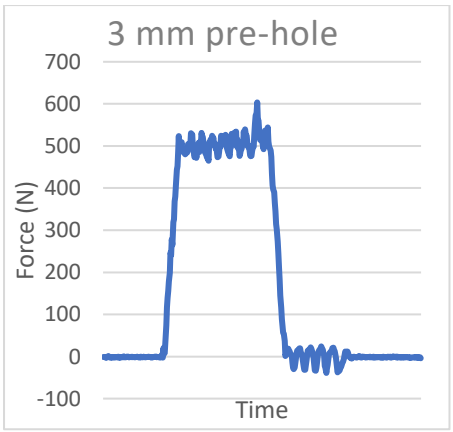

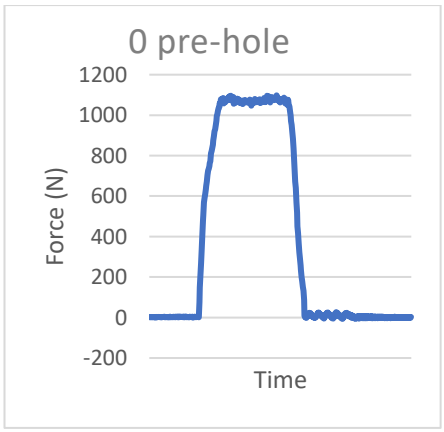

Maraging steel, As-built, 5° recoater angle

Axial drilling force for various pre-holes, Printing inclination 45°

4.2 mm drill

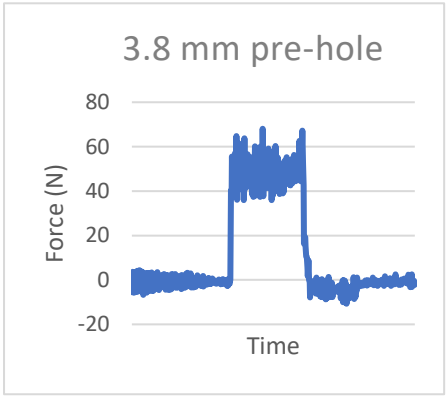

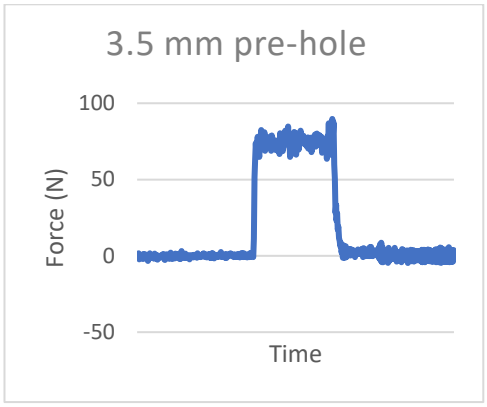

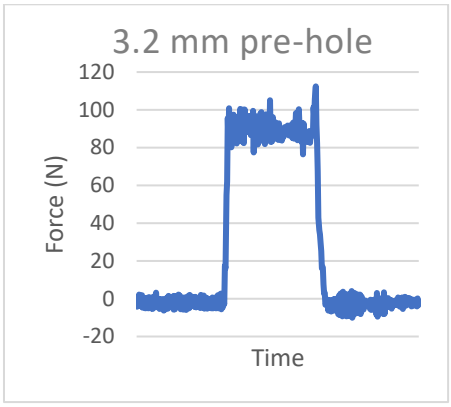

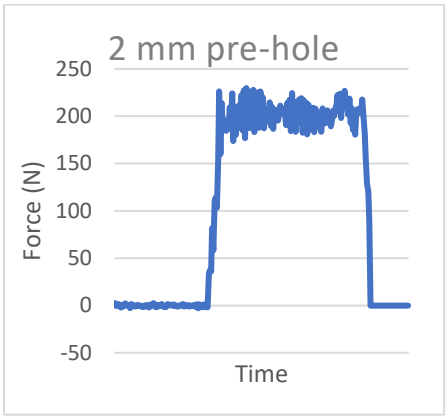

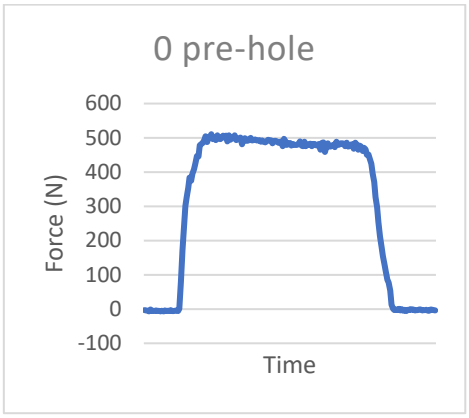

6.8 mm drill

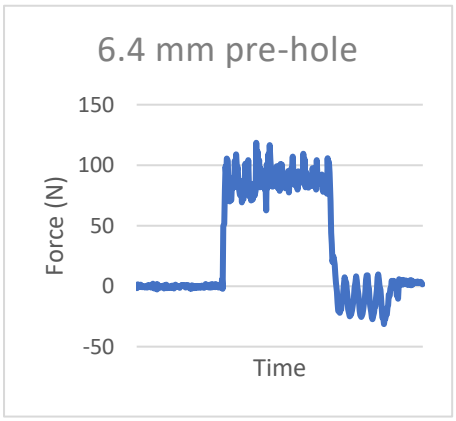

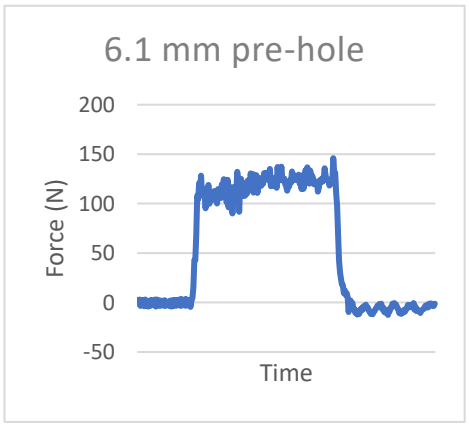

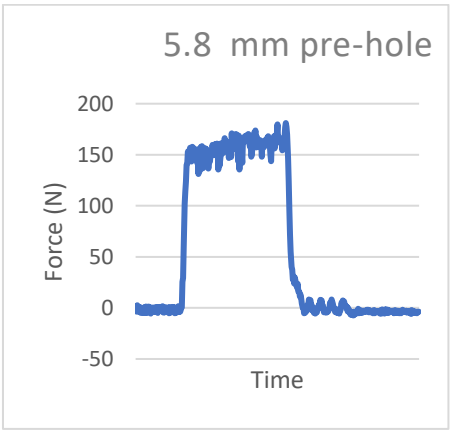

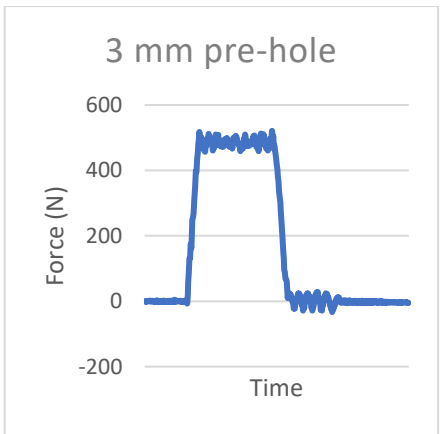

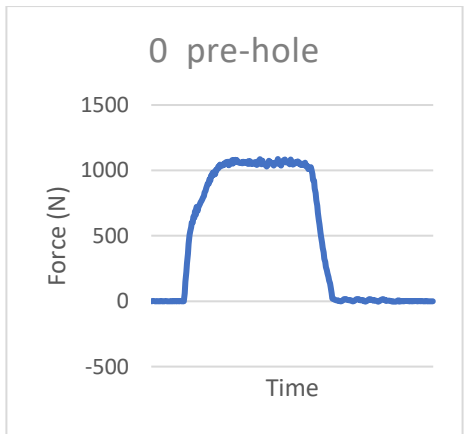

Maraging steel, As-built, 5° recoater angle

Axial drilling force for various pre-holes, Printing inclination 60°

4.2 mm drill

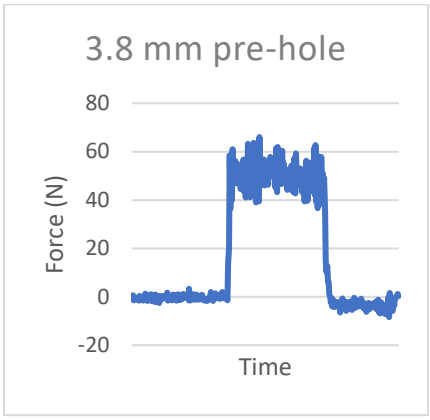

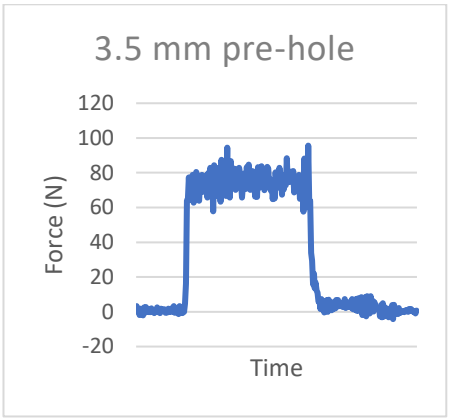

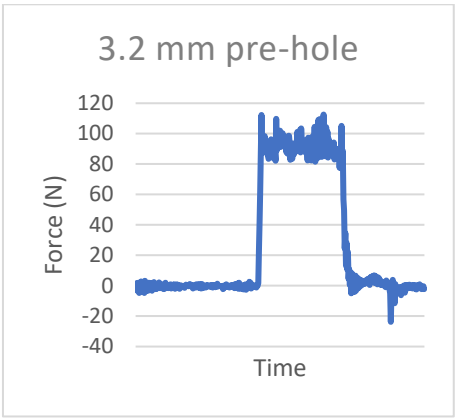

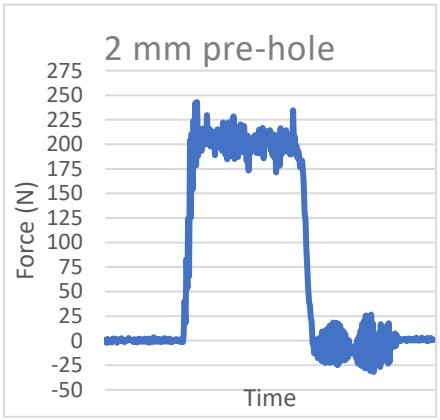

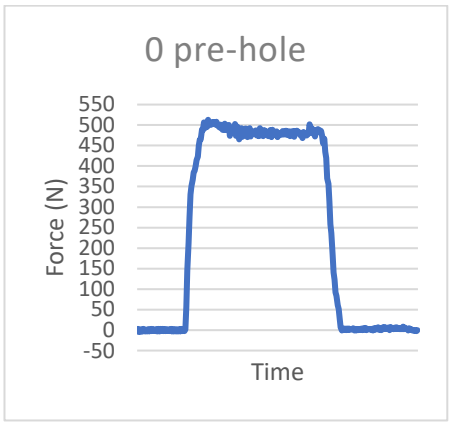

6.8 mm drill

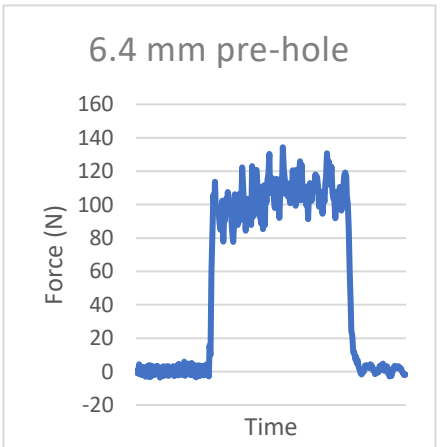

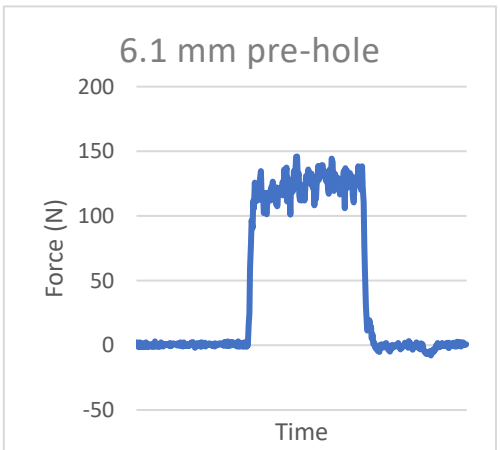

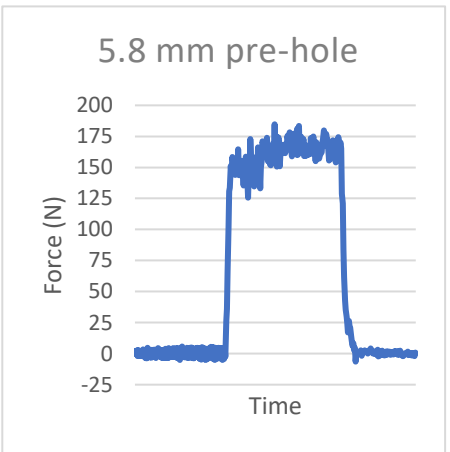

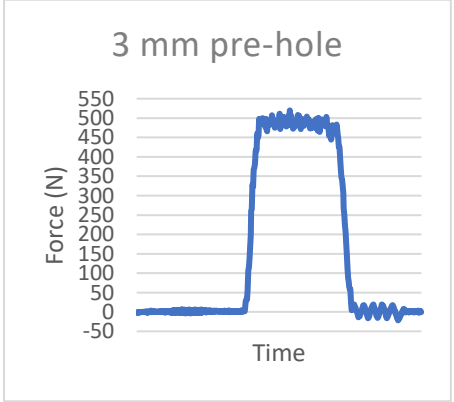

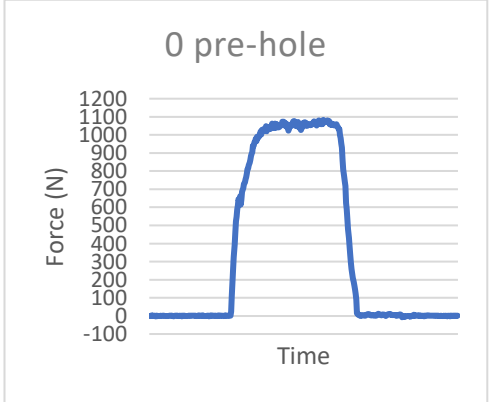

Maraging steel, As-built, 5° recoater angle

Axial drilling force for various pre-holes, Printing inclination 90°

4.2 mm drill

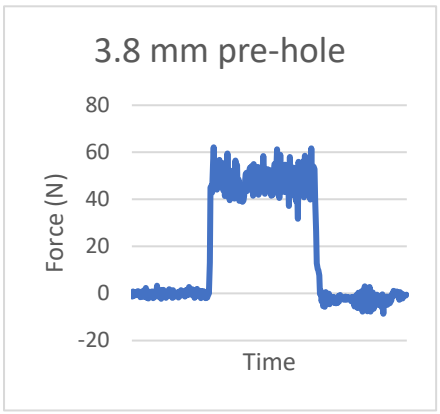

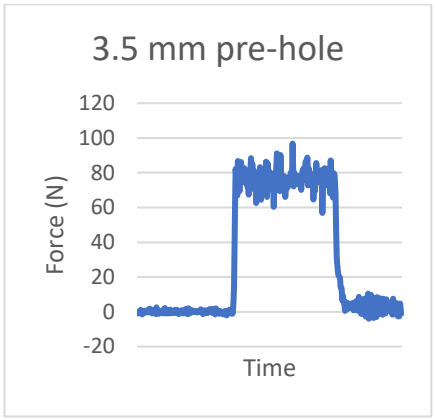

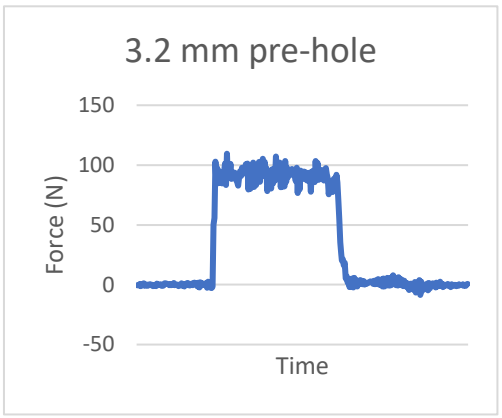

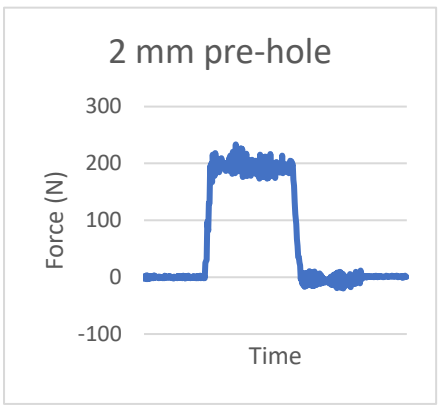

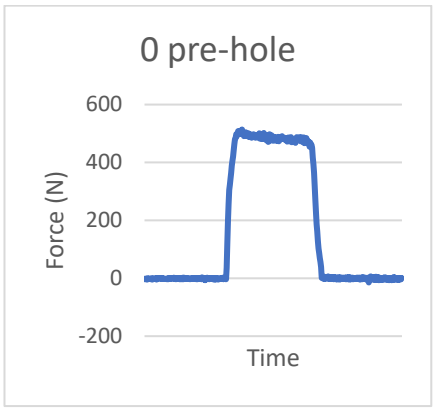

6.8 mm drill

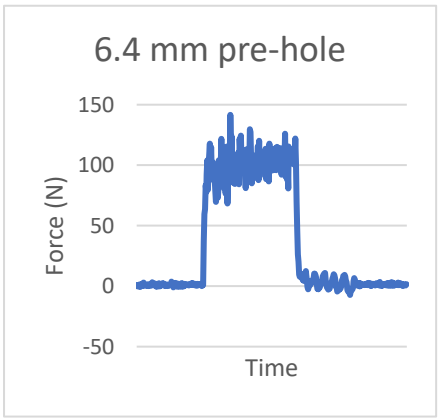

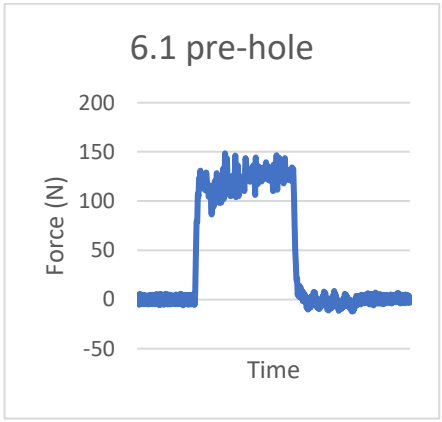

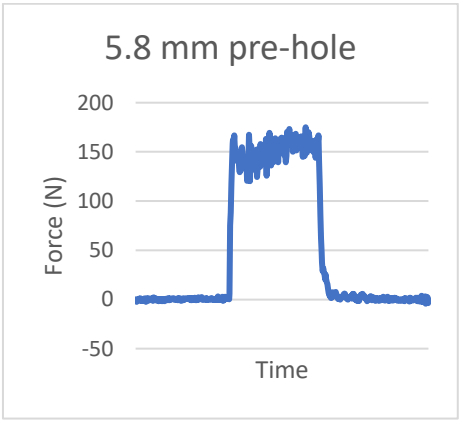

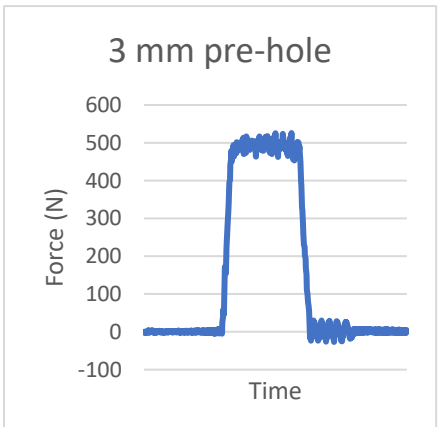

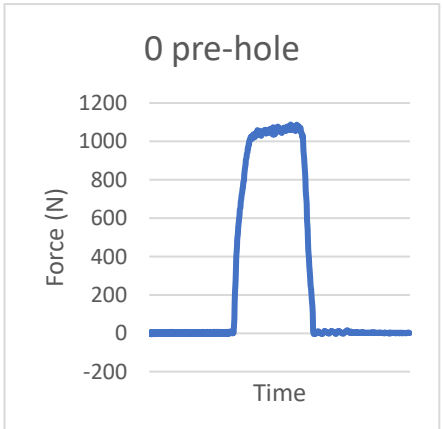

Maraging steel, Solution Treated, 5° recoater angle

Axial drilling force for various pre-holes, Printing inclination 0°

4.2 mm drill

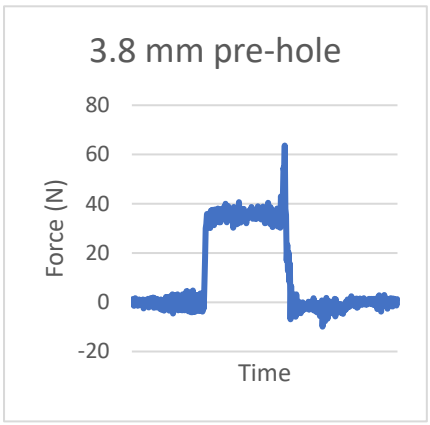

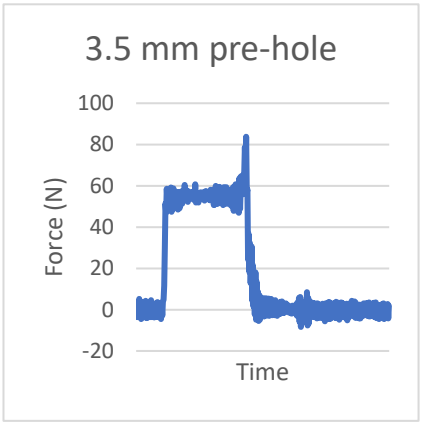

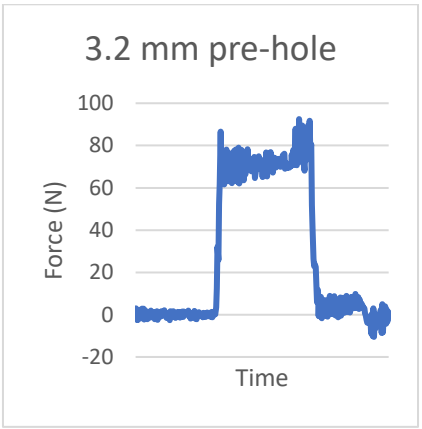

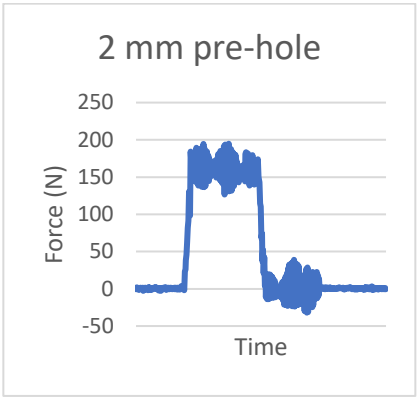

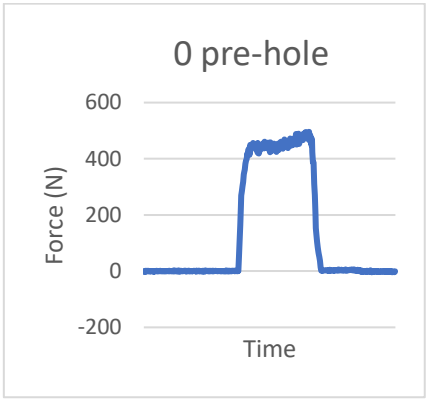

6.8 mm drill

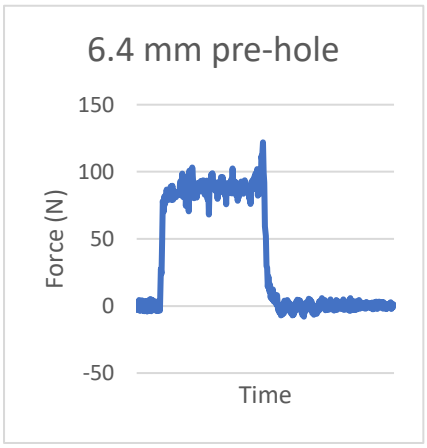

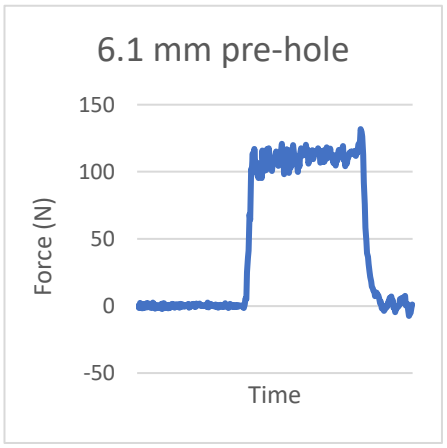

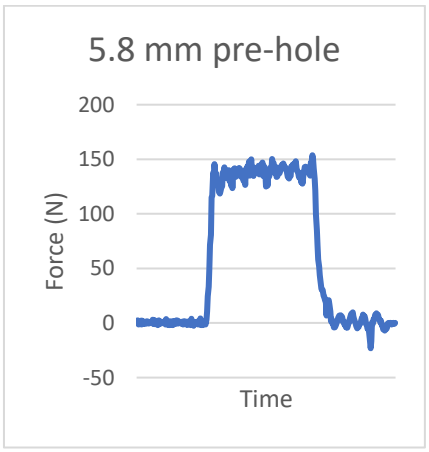

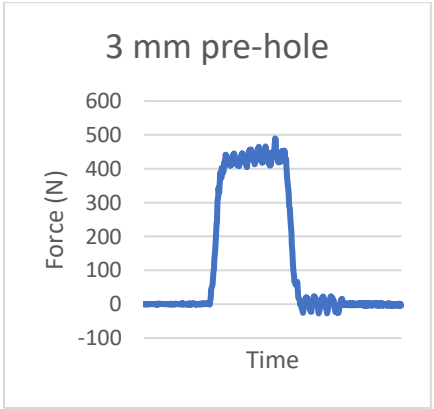

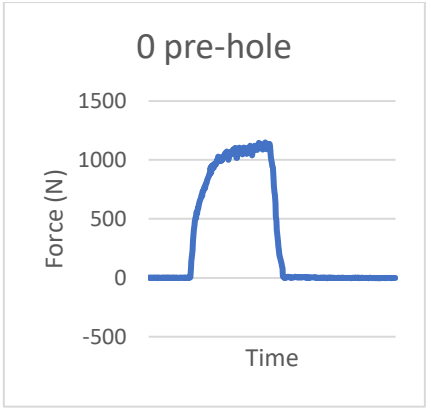

Maraging steel, Solution Treated, 5° recoater angle

Axial drilling force for various pre-holes, Printing inclination 30°

4.2 mm drill

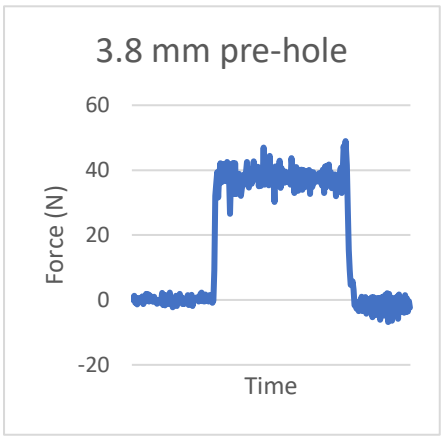

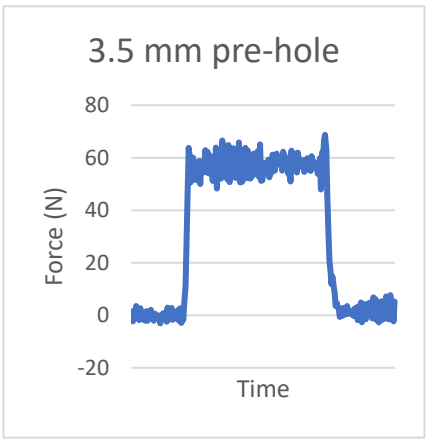

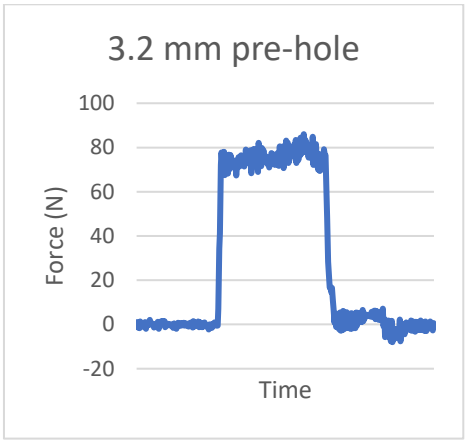

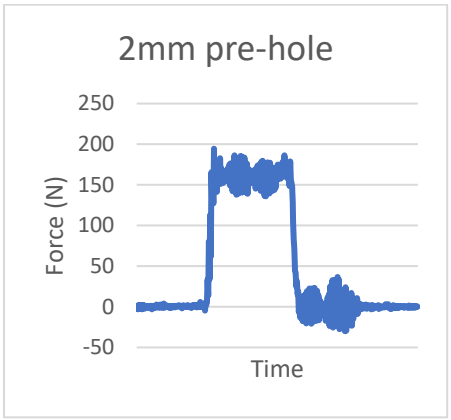

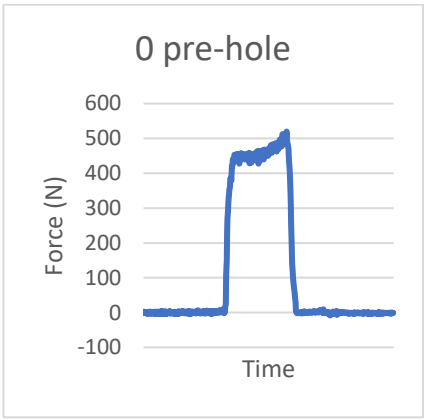

6.8 mm drill

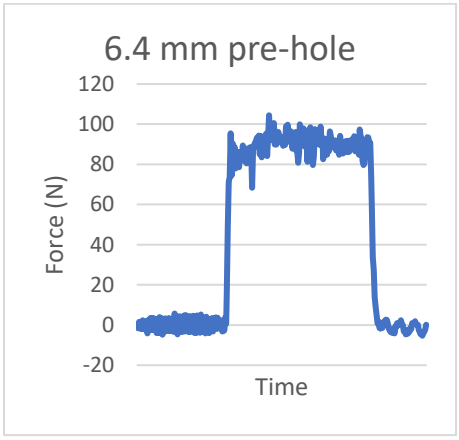

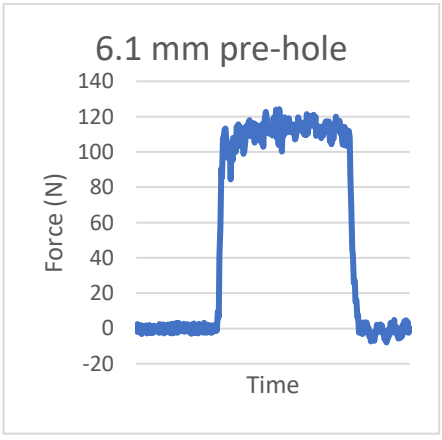

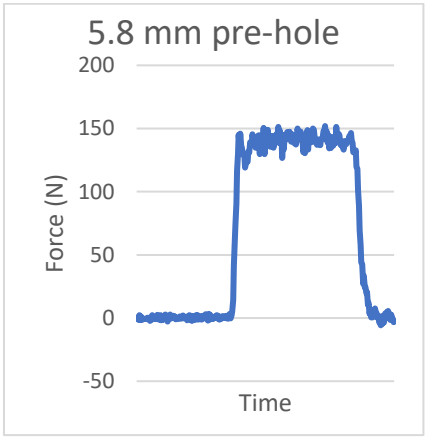

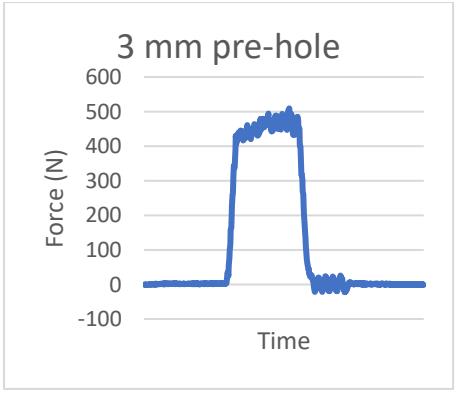

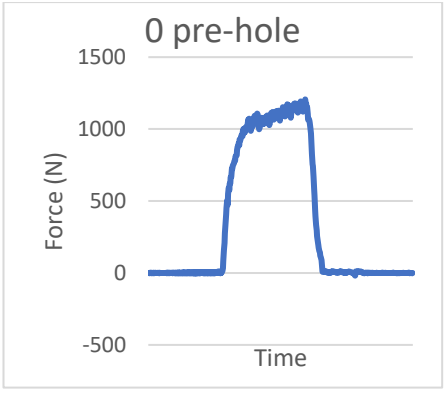

Maraging steel, Solution Treated, 5° recoater angle

Axial drilling force for various pre-holes, Printing inclination 45°

4.2 mm drill

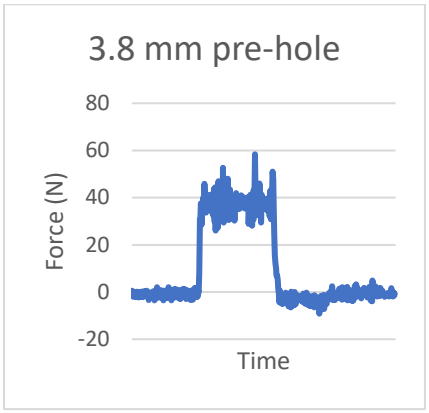

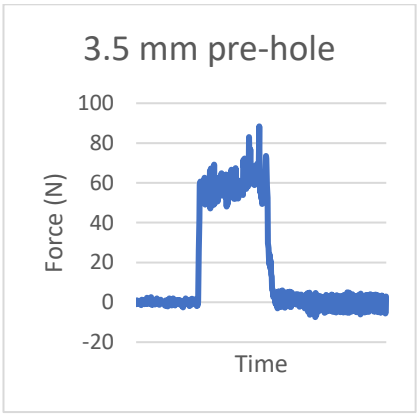

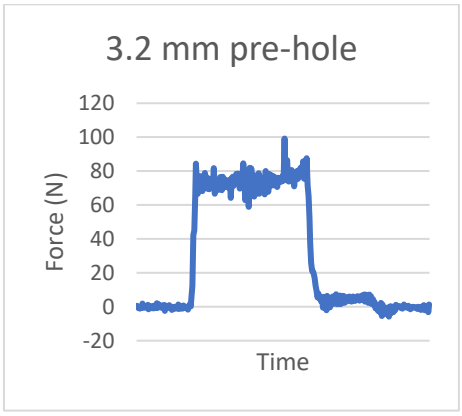

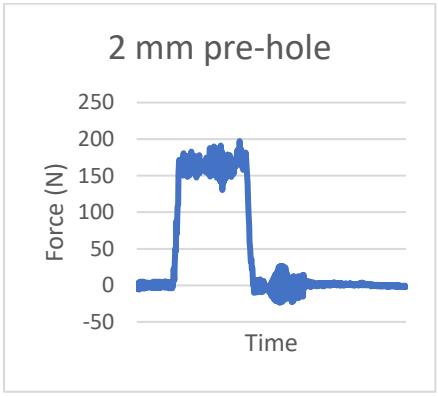

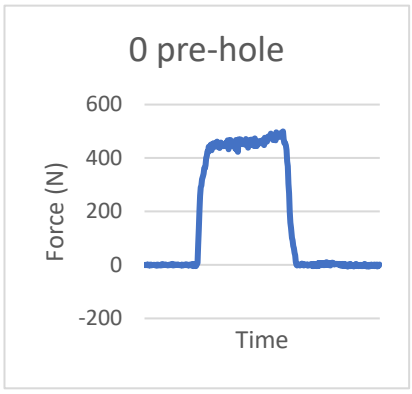

6.8 mm drill

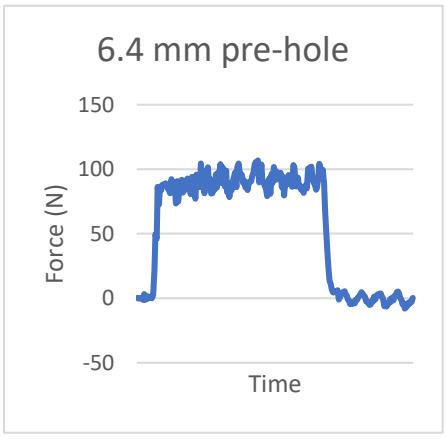

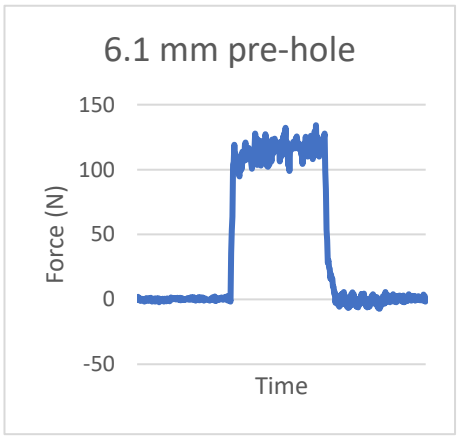

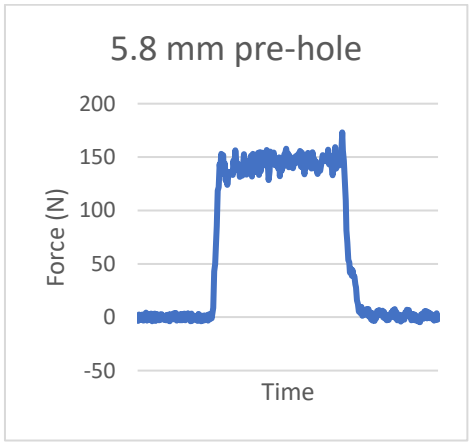

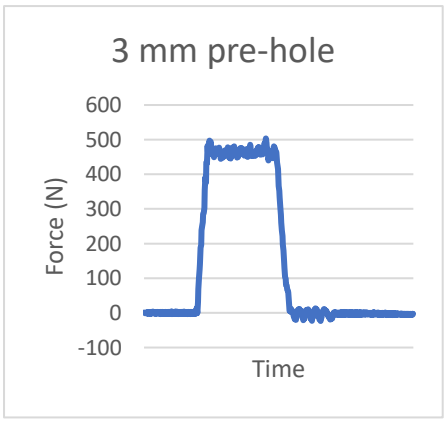

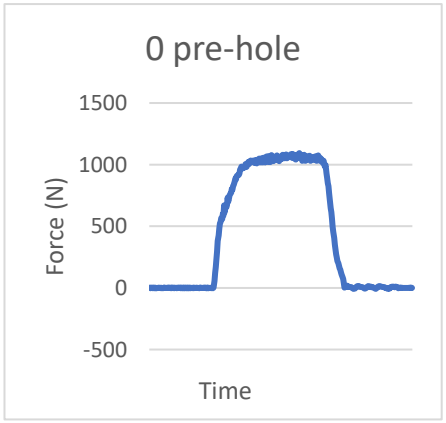

Maraging steel, Solution Treated, 5° recoater angle

Axial drilling force for various pre-holes, Printing inclination 60°

4.2 mm drill

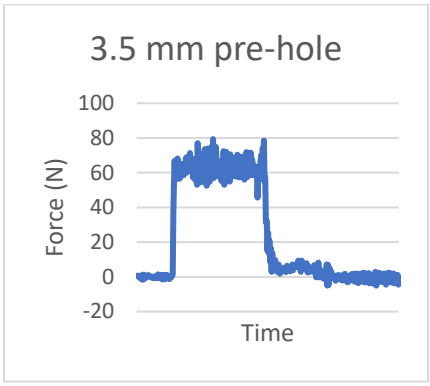

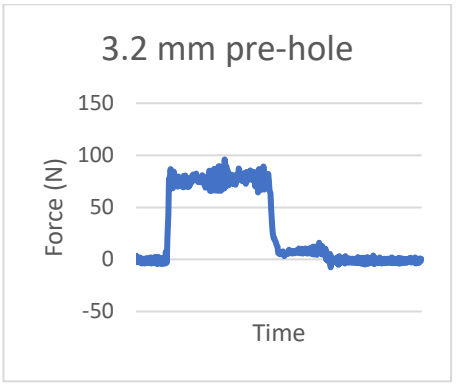

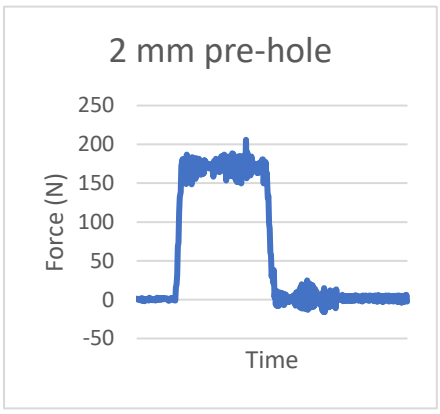

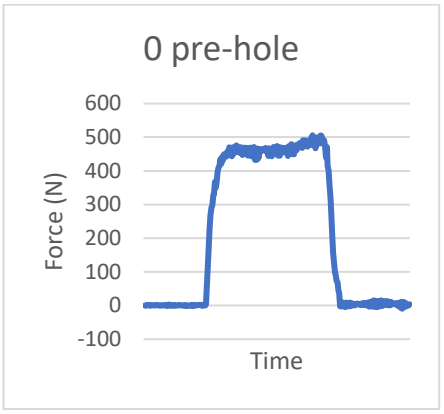

6.8 mm drill

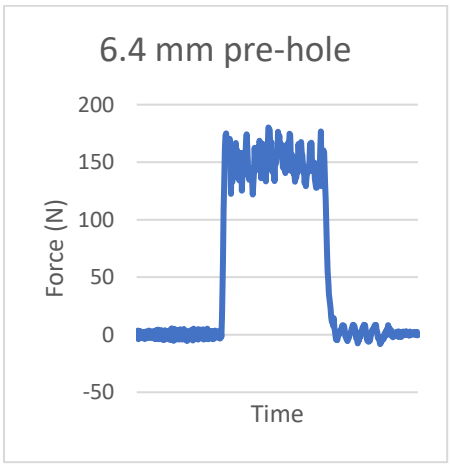

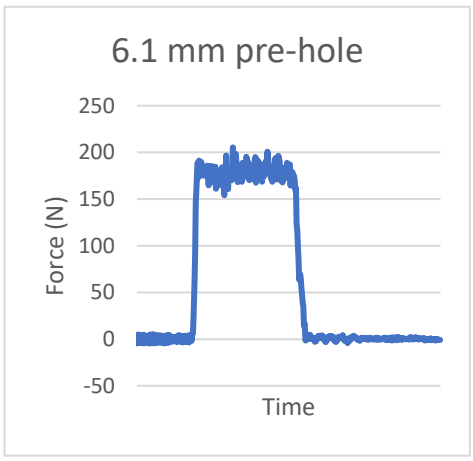

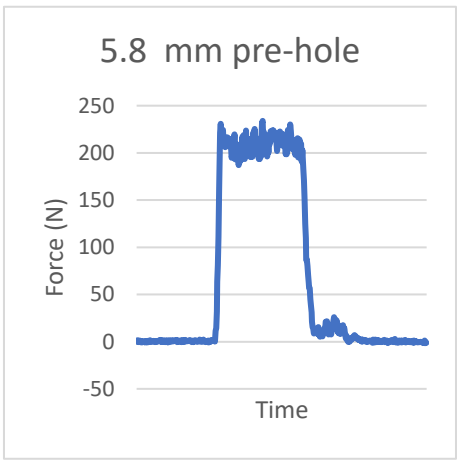

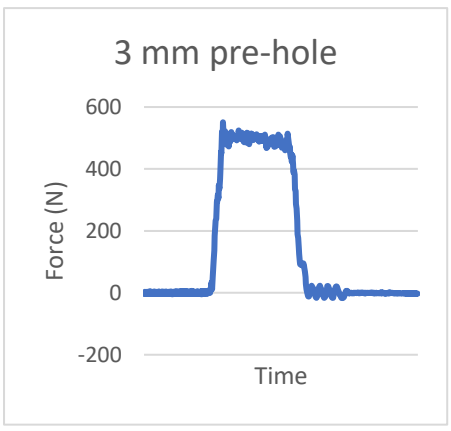

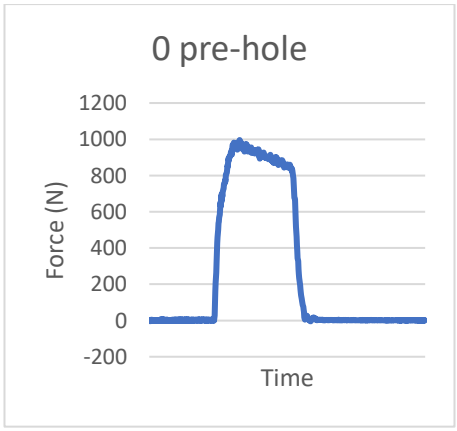

Maraging steel, Solution Treated, 5° recoater angle

Axial drilling force for various pre-holes, Printing inclination 90°

4.2 mm drill

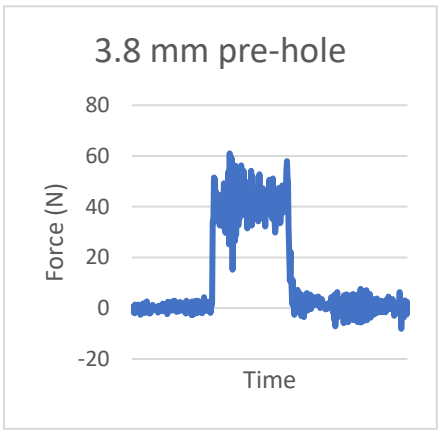

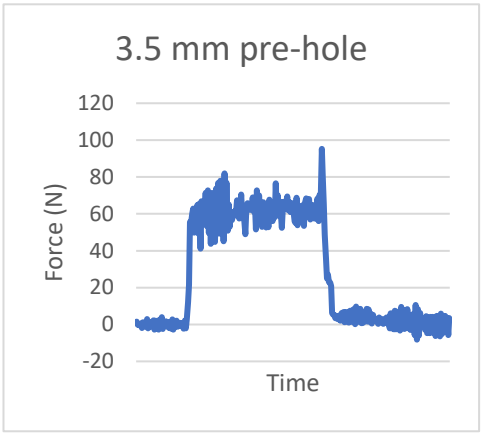

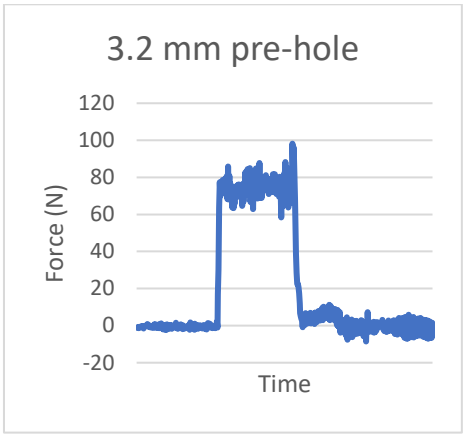

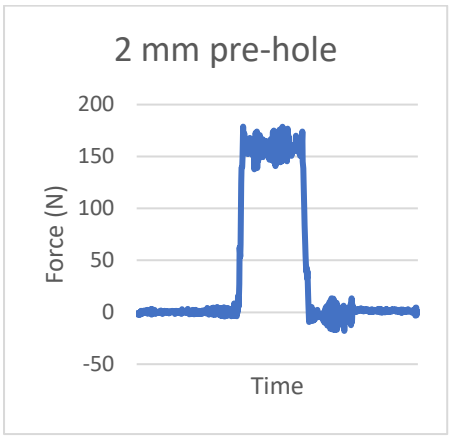

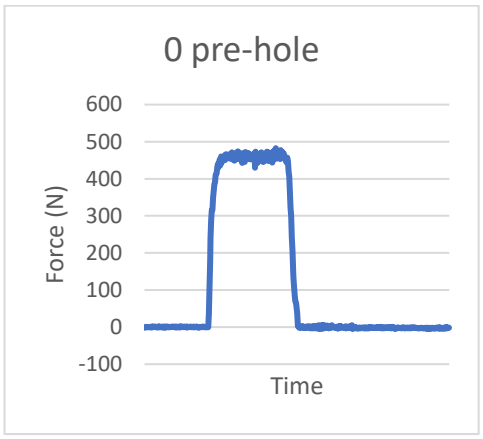

6.8 mm drill

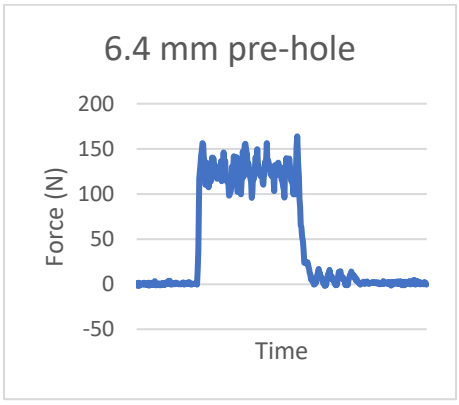

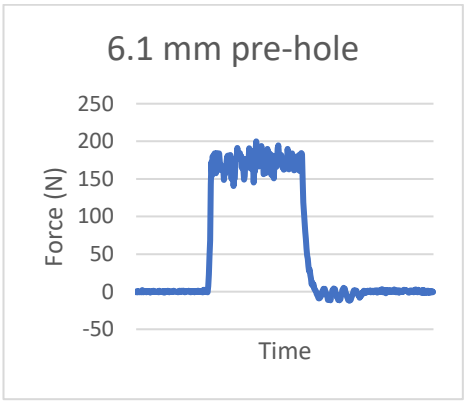

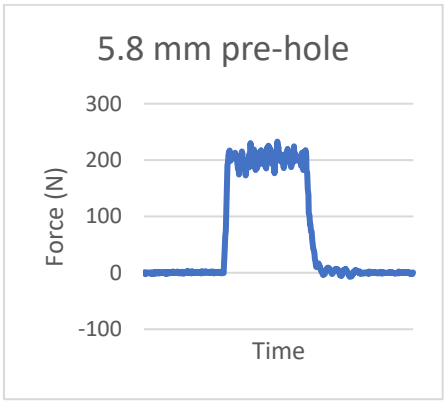

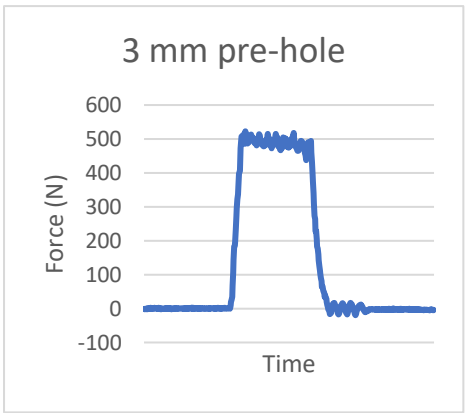

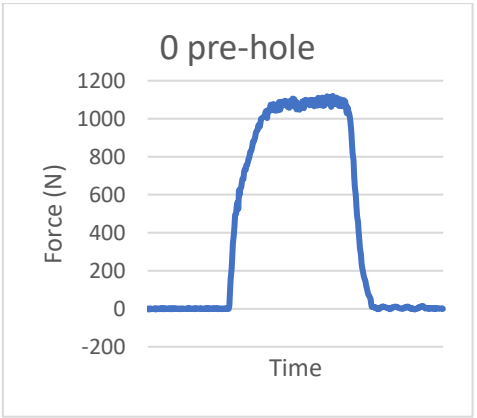

Maraging steel, Solution Treated, 45° recoater angle

Axial drilling force for various pre-holes, Printing inclination 0°

4.2 mm drill

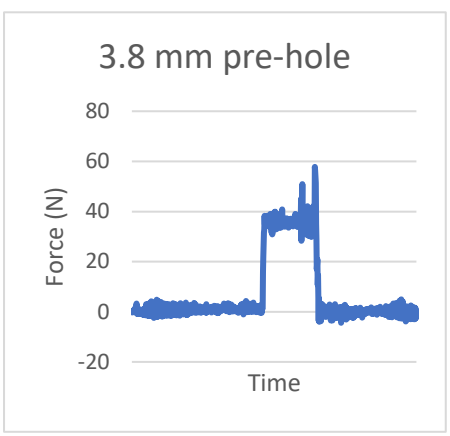

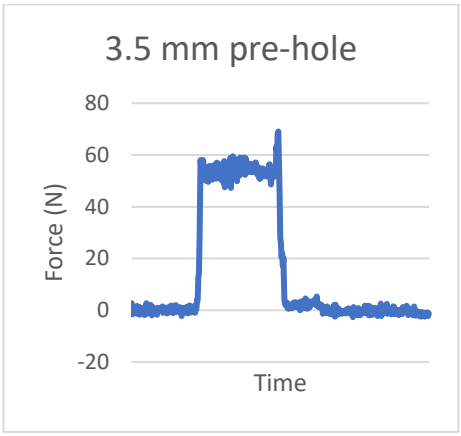

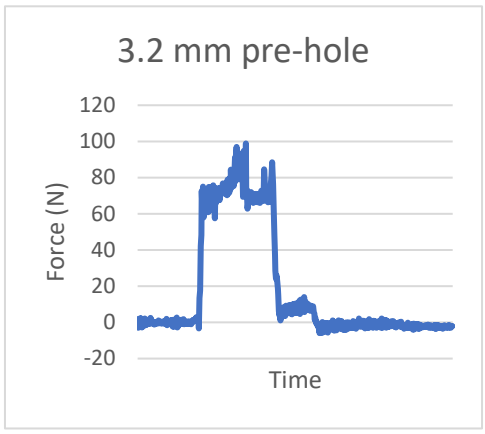

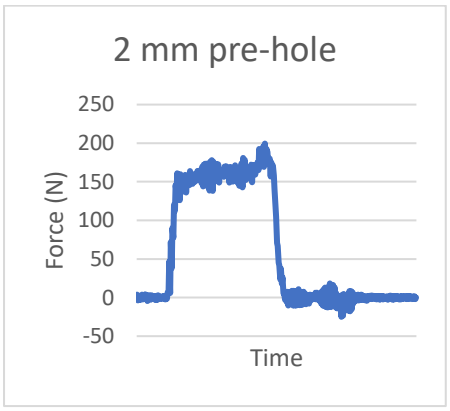

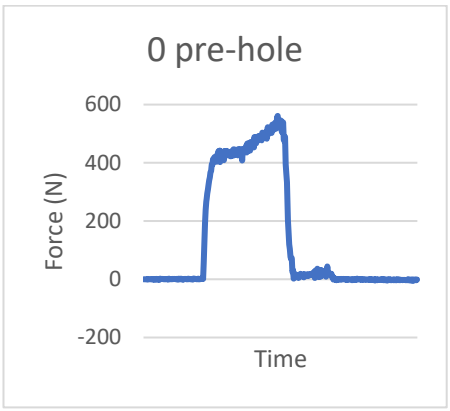

6.8 mm drill

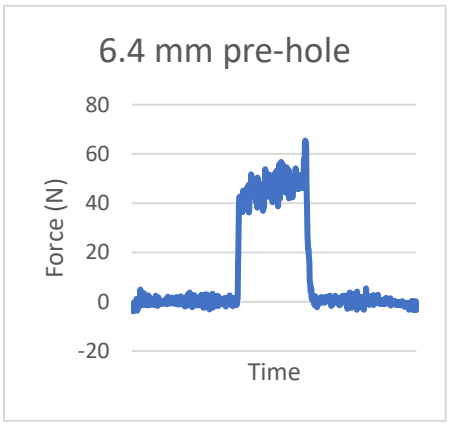

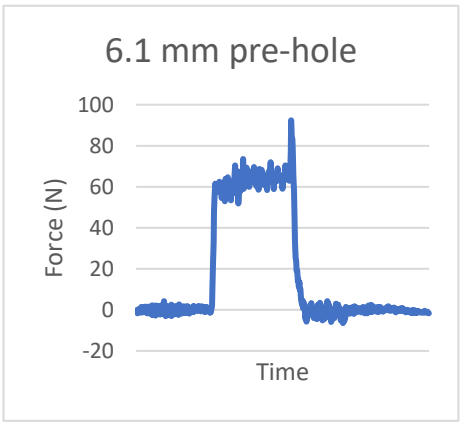

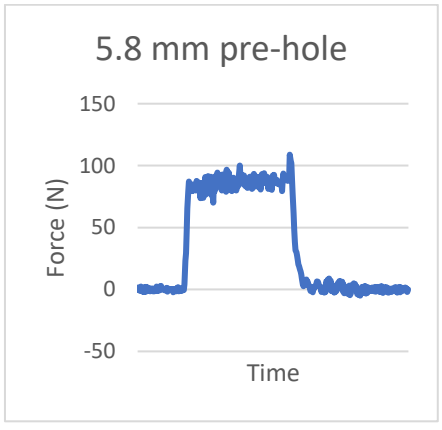

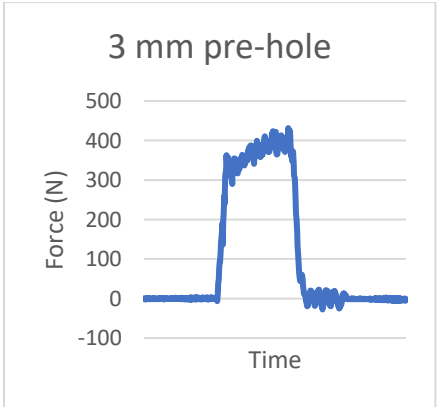

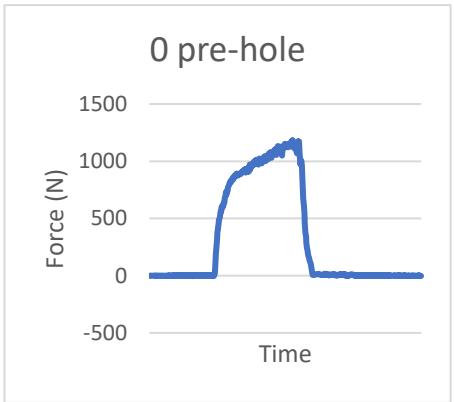

Maraging steel, Solution Treated, 45° recoater angle

Axial drilling force for various pre-holes, Printing inclination 30°

4.2 mm drill

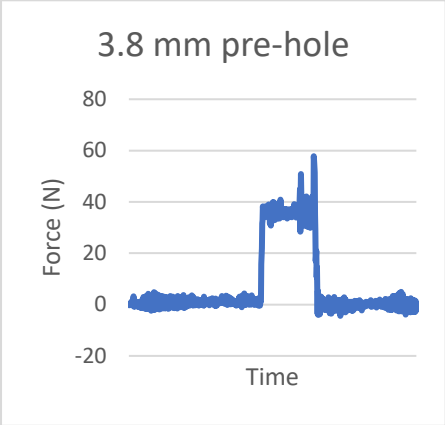

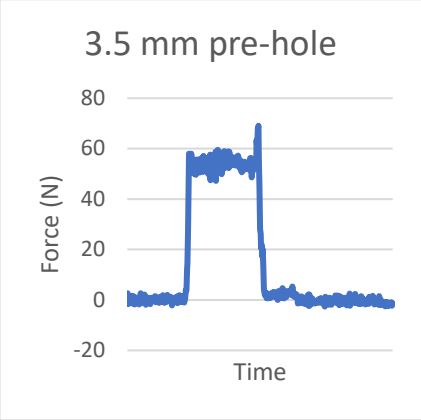

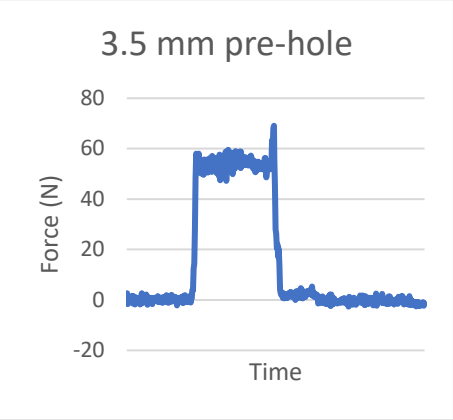

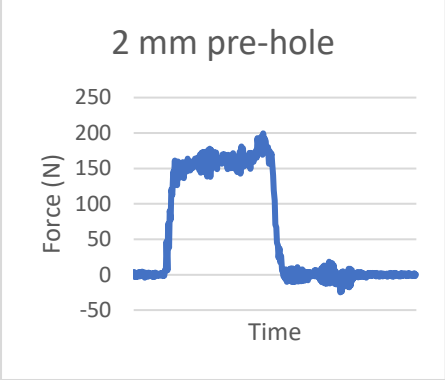

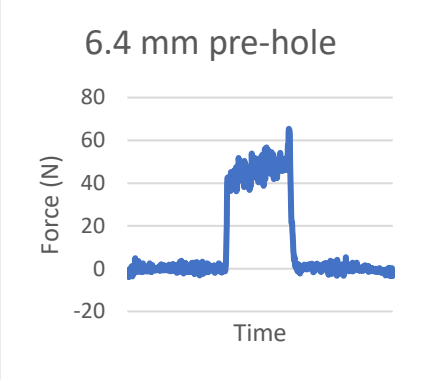

6.8 mm drill

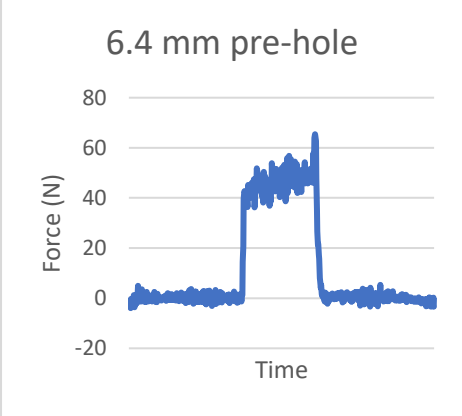

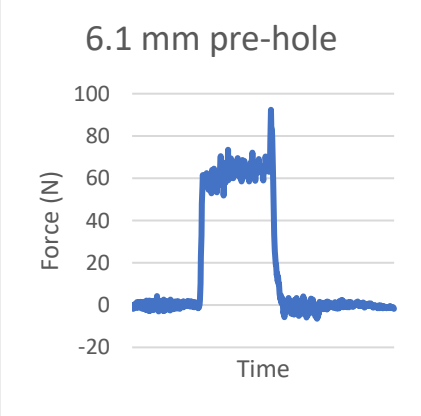

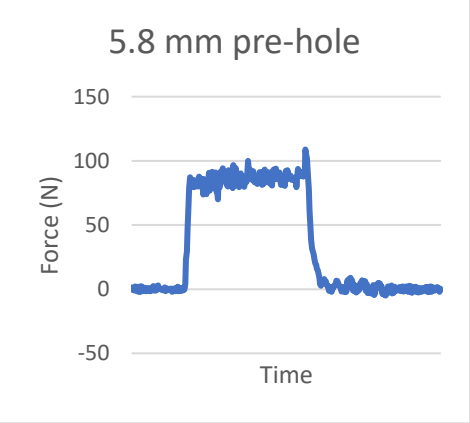

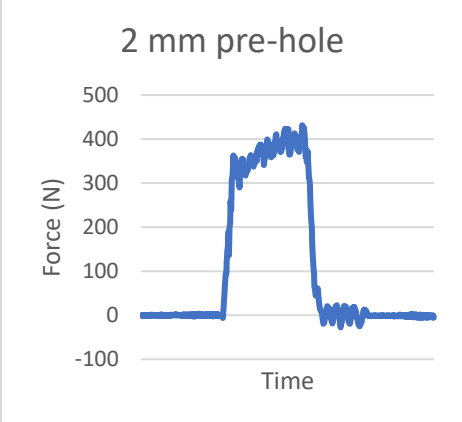

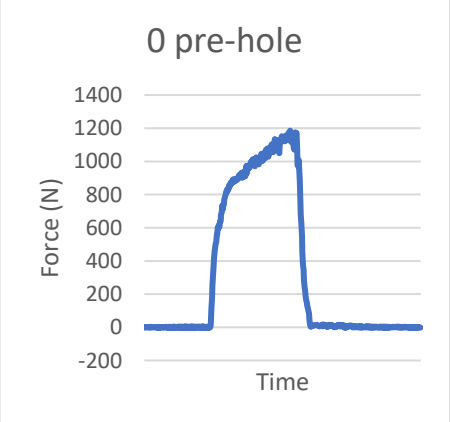

Maraging steel, Solution Treated, 45° recoater angle

Axial drilling force for various pre-holes, Printing inclination 45°

4.2 mm drill

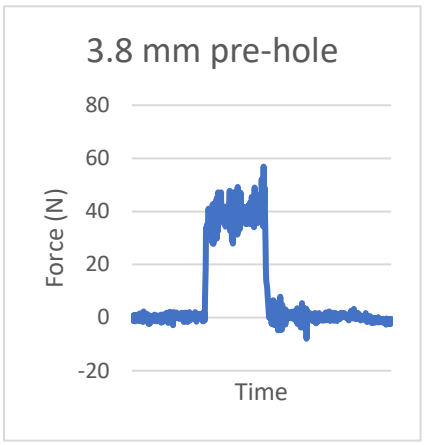

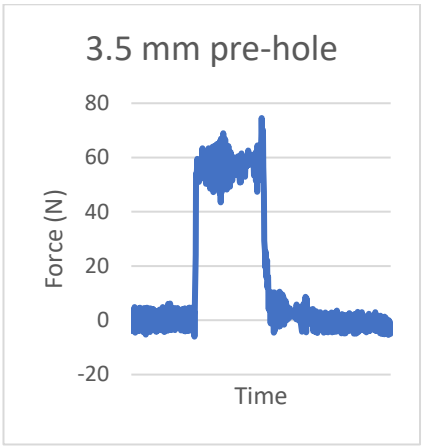

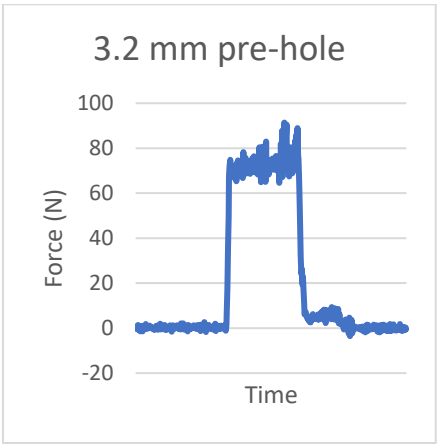

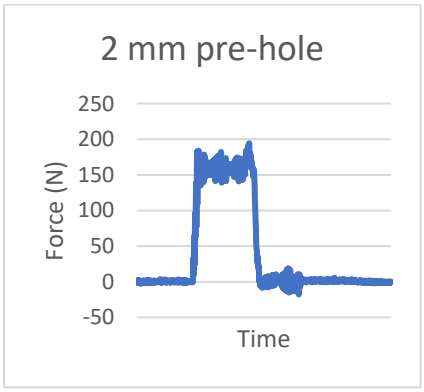

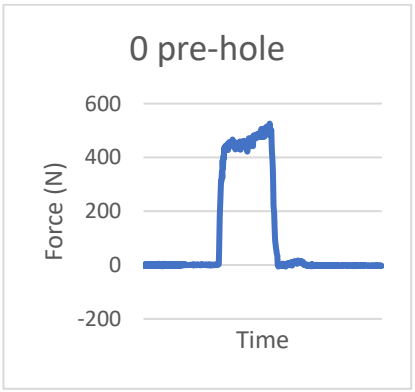

6.8 mm drill

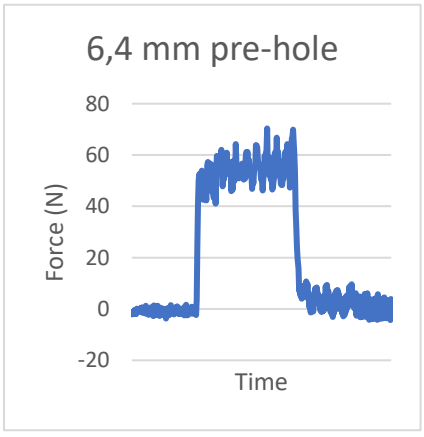

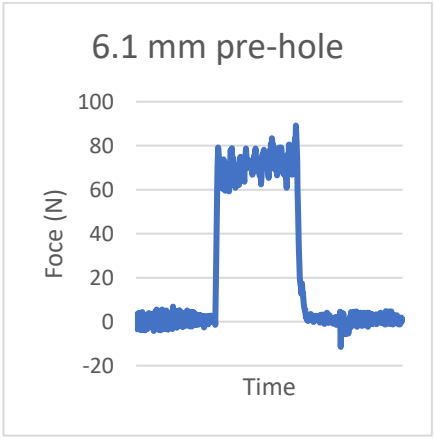

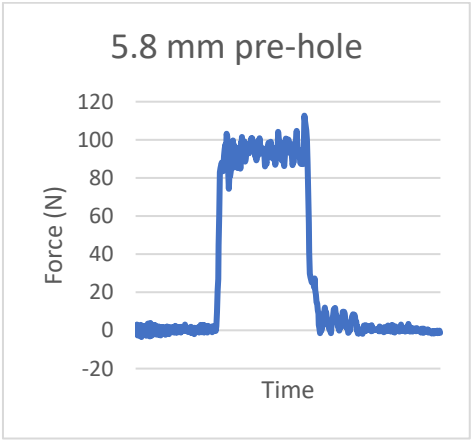

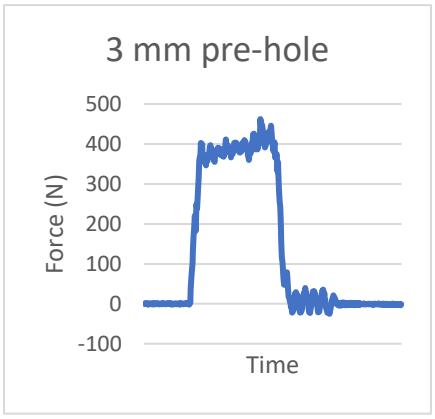

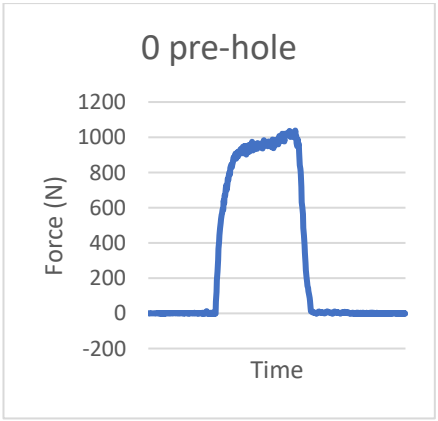

Maraging steel, Solution Treated, 45° recoater angle

Axial drilling force for various pre-holes, Printing inclination 60°

4.2 mm drill

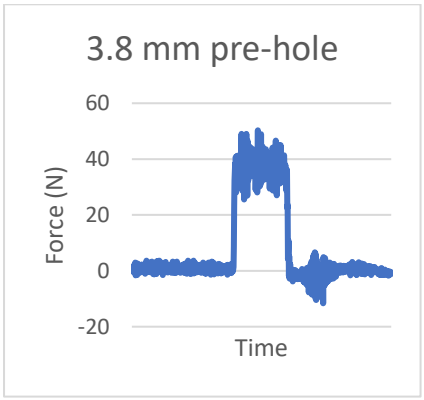

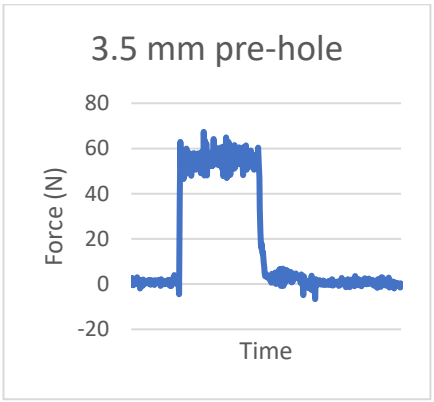

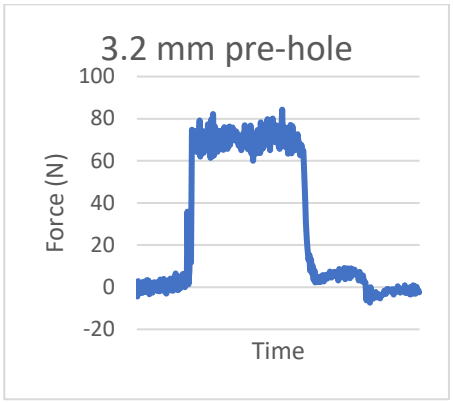

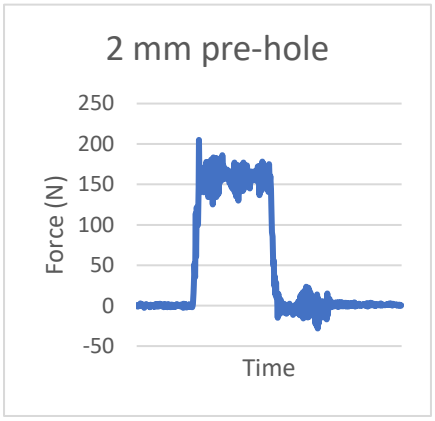

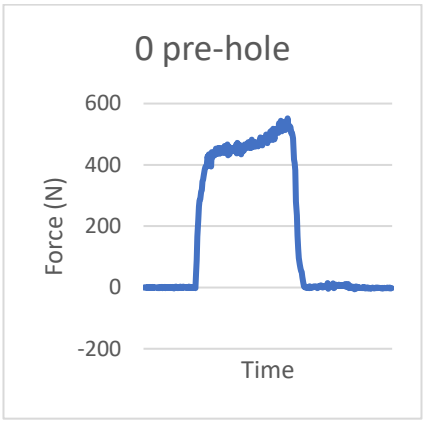

6.8 mm drill

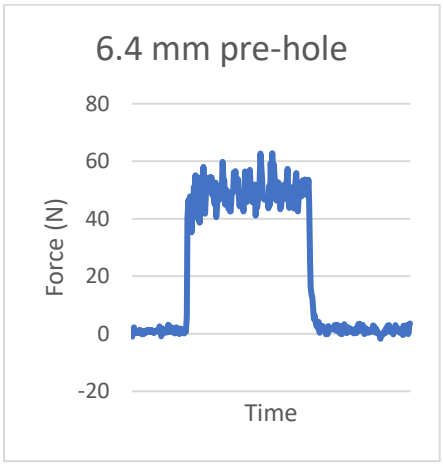

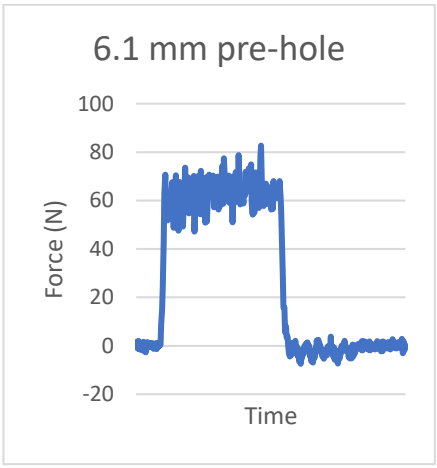

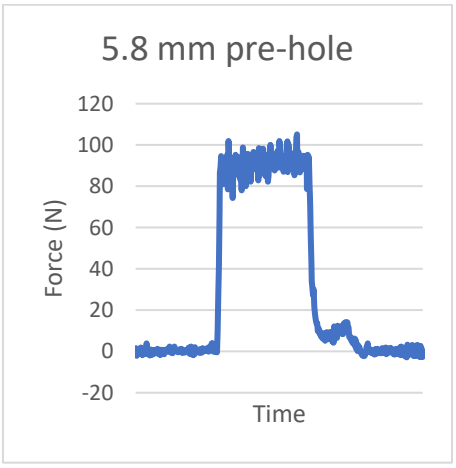

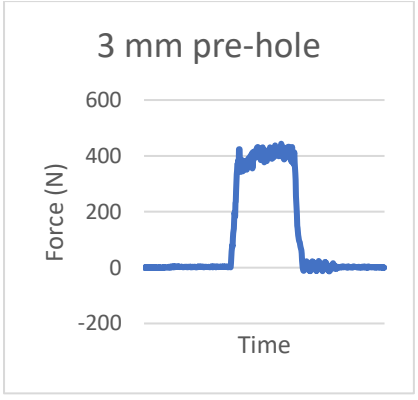

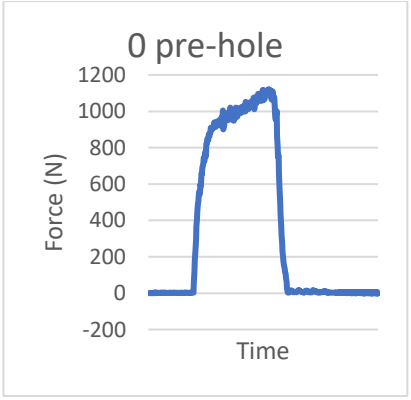

Maraging steel, Solution Treated, 45° recoater angle

Axial drilling force for various pre-holes, Printing inclination 90°

4.2 mm drill

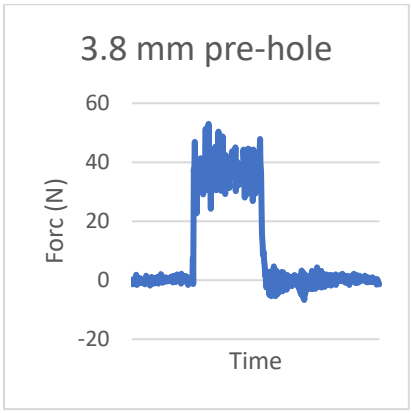

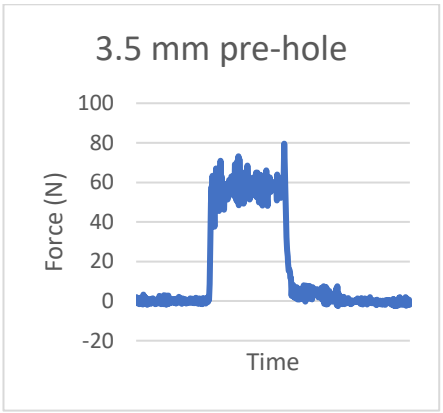

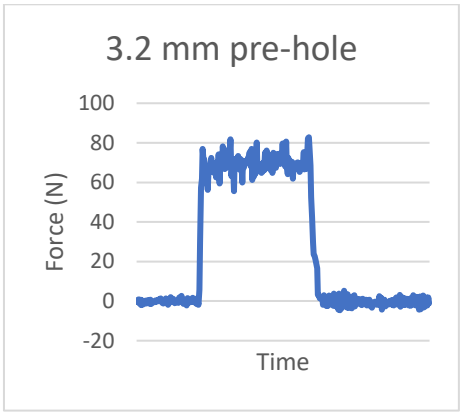

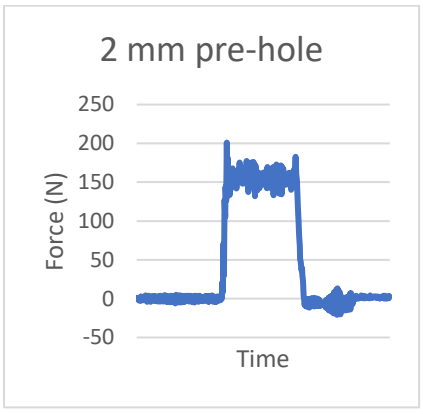

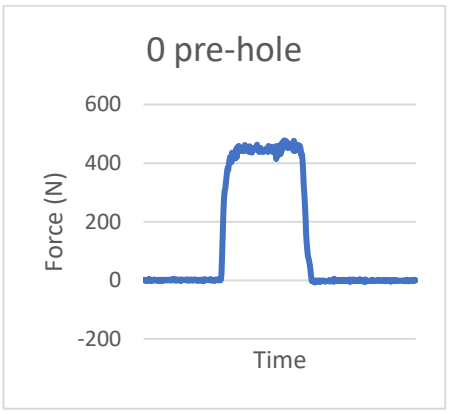

6.8 mm drill